Thermal transport in heterogeneous groundwater systems: Dynamics and flow estimation

Dylan Irvine

School of the Environment

Flinders University

A thesis submitted for the degree of

Doctor of Philosophy

August 7, 2014

Declaration

I certify that this thesis does not incorporate without acknowledgment any material previously submitted for a degree or diploma in any other university; and that to the best of my knowledge and belief it does not contain any material previously published or written by another person except where due reference is made in the text.

.....
Dylan Irvine

Coauthorship

This PhD thesis was produced as a series of journal publications in leading international scientific journals. Chapters 2 - 4 were written as independent journal papers. At the time this thesis was completed, one journal paper (chapter 3) was published, one was accepted and in the final stages of copy editing (chapter 2), and another (chapter 4) was undergoing revision and is expected to be published in due course.

I am the first author on all journal publications and was responsible for leading and conducting the majority of research contained in them, including the final writeup and publication of the research.

The papers in this thesis have benefitted from ongoing advice and input of my supervisors, coauthors and the peer review process. I acknowledge their valuable advice and important contributions.

Additionally, I acknowledge the contribution of the two anonymous reviewers who reviewed this thesis.

Acknowledgements

This thesis would not have been possible without the help and support from a great number of people.

I would like to thank my wife Sarah and my family for their support throughout my studies.

To my supervisors, many thanks for all of your support. Craig, you are the reason why I chose to study hydrogeology. Your passion and enthusiasm are contagious. Thank you. Adrian, I especially appreciate your attention to detail. Heather, if you did not take me on for the project with you, I may have never taken up Python which I have found to be an incredibly useful tool.

To everyone in the Earth Science building at Flinders University. It was such a joy to come to work each day, being surrounded by so many incredibly friendly people. To my office mates Jim and Saskia, and the rotation of Ilka, Hugo, Donmei and Marco, thanks for the memories.

To my friends who share a passion for temperature and density dependent hydrobiochemistry (you know who you are), many thanks. I am sure that we will be great friends for life. May you continue on with your endeavours.

And of course, I have to thank the organisations who funded me throughout my candidacy. This work was supported by: 1) an Australian Postgraduate Award, 2) the National Centre for Groundwater Research and Training (NCGRT), and 3) the Western Australian Geothermal Centre of Excellence (WAGCOE).

Summary

The use of water temperature as a tracer to infer rates of fluid flow, and determine subsurface properties has gained popularity in recent years, with review articles on heat as a tracer to infer groundwater–surface water exchange (Anderson 2005; Constantz 2008; Rau et al. 2014), heat as a tracer in hydrogeology (Anderson 2005), and the use of heat as a tracer for deep groundwater processes (Saar 2011). Heat is a popular tracer because both natural variations in water temperature (e.g. diurnal temperatures in streambed materials), or applied (e.g. input temperature can be monitored in aquifer storage and recovery systems) temperatures can be analysed. Other benefits of temperature measurements include the fact that water temperature can be measured without the need for laboratory analysis, and it can be collected quickly and easily from point measurements, to the use of Distributed Temperature Sensors to record temperature both temporally and spatially. With the increase in popularity in the use of temperature in hydrogeology, an understanding of the influence of aquifer heterogeneity on thermal transport in groundwater is required.

Anderson (2005) highlights that a revival of the use of temperature measurements in hydrogeology has been promoted by the availability of inexpensive temperature data loggers, and increased availability of numerical codes to simulate joint water flow and thermal transport. Temperature measurements could be useful in a range of contexts, as thermal transport occurs on a range of spatial scales, and is involved in a number of processes. With heterogeneity of porous media also occurring from the pore scale to the basin scale, the understanding of how heterogeneity influences thermal transport is vital to understand where the use of heat may be useful to understand groundwater systems, and to identify any limitations to its use. This body of work addresses the influence of aquifer heterogeneity on the transport of heat in porous media on scales from the kilometre scale down to the centimetre scale, and across a range of processes. Specifically, this work investigates: 1) the influence of aquifer heterogeneity on the potential for thermal free convection, 2) the influence of aquifer heterogeneity on the interpretation of applied heat and solute groundwater tracers, and 3) the influence of streambed heterogeneity on the use of temperature time series to infer groundwater–surface

water exchange.

The first part of this study investigates the potential for thermal free convection in the Yarragadee aquifer in the Perth metropolitan area in Western Australia. It does so by utilising a stratigraphic forward model of the aquifer, which provides a realistic, and plausible heterogeneous structure of the aquifer, something that is lacking in existing investigations of the influence of aquifer heterogeneity on the potential for free convection. The key question was whether the inclusion of heterogeneity in simulations of coupled heat and water flow would prevent the occurrence of free convection. We show that the influence of heterogeneity may not be sufficient to prevent the occurrence of thermal free convection, and identify regions where convection is most likely. This study provides further evidence for the presence of thermal free convection in the Perth metropolitan area, which will assist in the search for low temperature geothermal energy sources in Western Australia.

The second part of this study investigates the influence of aquifer heterogeneity on the interpretation of applied solute and heat tracers to determine pore water velocity in heterogeneous aquifers. It does so through the use of numerical simulations of groundwater flow, solute and heat transport in synthetic heterogeneous aquifers. Aquifer heterogeneity is represented using geostatistical properties that span the range found across highly instrumented sites such as the Borden, Cape Cod and the MADE sites. The goal was to identify any benefits or drawbacks of the use of applied heat or solute tracers. We show that interpretations of a heat tracer yielded the lowest variance in estimates of velocity. This means that estimates of velocities inferred from heat tracers will be closer to the mean velocity, which may be a key benefit. The higher variance in estimates of velocity from interpretation of the solute tracer may provide more insight about aquifer heterogeneity.

The final part of this study investigates the influence of streambed heterogeneity on the Hatch et al. (2006) analytical solutions that use temperature time series to determine groundwater– surface water interactions. It does so through the use of numerical models which generate synthetic temperature time series data, which are used to estimate vertical fluxes. The benefits of this approach is that

the analytical models can be tested where fluxes are known. We show that generally, the Hatch et al. (2006) equations perform fairly well for losing streams. We show that failure of the Amplitude Ratio method, and large variations in estimated fluxes over small distances from the Phase Shift method can be attributed to streambed heterogeneity. This research demonstrates that even when the assumption of 1D and homogeneous flow is violated, that the Hatch et al. (2006) equations perform well, and can provide detailed understanding of fluxes in heterogeneous streambeds.

Following Anderson's (2005) review, temperature measurements are becoming a more widely used tool in hydrogeology, including contexts ranging from groundwater–surface water interaction, to the identifying the location of fractures. With the use of temperature measurements on the increase in hydrogeology, it is important to understand the influence of heterogeneity in porous media on thermal transport and the estimation of flow rates from water temperature.

Contents

List of Figures

List of Tables

Chapter 1

Introduction

1.1 Research problem

Thermal transport theory has played an important role in the development of the theory of subsurface groundwater flow (Anderson 2005). When Darcy (1856) presented the law for subsurface groundwater flow, similar equations had previously been published for the molecular diffusion in liquids (Fick 1855), conduction of electricity (Ohm 1827) and conduction of heat through solids (Fourier 1822). Anderson (2005) highlights that Darcy would certainly have been aware of Fourier's work prior to conducting his experiments. Thermal transport was also fundamental in the development of the Theis (1935) solution to predict drawdown in a confined aquifer (or to be used inversely to determine aquifer transmissivity), which was developed from an analogy with thermal transport (Renard 2005). In fact, work on the conduction of heat in solids by Carslaw and Jaeger (1959) has continued to be used as a source for analytical solutions for groundwater problems (e.g. Hall and Moench 1972; Taniguchi et al. 1999; Townley and Trefry 2000).

A number of key papers on the use of heat as a groundwater tracer appeared in the 1960s, with analytical solutions to determine infiltration of surface water into the subsurface presented by Suzuki (1960), Stallman (1965), and Bredehoeft and Papadopulos (1965). However, with the importance of understanding issues relating to water quality, research on transport processes in groundwater have largely focussed on the transport of solutes. Research into solute transport in water has covered issues ranging the salinisation of wells caused by seawater intrusion (e.g. Pinder and Cooper 1970; Voss and Souza 1987), to issues relating to the transport of pollutants (e.g. Frind 1982; or the famous case of Woburn Massachusetts outlined in Bair and Metheny 2002).

Heterogeneity in porous media leads to the dispersion of a solute plume. Heterogeneity of porous media occurs on a range of scales, from the pore scale, to

the basin scale, both within and between different geological layers. Gelhar et al. (1992) performed an extensive review of field scale values of dispersivity of solutes, demonstrating that dispersivity of solutes increases with spatial scale. The influence of aquifer heterogeneity on the transport of solutes has been investigated both in the field (e.g. Sudicky 1986; LeBlanc et al. 1991) and numerically (e.g. Burnett and Frind 1987; Larocque et al. 2009).

With the number of methodologies that use temperature measurements to infer processes in hydrogeology increasing, and with the availability of automated analysis software (e.g. VFLUX by Gordon et al. 2012), the use of water temperature in problems relating to groundwater has made a resurgence. Thermal transport in groundwater occurs on scales ranging from the sub-metre scale, through to basin scale processes. For example, water temperature is used to determine interaction between surface water and groundwater on the tens of centimetre scale (e.g. Bredehoeft and Papadopulos 1965; Hatch et al. 2006). On scales of tens of metres, temperature measurements has also been used to identify high hydraulic conductivity zones between wells (Macfarlane et al. 2002; Pavelic et al. 2006), as well as in the identification of the location of fractures (Leaf et al. 2012; Banks et al. 2014), and to determine thermal transport properties (Vandenbohede et al. 2009). Uses of heat measurements to constrain larger scale processes include the measurement of spring temperatures to constrain basin scale permeability (see Saar 2011 for a review). Also of interest on large scales is whether thermal free convection can occur, which transports heated water towards the surface that can be ustilised for low temperature geothermal energy production. Temperature measurements are becoming widely used, although research into the influence of heterogeneity on thermal transport is limited.

With the increased use of heat in hydrogeology, investigations into the influence of aquifer heterogeneity on thermal transport in groundwater are required. Investigations into the influence of heterogeneity in porous media on thermal transport in groundwater have been performed in the context of thermal energy storage and recovery (Ferguson 2007), and the extent of a thermal plume generated from a groundwater heat exchanger (Hidalgo et al. 2009). However, the focus of these studies was not on the use of temperature for flow rate estimation. Schornberg et al. (2010), and Ferguson and Bense (2011) investigated the influence of streambed

heterogeneity on the use of the Bredehoeft and Papadopulos (1965) equation for upwelling flows (with Ferguson and Bense (2011) also investigating the use of the Turcotte and Schubert (1982) equation). These studies show that regions where conduction of temperature into regions of low flow led to error in flux estimations. However, the influence of heterogeneity in porous media on the use of heat as a tracer on larger (e.g. tens of metre) scales has not been widely investigated.

With increased capabilities of collecting time series of point or spatially distributed temperatures and increased capability of numerical modelling codes, the use of temperature in groundwater problems is expected to increase. Generally, this thesis focuses on the influence of heterogeneity in porous media on thermal transport in order to provide understanding of how heterogeneity may influence estimates of groundwater flow rates, or the flow dynamics within an aquifer. All investigations contained in this thesis involve numerical simulations of thermal transport. This thesis specifically investigates thermal transport in three separate contexts, and on three spatial scales:

Firstly, the influence of aquifer structure on the flow dynamics and potential for thermal free convection in deep aquifers (kilometre scale) requires attention. Typically, field scale numerical investigations of the potential for thermal convection are performed with homogeneous aquifer properties (e.g. Magri et al. 2010; Sheldon et al. 2012), or with random permeability distributions (e.g. Kühn et al. 2006). A more reliable determination of the likelihood for thermal free convection can be expected from numerical simulations whose permeability distribution is determined by the geology of the aquifer of interest. A potential method to investigate the potential flow dynamics of very deep aquifers is to constrain stratigraphic forward simulations of aquifer structure with measurements of porosity and grain size. With the structure of the permeability field playing an important role in the potential for, and onset or decay of free convection (e.g. Prasad and Simmons 2003; Simmons et al. 2010), the use of geologically informed permeability fields is important in the investigation for likely locations of thermal free convection.

Secondly, Anderson (2005) highlights that researchers are just beginning to realise the benefits of the use of temperature measurements in a range of hydrogeolog-

ical settings. One of the key uses of water natural temperature variations is to determine water flow rates or recharge (e.g. Suzuki 1960; Taniguchi 1993). These processes typically require temperature measurements on the tens of metres scale. The use of heat as a tracer in groundwater is not limited to natural temperature variations. For example, the use of heat as an applied groundwater tracer can be used to determine high permeability zones (Macfarlane et al. 2002; Pavelic et al. 2006). If temperature measurements are to become more widely used to determine groundwater flow, the key benefits and drawbacks of the use of temperature measurements to infer flow rates must be identified. While field investigations of the use of heat as a tracer, and numerical investigations into the influence of heterogeneity on heat transport have been performed, a general understanding on the influence of aquifer heterogeneity on flow rates interpreted from temperature observations is required.

Finally, the use of temperature time series to infer interaction between streams and groundwater has become a popular technique. This process requires measurements of temperature on a sub-metre scale. The use of heat as a tracer in a stream setting allows the estimation of fluxes without the need for measurements or estimates of hydraulic conductivity, which is a key drawback for the use of hydraulic methods (e.g. using vertical head gradients and measured or estimated hydraulic conductivities). The assumptions of analytical models based on the Stallman (1965) equation (e.g. Hatch et al. 2006; Keery et al. 2007), include that flow is both vertical and 1-dimensional, and that streambed properties are homogeneous. Recent work has investigated the influence of multidimensional flow fields (e.g. Lautz 2010; Roshan et al. 2012; Cuthbert and McKay 2013), as well as uncertainty in thermal diffusivity or the influence of sensor accuracy (Shanafield et al. 2011). While the effect of streambed heterogeneity on the use of the Bredehoeft and Papadopoulos (1965) equation has been assessed (e.g. Schornberg et al. 2010; Ferguson and Bense 2011), no investigations into the influence of streambed heterogeneity on the equations based on the Stallman (1965) model have been performed, and the influence of heterogeneity on the estimation of downwelling fluxes has not been assessed. There is a need to determine the influence of streambed heterogeneity on the reliability of thermal time series analytical models.

1.2 Research aims

This PhD broadly addresses the influence of heterogeneity of porous media on thermal transport by subsurface water flow. Three separate processes (each on a different spatial scale) are investigated, with a focus on both natural and applied temperature variations as means to determine water flow rates, and the potential for the use of elevated groundwater temperatures as an energy resource. The scales covered in this thesis range from the sub-metre and tens of metre scale, to the kilometre scale. All studies in this thesis are based on numerical simulations of heat and fluid flow. This body of work specifically investigates:

i. The control of aquifer heterogeneity on flow dynamics, including the potential for thermal free convection in the Yarragadee Aquifer, in the Perth metropolitan area, Western Australia (kilometre scale). Through the use of a stratigraphic forward model, this study uses geologically based permeability distributions to identify potential regions where thermal free convection is likely to occur.

ii. How the interpretation of applied temperature and solute tracers are influenced by various degrees of aquifer heterogeneity (tens of metre scale). Additionally, benefits and drawbacks of the use of heat as an applied tracer in heterogeneous aquifers are identified.

iii. The influence of streambed heterogeneity on 1D analytical solutions that use diurnal temperature signals to estimate groundwater– surface water exchange fluxes (sub-metre scale). This study identifies the error introduced by multi-dimensional flow for different degrees of heterogeneity and at different depths in the estimation of downwelling fluxes.

These specific knowledge gaps are the focus of three manuscripts presented in Chapters 2 through to 4. One of these manuscripts is now in press, and two are under review. Conference proceedings from work contained in this thesis are presented in Appendices A through to C.

1.3 Contribution of this PhD

This PhD explores the influence of heterogeneity of porous media on the transport of temperature in subsurface water flow. It does so through the use of controlled numerical studies to either produce synthetic data which is analysed, or to observe the influence of aquifer heterogeneity on the flow dynamics of an aquifer system. Key advantages of the use of numerical simulations include the fact that the answer (for example, groundwater flow rates) is known, the physics of a system can be easily observed without the limitation of many field data collection approaches, or that processes that can take thousands of years can be simulated in a matter of hours. This research investigates thermal transport in a range of heterogeneous environments and on a range of spatial scales, including: i.) The investigation of the influence of aquifer heterogeneity on the potential for thermal free convection in the Perth Basin, with thermal transport on the kilometre scale. This study demonstrates a step forward in the representation of realistic aquifer heterogeneity which would be of use in future investigations into free convection. Results identify regions in the Perth Basin where thermal convection is most likely. ii.) The investigation of the interpretation of heat as an applied groundwater tracer on the scale of tens of metres. This investigation shows that groundwater flow rates estimated from solute and temperature tracers may not agree, where a temperature tracer is more likely to provide a better estimate of mean flow rates, and a solute tracer will show more variability in flow rates, providing more information on aquifer heterogeneity. And iii.), the investigation of the influence of streambed heterogeneity on the interpretation of fluxes from temperature time series data (on the sub-metre scale). This investigation demonstrated that the violation of the assumption of 1D homogeneous flow does not rule out the use of temperature time series data to estimate groundwater– surface water exchange fluxes. The study also demonstrates that failure of the Hatch et al. (2006) amplitude ratio method can be attributed to streambed heterogeneity, and that where the amplitude ratio method cannot be used, that flux estimates from the phase shift method are unreliable.

These findings will contribute to the interpretation of heat as a tracer in the case of both applied and natural temperature variations, and demonstrates the use of a new approach to representing aquifer heterogeneity in the study of thermal free

convection. In the case of the Perth Basin, regions most likely to host thermal free convection have been identified.

Chapter 2

Investigating the influence of aquifer heterogeneity on the potential for thermal free convection in the Yarragadee Aquifer, Western Australia

Accepted for publication in *Hydrogeology Journal*: Irvine, D.J., H.A. Sheldon, C.T. Simmons, A.D. Werner, and C.M. Griffiths. Investigating the influence of aquifer heterogeneity on the potential for thermal free convection in the Yarragadee Aquifer, Western Australia

2.1 Abstract

The potential for thermal convection in aquifers is strongly influenced by permeability. Permeability is highly heterogeneous within aquifers, and spatial distributions of permeability are rarely well-constrained by measurements, making it difficult to determine the potential for thermal convection in a given aquifer. In this study, this difficulty is overcome through the use of a stratigraphic forward model (SFM). The SFM simulates the processes of deposition, burial and compaction of the aquifer, yielding a geologically plausible permeability field that is conditioned through measured permeability-porosity relationships. The aim of this study is to determine the influence of aquifer heterogeneity on the potential for thermal convection in the Yarragadee Aquifer, Western Australia. Permeability distributions from the SFM of the Yarragadee Aquifer are analysed through calculation of the thermal Rayleigh number (a stability criterion) from vertically averaged permeability, and numerical hydrothermal simulations with permeability distributions taken from the SFM. Results from the numerical simulations demonstrate that thermal convection can occur with the inclusion of geologically informed heterogeneity. These findings are supported by Rayleigh number calculations that indicate that convection is most likely to occur on the eastern side

of the aquifer where it is thick and has high average permeability.

2.2 Introduction

The Yarragadee Aquifer is part of the Perth Basin, an elongate rift basin trending north-south along the south-western margin of Australia (Fig. 2.1) (Playford et al. 1976). The Yarragadee Aquifer is highly permeable and has thicknesses that exceed 2500 m in places (Davidson 1995). It has been suggested that the Yarragadee Aquifer has the potential for hosting thermal free convection (where free convection relates to heat transport due to differences in water density, rather than the heat transported by flowing groundwater, which is known as forced convection). The process of thermal free convection can create areas of anomalously high temperature at shallow depths, which could provide a source of geothermal energy (Sheldon et al. 2012; Schilling et al. 2013). Anomalously hot groundwater at shallow depths can reduce the cost of geothermal energy extraction, as greater drilling depths result in higher costs. Understanding whether convection is possible, where convection cells may occur, and the likely magnitude of temperature enhancement in those convection cells, is useful for identifying regions to explore for geothermal energy.

A number of factors control the likelihood of thermal convection in aquifers, including aquifer thickness, geothermal gradient, and permeability. Permeability can span several orders of magnitude within an aquifer, and varies spatially on length scales ranging from centimetres to hundreds of metres, hence it is the most important parameter in controlling the occurrence of convection (Prasad and Simmons 2003; Simmons et al. 2010). The potential for thermal free convection in geometrically simple and homogeneous systems can be determined by calculating the thermal Rayleigh number, Ra_T (e.g. Domenico and Schwartz 1998):

$$Ra_T = \frac{k\alpha\rho_0^2 c_w g H \Delta T}{\mu \kappa_b}, \tag{2.1}$$

where all parameters and units are defined in Table 2.1. Note that Ra_T is proportional to permeability (k). Convection is predicted to occur if Ra_T exceeds a critical value, Ra^* (see Eqn. 2.8). However, application of Ra_T analyses to aquifers is problematic, because the permeability is strongly heterogeneous. Ra_T

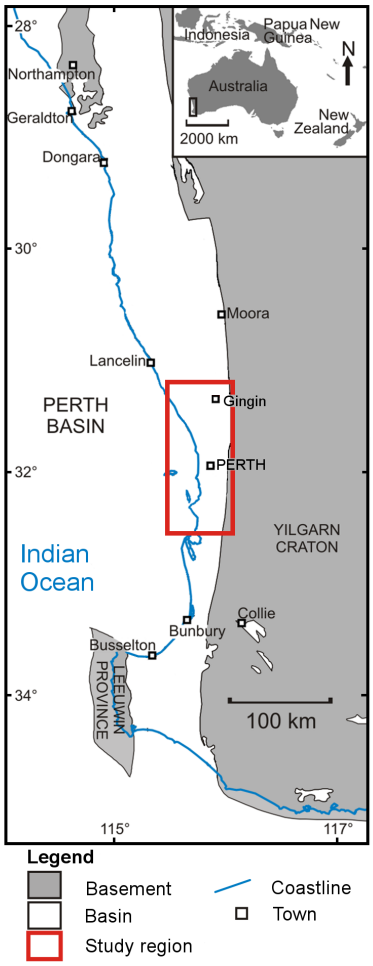

Figure 2.1: Location of the study area in the Perth Basin. Red box indicates the extent of the Perth Metropolitan Area (PMA) considered in this study. Inset shows location of the Perth Basin map within Australia. Adapted from Sheldon et al. (2012)

may be calculated from average permeability if the permeability distribution is known, but this may not be a reliable indicator of convection because the existence of low-k layers might inhibit convection, even if the average permeability suggests that it should be possible (Simmons et al. 2001). Furthermore, the spatial distribution of k in aquifers is rarely well-constrained by measurements. An alternative approach for determining the potential for convection is to use numerical hydrothermal simulations incorporating realistic k distributions. Yet even this approach is hampered by lack of information about the spatial distribution of k.

Table 2.1: Nomenclature for Rayleigh number analysis and numerical modelling

Symbol	Definition (units)
Ra_T	Thermal Rayleigh number (-)
Ra^*	Critical Rayleigh number (-)
k, k_v, k_h, k_v^*	Permeability, vertical, horizontal and critical vertical permeability (m^2)
α	Thermal expansion coefficient (1/°C)
ρ_0	Reference fluid density (kg/m^3)
c_w	Specific heat capacity of water (J/kg/°C)
g	Gravity (m/s^2)
H	Aquifer thickness (m)
T_{base}, T_{top}	Temperature at the base and top of the layer (°C)
$\Delta T = T_{base} - T_{top}$	Temperature difference across layer (°C)
θ	Porosity (-)
$\kappa_b = (1-\theta)\kappa_s + \theta\kappa_w$	Thermal conductivity of the bulk (W/m/°C)
κ_s, κ_w	Thermal conductivity of solid and water (W/m/°C)
W	Expected width of convection cell (m)

The plausibility of thermal free convection in the Yarragadee Aquifer in the Perth Metropolitan Area (PMA) has been the focus of recent studies, which have used Ra_T analyses and numerical simulations based on estimates of average k in the Yarragadee Aquifer. Sheldon et al. (2012) investigated whether thermal convection could explain elevated temperatures observed in some parts of the PMA. In their study, they calculated Ra_T for a range of aquifer thicknesses, average k, and geothermal and salinity gradients representative of the PMA. Numerical simulations using simple aquifer geometry showed that thermal convection is possible with homogeneous and anisotropic hydraulic and thermal parameter values that may be representative of the Yarragadee Aquifer, and could explain the high temperatures observed at shallow depths in parts of the PMA. Schilling et al. (2013) used a 3D hydrogeological model of the PMA (Corbel et al. 2012a) to investigate the impact of realistic 3D aquifer geometry on convection in the Yarragadee Aquifer. Their study demonstrated that the occurrence and geometry of convection cells is influenced by the 3D shape of the aquifer and by the k of faults that cut through it. They also found that groundwater flow driven by meteoric recharge can cause convection cells (should they occur) to migrate over geological time, although they are essentially stationary on human time scales.

These quasi-stationary thermal highs could be viable targets for geothermal energy extraction. However, while the abovementioned studies suggest that thermal convection may be a significant process in the Yarragadee Aquifer, only homogeneous aquifer k conditions have been assessed.

The Yarragadee Aquifer is known to be highly heterogeneous, with measurements of k spanning more than five orders of magnitude (CSIRO 2007; Timms et al. 2012). The high degree of heterogeneity in k is due to the deposition of the Yarragadee Aquifer in a braided stream setting, with coarse-grained channel fill deposits, as well as fine-grained floodplain deposits and marine incursions (Playford et al. 1976). Given the importance of k in evaluating the potential for thermal convection, and the high degree of heterogeneity in the Yarragadee Aquifer, an analysis of the influence of aquifer heterogeneity on the potential for thermal convection in the Yarragadee Aquifer is required.

Early research into the influence of heterogeneity on convection by McKibbin and OSullivan (1980) and McKibbin and Tyvand (1983) represented aquifer heterogeneity as alternating horizontal layers of high-k and low-k. These studies identified that thermal convection can occur on a local scale (within a single layer) or on a larger scale (across several layers). Whether convection occurs on a local or larger scale depends on both the k and relative thicknesses of low and high-k layers. More recently, numerical investigations into the influence of k on free convection processes have been performed using multi-Gaussian k distributions (e.g. Prasad and Simmons 2003; Sharp and Shi 2009; Simmons et al. 2010). These studies demonstrated that heterogeneities can stimulate instabilities (i.e. convection) at early times, but can also promote stability at late times. Simmons (2005) highlights the need for research on variable-density flow processes in realistic heterogeneity structures.

Investigations into the influence of aquifer heterogeneity on the potential for free convection (solute or thermal) in specific geologic units have typically represented k as simple layers, or as stochastic distributions, because of the difficulty in obtaining sufficient data to represent the true spatial distribution of k. For example Kühn et al. (2006) investigated the influence of heterogeneity on the potential for thermal convection in the Urquhart shale near Mount Isa in Queensland, north

eastern Australia. Their study tested both homogeneous k values for the different geological units, and cases where the k distributions of the Urquhart shale and surrounding faults were normally distributed. Kühn et al. (2006) found that the flow behaviour was similar in simulations where aquifer units were homogeneous or heterogeneous, and that the dip of the main permeable unit controlled the distribution of convection cells. Sharp and Shi (2009) used geostatistical distributions of k (differentiated by their mean, standard deviation and correlation structure) to investigate the likelihood of convection in low-k media, highlighting that classical Ra_T analyses are over-sensitive in heterogeneous, low-k strata. Their study demonstrated that overlying or underlying high-k layers can promote free convection and convective flux across low-k layers. They found that the likelihood of convection occurring increased with mean k, standard deviation of k, vertical correlation lengths, and with connectedness of high k zones.

The aim of this study is to determine the influence of aquifer heterogeneity on the likelihood of thermal convection in the Yarragadee Aquifer. Unlike previous investigations, this study uses the output from a geological stratigraphic forward model (SFM) that has been conditioned by the measured k and porosity (θ) data from the study area. The SFM provides a 3D k distribution that is representative of the k distribution in the Yarragadee Aquifer. First, the calculation of Ra_T, which required the calculation of equivalent average homogeneous k and θ from their heterogeneous distributions in the SFM, allows for a first-order investigation of the likelihood of convection in various locations in the SFM. The calculation of Ra_T allows for the determination of critical k values, where convection in equivalent homogeneous, anisotropic media is expected to occur. These critical k values are compared against the k-depth profiles at various locations in the SFM. Finally, the findings from the Ra_T and critical k calculations are compared with hydrothermal simulations that incorporate the heterogeneous k distributions of the SFM. This numerical simulation approach allows for an assessment of the validity of the use of Ra_T analyses and critical k values to determine the likelihood of free convection in heterogeneous geological units such as the Yarragadee Aquifer.

2.3 Yarragadee Aquifer

2.3.1 Hydrogeological setting

Numerous reviews of the hydrogeology of the Perth Basin (which includes the Yarragadee Aquifer) exist, including reports by Playford et al. (1976), Davidson (1995), Mory and Iasky (1996), and Crostella and Backhouse (2000). The hydrogeology of the Yarragadee Aquifer is briefly discussed here. For a more detailed description, see the references above.

The Perth Basin (Figure 2.1) extends for approximately 700 km along the coastline of Western Australia (Crostella and Backhouse 2000). The Basin is bounded to the east by the Darling Fault, which separates it from the Yilgarn Craton, and extends to the continental shelf to the west. A schematic hydrogeological cross section of the shallow Perth Basin within the PMA is shown in Figure 2.2. There are three major aquifer units in this area: the Superficial, the Leederville and the Yarragadee Aquifer. The focus of this investigation is the Yarragadee Aquifer (see Figure 2.2), because it is thick, typically between 1000 and 3000 m (Davidson 1995), which makes it the most likely aquifer to host convection in the PMA (Sheldon et al. 2012). The Yarragadee Aquifer comprises interbedded sandstones, siltstones and shales from the Jurassic and Cretaceous period (Playford et al. 1976). For the purpose of the present investigation, the confining beds above and below the Yarragadee Aquifer are considered as continuous low-k layers (1.8×10^{-17} m^2), although in reality it is connected with the overlying Leederville and Superficial Aquifers in some places.

Measurements of k and θ have been recorded for cores from four deep (approximately 4 km) petroleum exploration wells that penetrate the Yarragadee Aquifer (Timms et al. 2012). These measurements provide an understanding of the range of k and θ in the Yarragadee Aquifer, and their relationship as a function of grain size. However, these data do not provide information on the spatial distribution of k and θ values. Information about the vertical distribution of k can be obtained by using the k-θ measurements to estimate θ and k from wireline logs (e.g. sonic logs) of exploration wells (Timms et al. 2012). Wireline logs provide excellent vertical resolution, but with the sparse distribution of observation wells,

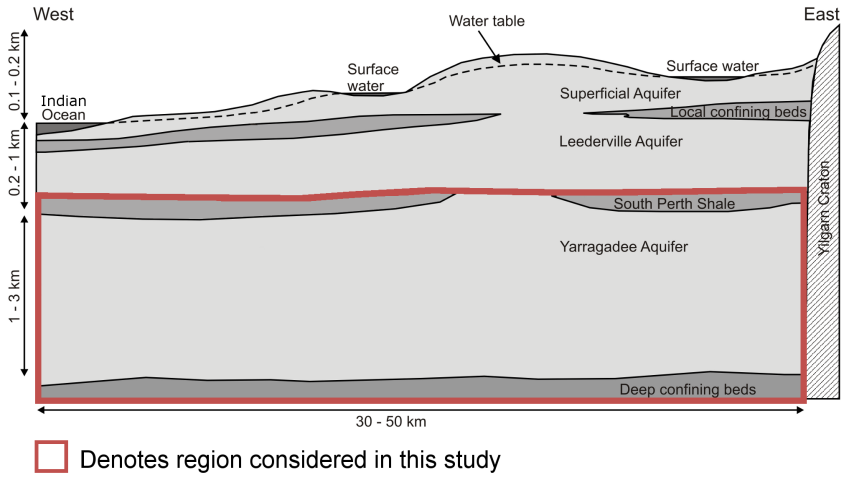

Figure 2.2: Schematic hydrogeological cross-section through the PMA. Note vertical exaggeration. Region within the red box is considered in this study. The South Perth Shale is treated as a continuous layer for this study, although in reality there are gaps allowing recharge from the overlying aquifers. Adapted from Sheldon et al. (2012)

this too provides little detail on the horizontal distribution of k and θ values. One solution to the data short-comings is to use interpretations of the wireline logs to inform geostatistical representations of the aquifer permeability, however there is no guarantee that these k-fields will be representative of the aquifer given the limited number of measurements. An alternative approach is to use available field data and geological understanding to condition stratigraphic forward models. The use of a stratigraphic forward modelling approach is more likely to produce geological distributions that have a physically realistic basis than geostatistically modelled k-fields because stratigraphic forward models simulate the processes that led to the deposition of the aquifer material.

2.3.2 Stratigraphic forward model

The stratigraphic forward modeling code Sedsim (Tetzlaff and Harbaugh 1989; Griffiths et al. 2001) simulates the physical processes that deposited, eroded, transported and modified geological formations using a modified form of the Navier-Stokes equations (Timms et al. 2012). A brief description of the modelling process is given below. For a detailed discussion of the Sedsim modelling

procedure in the Perth Basin, see Corbel et al. (2012b) and Timms et al. (2012).

Sedsim simulates the deposition of sediment of varying grain size on a subsiding basement with various sediment sources. The SFM used in this study simulated the deposition of the Yarragadee Aquifer over a period of 15.8 million years, with the deposited sediment comprising four different grain sizes. Deposition was modelled in time steps of 60,000 years although not all layers are preserved at every location. The output of the SFM is a value of compacted porosity θ, and thicknesses of four different siliciclastic grain sizes, and hence the total thickness of the preserved sediment for each time step at each grid node.

The inputs for the SFM include the initial topography/bathymetry of the basement, a time series of sea levels from start to finish of the simulation, and the distribution of the four selected input siliciclastic grain sizes (Timms et al. 2012). The diameters (d) of the four grain sizes were selected from samples taken from four deep petroleum wells, which provided values of $d_1 = 0.45$ mm for coarse material (e.g. coarse sand), $d_2 = 0.15$ mm for medium material (e.g. medium to fine sand), $d_3 = 0.03$ mm for silt, and $d_4 = 0.0003$ mm for clay.

The SFM simulation of the Yarragadee Aquifer in the PMA is a subset of a larger model of the Perth Basin. The modelled area represented by the SFM is shown in Figure 2.1. The extent of the simulation of the Yarragadee Aquifer within the PMA is 152.1 km north-south, and 63.1 km east-west. The discretisation of the model is $\Delta x = \Delta y = 3710$ m, and the thickness (Δz) of the elements depends on the degree of deposition/erosion in each element. If the amount of erosion exceeds the deposition within a time step, an element can have zero thickness. The non-zero elemental thickness typically ranges between 0.1 to 85 m, with a mean value of 7.6 m. The process of simulating the formation of the Yarragadee Aquifer was an iterative process, with the output of the model (θ and average grain size of each element in the model) calibrated against the facies observed from four deep petroleum wells that were used to determine the grain sizes in the simulation (Timms et al. 2012).

In order to use the output of the SFM to investigate the potential for thermal convection in the Yarragadee Aquifer, the calculation of k from the θ and grain

size distributions is required. The process of these calculations is outlined in Section 2.3.3.

2.3.3 Calculating permeability from the stratigraphic forward model

Relationships between laboratory measurements of permeability, porosity and grain size from four deep wells, as outlined in Timms et al. (2012), are used to calculate a value of k in each element of the SFM. The k-θ pairs presented in Figure 2.3 are divided into materials that are classified as coarse (d >0.2 mm, top figure), intermediate (0.2 >d >0.05 mm, centre figure), and fine (d <0.05 mm, bottom figure). For each plot shown in Figure 2.3, the measured k-θ data are presented as white circles. The solid line denotes the best fit obtained using a power law, and the dashed lines are the upper and lower estimates of the k-θ relationship. Details of the fitting process are given below. All fitting parameters and descriptions of materials in each grain size range are presented in Table 2.2.

Table 2.2: Fitting parameters a and b, and standard error SE of ln$k$ of laboratory measurements of porosity and permeability for Equation 2.2 – 2.4

Mean grain size of SEDSIM model (mm)	Material Description	a	b	$SE(\ln(k))$
> 0.2	Coarse (e.g. river channel fill)	1.8×10^8	7.8	1.9
0.2–0.05	Intermediate (e.g. cross laminated sandstone with clay flaser)	1.9×10^6	6.5	0.9
< 0.05	Fine (e.g. swamp/ lagoonal deposits, overbank deposits)	1.1×10^3	2.7	1.7

The power law fit employed to determine the best fit k (k_{best}) is:

$$k_{best} = a\theta^b, \tag{2.2}$$

where a and b are fitting parameters. For any given θ, there is significant variability in measured values of k. In order to capture this variability, relationships were determined to capture an upper estimate of k (k_{upper}) and lower estimate of k (k_{lower}) for any given value of θ. These upper and lower estimates are calculated using $\pm$ 1 standard error (SE) of ln(k) using the equations:

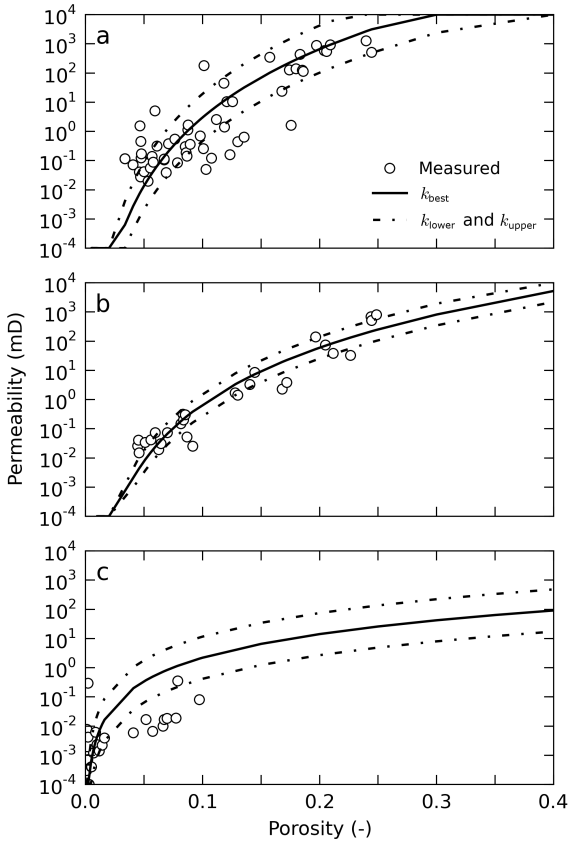

Figure 2.3: Measured permeability and porosity for: (a) coarse grained materials (grain size >0.2 mm); (b) intermediate material (grain size 0.2 to 0.05 mm);(c) fine grained materials (<0.05 mm). White circles represent measurements, solid lines denote best fit (k_{best}) from Equation 2.2, dashed lines represent k_{upper} and k_{lower} from Equations 2.3 and 2.4

$$k_{lower} = e^{k_{best} - SE(lnk))}, \tag{2.3}$$

$$k_{upper} = e^{k_{best} + SE(lnk))}. \tag{2.4}$$

The relationships developed in Equations 2.2, 2.3 and 2.4 are used to calculate the three estimated k distributions (k_{lower}, k_{best}, k_{upper}) using a five-step process:

1. Calculate the mean grain size (d_{avg}) of each SFM element,
2. Select the k-θ relationship to convert SFM output to k based on d_{avg},
3. Calculate an adjusted porosity (θ_{adj}) to account for elements with high clay fractions (as clay has high θ, but low-k, see explanation below),
4. Determine k from the d_{avg} and θ_{adj},
5. Apply maximum and minimum cut off values for k.

The mean grain size (d_{avg}, step 1) of each element in the SFM was calculated from the fraction of each grain size material (G_1, ..., G_4) and the grain size of each fraction (d_1, ..., d_4) using the equation:

$$d_{avg} = \sum_{i=1}^{4} G_i d_i. \tag{2.5}$$

It is noted that the k-θ relationship is rather poorly defined for the fine-grained material (bottom plot in Figure 2.3), especially for $\theta > 0.05$ where many of the measurements fall below the k_{lower} curve. However, with the application of Equation 2.5 to each element in the SFM, the distribution of d_{avg} (by volume) is only 6 % fine grain material. The intermediate grain size material (which displays the least variability) makes up 65 %, and the coarse material makes up 29 % of the Yarragadee Aquifer. In total, approximately 4 % of the volume of the aquifer was fine grained material with $\theta > 0.1$. However, these elements with over-exaggerated k values were limited to the western side of the domain, and were not included in any of the following analyses.

The value of d_{avg} is used to determine which relationships of the k-θ data are used to calculate k (step 2). Some elements with a high clay fraction (large value of G_4) had rather high θ which would result in unrealistically high k, therefore the θ of each element was adjusted to eliminate the θ associated with the clay fraction (step 3):

$$\theta_{adj} = \theta(1 - G_4) \tag{2.6}$$

The resulting θ_{adj} is used in Equations 2.2, 2.3 and 2.4 to calculate k_{lower}, k_{best} and k_{upper} values for each element in the SFM (step 4). The use of θ_{adj} in the calculation of k produces a conservative (lower) k value as $\theta_{adj} < \theta$.

Finally, to ensure a realistic range of k values, cut off values were applied to limit the range of k between 1×10^{-10} and 1×10^{-19} m^2 (step 5).

2.4 Rayleigh number analysis of the Yarragadee Aquifer

Keeping in mind the limitations of Ra_T analyses in heterogeneous systems, the k distributions derived from the SFM can be analysed in two ways to determine the likelihood of thermal convection: 1) Calculating Ra_T/Ra^* from the average permeability at each xy location in the SFM; and 2) Comparing the k-depth (z) profile at a given xy location in the SFM with the critical permeability that is required for convection in an equivalent homogeneous medium. It is worth reiterating that the derivation of Ra_T and Ra^* assumes that the system has both homogeneous properties and a simple geometry and boundary conditions. The assumption of homogeneous properties is a particular issue for k, which can be highly variable. Numerous researchers have identified that the use of average k to determine whether or not convection will occur in heterogeneous porous media is insufficient and problematic (e.g. Simmons et al. 2001; Prasad and Simmons 2005; Sharp and Shi 2009; Simmons et al. 2010). The Ra_T analysis presented here should therefore be seen as only a preliminary investigation into the potential for thermal free convection in the Yarragadee Aquifer.

A representative average value of k is required for calculation of Ra_T, which is represented here by using the average vertical k (k_v) at each xy location in the SFM. This average k is calculated from the thickness and k of each layer within the aquifer at each xy location, according to the following equation (e.g. Domenico and Schwartz 1998):

$$k_v = \frac{\sum_{i=1}^{n} m_i}{\sum_{i=1}^{n} m_i / k_i}, \tag{2.7}$$

where m_i is the element thickness, k_i is the element permeability, and n is the number of elements in the SFM at the required xy location. The k_v value given by Equation 2.7 is a conservative (low) estimate of k, as the value of k_v according to Equation 2.7 is dominated by the lowest k values.

The value of Ra^* depends on the boundary conditions and the properties of the system. Assuming an equivalent homogeneous and anisotropic k and constant temperature boundary conditions at the top and bottom of the aquifer, following Epherre (1975), Ra^* is calculated as:

$$Ra^* = \pi^2 (1 + \sqrt{k_v / k_h})^2, \tag{2.8}$$

where k_h is the average horizontal k given by (e.g. Domenico and Schwartz 1998):

$$k_h = \frac{\sum_{i=1}^{n} m_i k_i}{\sum_{i=1}^{n} m_i}, \tag{2.9}$$

with m_i and k_i being the element thicknesses and permeabilities at the given xy location, as before. Ra^* therefore varies with xy location in the SFM, because the ratio k_v/k_h varies.

For the calculation of Ra_T, values for ρ_0 and c_w are assumed to be homogeneous, with values of 1000 kg/m^3 and 4200 J/kg/°C respectively. The value for was set to 0.00021 (1/°C). The value of ΔT is calculated from the thickness of the Yarragadee Aquifer from the SFM and assuming a thermal gradient of 0.025 °C/m, which is representative for the Yarragadee Aquifer in the PMA (Reid et al. 2012). Values of κ_b are calculated as $\kappa_b = (1-\theta)\kappa_s + \theta\kappa_w$, where the arithmetic average θ of a section of the SFM, $\kappa_w = 0.65$ and $\kappa_s = 4.0$ W/m/°C are used. With the range of θ from the SFM, κ_b of an element ranges from 2.96 to 3.61 W/m/°C (with

a mean value of 3.33 W/m/°C). This range is consistent with the κ_b value suggested by Hot Dry Rocks Pty Ltd (2008), who obtained a value of 3.54 W/m/°C from a harmonic mean of two samples. The value of μ is calculated using the equation of state for water (Wagner et al. 2000) using the temperature and pressure at the depth of the midpoint of the aquifer for each xy location in the model.

Values of k_v and k_h were calculated at each xy location in the model, which were then used to calculate Ra_T and Ra^*. In Figure 2.4, maps of Ra_T/Ra^* are presented for k_{lower}, k_{best} and k_{upper}. Areas where $Ra_T/Ra^* \geq 1$ is where free convection is most likely to occur.

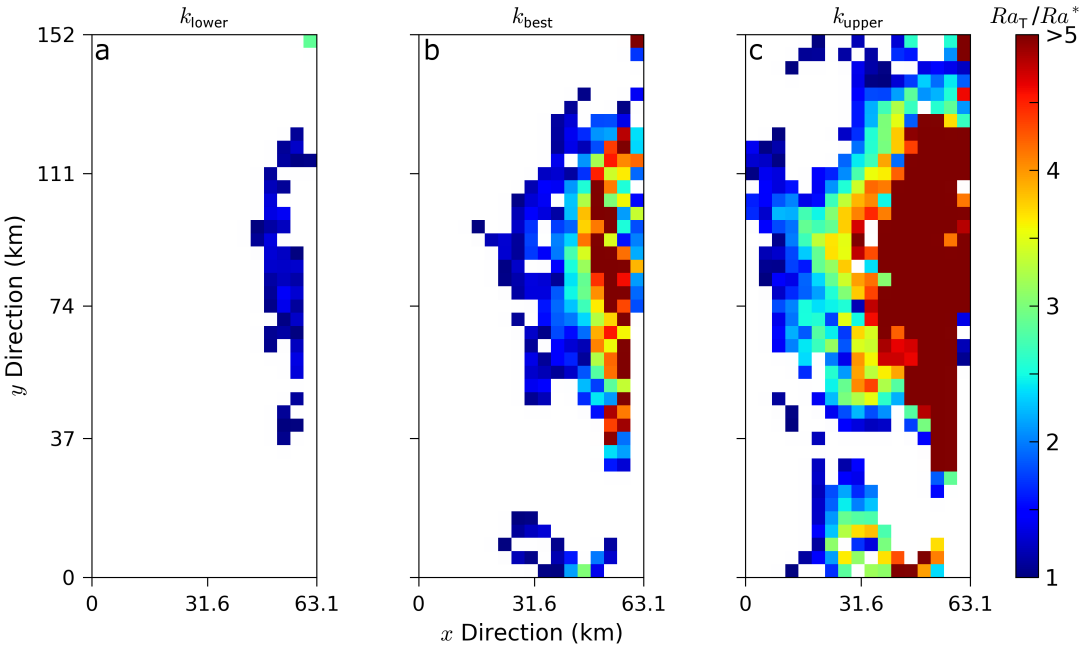

Figure 2.4: Maps of Ra_T/Ra^* in the Sedsim model domain calculated using a k_{lower}, b k_{best} and c k_{upper}. Thermal convection is expected to occur in equivalent homogeneous and anisotropic media where $Ra_T/Ra^* > 1$. Locations where $Ra_T/Ra^* < 1$ are shown in white

For all three interpretations of k in the SFM (i.e. k_{lower}, k_{best} and k_{upper}), the most likely regions for thermal convection are on the eastern side of the domain. These regions are relatively thick (often exceeding 2000 m), and have a higher percentage of coarse (highly permeable) sediment representing alluvial fan deposits that

accumulated along a fault scarp. In the k_{lower} map, the greatest value of Ra_T/Ra^* is approximately 1.5. For kupper, the eastern side of the SFM contains regions where $Ra_T/Ra^* \geq 5$. Interestingly, the northern part of the aquifer is also thick ($>$ 2500 m), however the Ra_T/Ra^* values are typically small (e.g. 0.10.7). This region contains a high proportion of low-k layers, which have a large influence on the value of k_v, which in turn reduces the value of Ra_T/Ra^*.

Another way of analysing the k distributions from the SFM is to compare k-z profiles at a given xy location with the critical k (k_v^*) that is required for convection, where k_v^* is calculated by:

$$k_{v^*} = \frac{\mu \kappa_b Ra^*}{\rho_0^2 c_w \alpha g H \Delta T} \tag{2.10}$$

A comparison of k_v^* with k shows that the percentage of the Yarragadee Aquifer in the PMA where $k > k_v^*$ is 36.9 % for k_{lower}, 62.4 % for k_{best} and 82.7 % for k_{upper}. A visual representation of this comparison is shown in Figure 2.5, where values of k_v^* are plotted along with the k_{best}-z profiles at five xy locations in the SFM.

The locations shown in Figure 2.5 were selected to cover a range of locations in the aquifer, thicknesses and Ra_T/Ra^*. The profile shown in Figure 2.5a has a large proportion of layers with sub-critical k values ($k < k_v^*$). The majority of the k values in Figures 2.5b, 2.5c and 2.5d exceed k_v^*, with a few layers where k is sub-critical. For the profile shown in Figure 2.5e, much of the upper part of the profile contains k values above k_v^*, and the lower part of the profile is made up of layers which are sub-critical. The plots in Figure 2.5 illustrate the problem with applying Ra_T analysis to a heterogeneous system: Even if the average k is sufficient for convection to occur, the occurrence of some low-k layers with sub-critical k could inhibit convection. Ra_T analysis alone cannot determine whether convection is possible in these heterogeneous k profiles. To assess the impact of heterogeneous k on the potential for thermal convection to occur in the Yarragadee Aquifer, the k_{lower}, k_{best} and k_{upper} distributions from five xy locations in the SFM are used in numerical hydrothermal simulations.

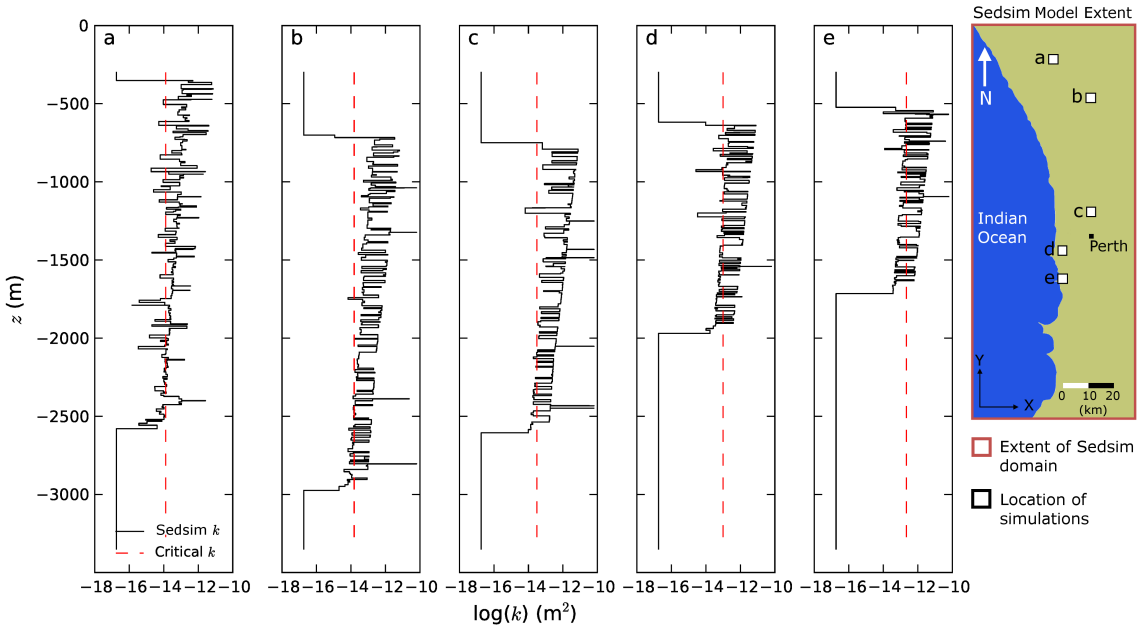

Figure 2.5: Log (k_{best}) versus depth, and map of locations of $k-z$ profiles. Black solid lines represent kbest from the SFM. Red dashed lines represent k_v^* calculated by Equation 2.10

2.5 Hydrothermal modelling

Hydrothermal simulations were performed using FEFLOW, a finite element modelling package that solves the equations of heat/mass transport and groundwater flow using a variable density and viscosity form of Darcys law. For all simulations, fluid density and viscosity were dependent on temperature, and the thermal expansion term (α) was also allowed to vary according to temperature, using the FEFLOW Beta-Gamma plugin (Magri 2009).

Simulations were performed in 2D domains, with each simulation scenario representing the k-z profile from a single xy location in the SFM (see Figure 2.5 for locations and k-z profiles used in the simulations). There was no variation in k across the width of the modeled domain. Discretisation of these 2D model domains resulted in meshes with 1.4 - 2.0 million elements. Extending the model domain into 3D, while maintaining the k-layering from the SFM, would have been computationally prohibitive. Simmons et al. (2010) highlight that 3D sim-

ulations are always more unstable than 2D; if convection can occur in 2D, it also is expected to occur in 3D. Furthermore, convection may be more likely to occur in 3D due to lateral discontinuities in low-k layers. Therefore the simulations presented here are expected to be conservative in their prediction of convection.

It was not possible to perform simulations using 2D cross-sections from the SFM (i.e. spanning more than one xy location in the SFM) because discontinuities in layering between adjacent blocks triggered convective upwellings, creating a misleading impression of the tendency for convection and the size of convection cells. This problem could be mitigated in future studies by improving the horizontal resolution of the SFM, or by smoothing the layering between adjacent blocks.

Discretising thinly layered structures (such as the layers from the SFM) is a challenge with an orthogonal quadrilateral mesh. It is generally recommended that element aspect ratios (e.g. $\Delta x : \Delta z$) should not exceed 4 (Anderson and Woessner 1992). Using this guideline with a quadrilateral mesh, the presence of a single thin layer would determine the lateral discretisation of the entire numerical model domain. For example, if a thin layer with 0.5 m thickness occurred, and the layer was to be discretised vertically with four elements, the lateral discretisation (Δx) required would be 0.5 m. With a model width of 10 km (which is typical of this study), 20,000 elements in the x direction would be required. An alternative, more flexible approach is to use a triangular mesh. In order to determine the suitability of a triangular mesh, a comparison of the results from triangular and quadrilateral meshes was undertaken for a test case. To discretise the domain for the test case with a reasonable number of quadrilateral elements, narrower model domains than those used in the remainder of the study were used. Also, layers less than 10 m thick were joined to adjacent layers, and represented with average properties for the joined layers (k_v, k_h, θ). Results from these hydrothermal simulations showed that macroscopic details (whether convection occurred or not and the number of convection cells) were in agreement for the quadrilateral and triangular meshes. Therefore, triangular meshes were used for the remainder of this study. The minimum possible internal angle of the triangular elements was set to 20°. Increasing the minimum internal angle to 30° (which produced approximately 2 to 3 times the number of elements) did not significantly affect results.

2.5.1 Modelling approach

All simulations use the k-z profiles from a single xy location in the SFM. Extra layers with low k were added to the top and bottom of the domain to limit the influence of thermal boundary conditions (Figure 2.6). The extra layers represent confining units above and below the Yarragadee Aquifer. The elevation of the top of the domain was -300 m, and the elevation of the bottom of the domain was -3350 m for all simulations. The thickness of the extra layers was dependent on the elevations of the top and bottom of the Yarragadee Aquifer in the SFM at each xy location. The properties of the extra layers were $K = 1{\times}10^{-10}$ m/s (where K is hydraulic conductivity at a reference temperature; see Appendix A, equivalent to $k = 1.8{\times}10^{-17}$ m^2) and $\theta = 0.05$ to ensure that conduction would be the predominant mode of heat transfer through these layers. For the conversion from k to K, see Appendix A.

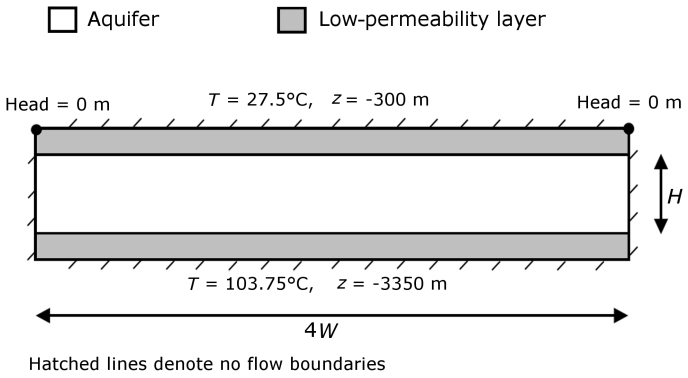

Figure 2.6: Conceptual model. Hatched lines indicate no-flow boundaries. H is the thickness of the aquifer, W is the expected width of a convection cell from Equation 2.11

While aquifer thickness (H) and k are key parameters in determining whether convection can occur, the width of the aquifer is also important, as the hydrogeologic properties and boundary conditions of the aquifer will determine the width of convection cells. Following Philips (1991), the expected width (W) of a convection cell in a homogeneous anisotropic medium can be calculated as:

$$W = H(k_h/k_v)^{0.25}, \tag{2.11}$$

where H is the thickness of the aquifer (excluding the extra low-K layers) and k_h and k_v are as previously stated. It is important to note, that the width of a convection cell is the distance from a thermal high to a thermal low. To ensure that there was room for convection cells to form, the width of the FEFLOW models was set at $4W$ based on the average horizontal and vertical permeabilities at the chosen location in the SFM. This width has been shown to be appropriate for the use of Ra^* to predict convection in homogeneous media by Weatherill et al. (2004). This approach led to the width of the model domains varying from location to location in the SFM domain, and for each interpretation of the k distribution at a given location.

Values of thermal parameters for the numerical simulations were $\kappa_s = 4.0$ W/m/°C, $\kappa_w = 0.65$ W/m/°C, $c_s = 850$ J/kg/°C, $c_w = 4200$ J/kg/°C and $\rho_s = 2650$ kg/m^3. Fluid density (ρ_w) was dependent on temperature, and all bulk properties were a function of θ from the SFM.

No-flow boundary conditions were applied at all boundary nodes except for the top-left and top-right nodes, where hydraulic head was set to 0 m (Figure 2.6). Constant temperature boundary conditions were applied to the top and bottom boundaries, with 27.5 °C at the top, and 103.75 °C at the bottom boundary. The initial thermal conditions of each modelling run was a linear increase in temperature with depth. With the exception of one simulation (shown in Figure 2.8b), all simulations were run for 5×10^7 days. For the simulation shown in Figure 2.8b, it was clear that convection was occurring, but the convection cells had not stabilised, and hence the model run time was extended to 1×10^8 days.

2.5.2 Modelling results and discussion

The results from numerical simulations are shown in Figure 2.7. For each k-z profile, temperature distributions from simulations using the k_{best}, k_{upper} and k_{lower} distributions are presented. Convection is indicated by undulating temperature contours, while horizontal temperature contours indicate a non-convecting, conductive case.

The results in Figure 2.7 show convection occurring for all scenarios with Ra_T/Ra^*

> 1, but also for some scenarios with $Ra_T/Ra^* < 1$. Furthermore, the number of convection cells (where convection occurred) exceeds the expected number of convection cells in all cases, with the exception of the k_{lower} case shown in Figure 2.7e, which has exactly four cells. These differences between the simulated behavior and that predicted by linear stability theory are not unexpected, because there are differences in the implicit and explicit assumptions in linear theory when compared to the simulated scenarios. Amongst other things, linear stability theory assumes homogeneous properties and ideal boundary conditions, whereas the simulations have heterogeneous properties and boundary conditions applied at some distance from the convecting layer. Furthermore, the theoretical prediction of convection cell width applies only when Ra_T is close to Ra^*; the number of cells is expected to increase and convection to become more chaotic as Ra_T increases above Ra^* (e.g. Phillips 1991), and this is confirmed by the simulations (e.g. increasing number of convection cells with increasing Ra_T/Ra^* in Figures 2.7b, c, d and e). To check that FEFLOW predicts the correct behavior in an ideal case, simulations were run using one of the finely-layered non-uniform meshes but with homogeneous properties (and with anisotropic k) extending across the full thickness of the model, and with fixed temperature boundary conditions at the top and base of the model. These ideal simulations predicted no convection with $Ra_T/Ra^* = 0.9$, and convection with exactly four cells for $Ra_T/Ra^* = 1.1$. This demonstration of the correct behavior in an ideal homogeneous and anisotropic case provides confidence in the ability of the numerical simulator and hence in the results for heterogeneous, non-ideal scenarios, and in particular confirms that the finely layered and non-uniform mesh does not unduly influence the results. These findings are consistent with previous studies of density-dependent flow using FEFLOW (e.g. Diersch and Kolditz 2002).

There are three non-convecting (conductive) scenarios in Figure 2.7, all with $Ra_T/Ra^* < 1$ (Figures 2.7a and 2.7d). Convection is triggered in these scenarios by increasing k (i.e. from k_{lower} to k_{best} or from k_{best} to k_{upper}). In the case shown in Figure 2.7a, convection does not occur for the k_{lower} or k_{best} distributions because of the dominance of low-k layers. This is illustrated by the $k_{best} - z$ profile shown in Figure **??**a, where much of the profile below -1700 m is sub-critical, and there is a high frequency of low-k layers in the upper part of the profile. For the cases of k_{lower} and k_{best}, the presence of sub-critical k layers inhibits convection

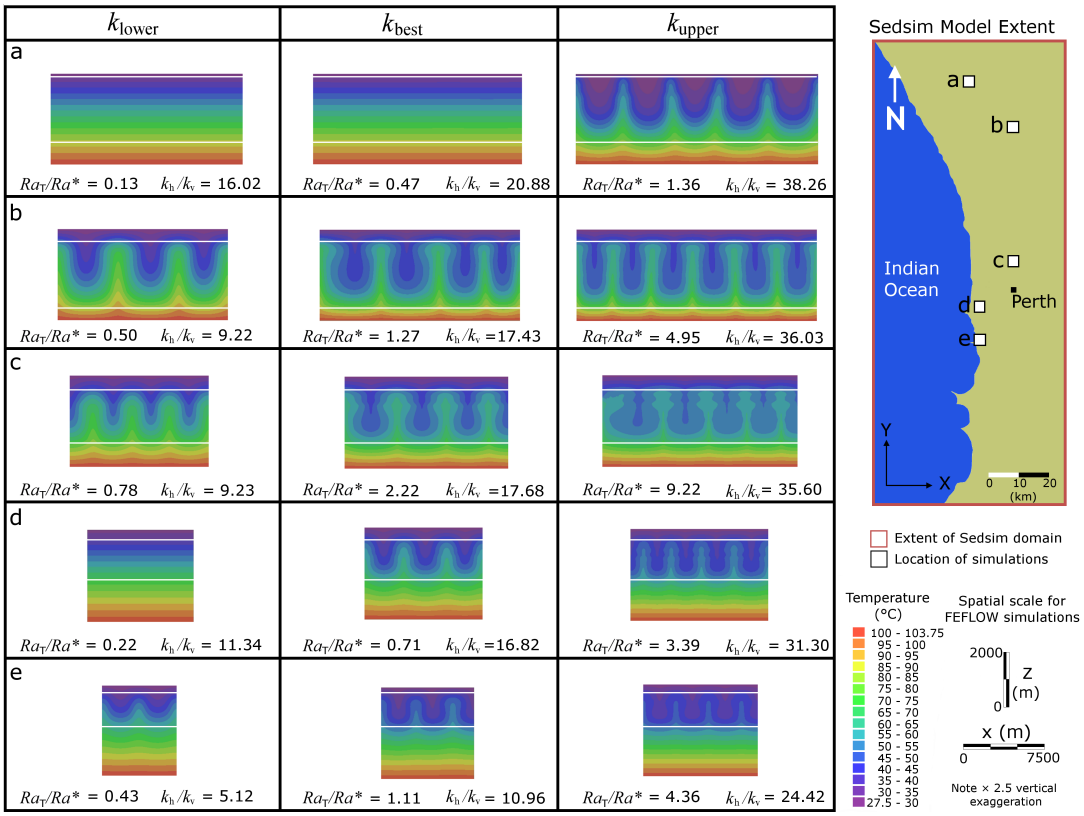

Figure 2.7: Temperature distributions from FEFLOW simulations, with aquifer permeabilities k_{lower} (left column), k_{best} (centre column) and k_{upper} (right column). White lines on the temperature distributions denote the extent of the SFM. a-e show the simulations within the Sedsim model (see locations a to e on the map). Note 2.5 × vertical exaggeration of the FEFLOW simulations. The widths of the models vary due to differences in the expected convection cell width as calculated by Equation 2.11, where all model widths are $4W$. The degree of anisotropy (K_h/K_v) is presented for each simulation

(Figure 2.7a). The influence of low-k layers can also be seen in other temperature profiles. For example in all interpretations of k shown in Figure 2.7c, a low-k zone (see Figure 2.5c) can be observed at approximately -1200 m. In this case, the presence of this low k layer causes the edges of the convection cells to pinch together, but does not prevent the convection cell from extending through the low k layer towards the surface. The k of this layer is not sufficiently small to prevent convection.

From the results shown in Figure 2.7, it is clear that low-k layers in the k-z pro-

file could influence the process of thermal convection in the Yarragadee Aquifer. To investigate the influence of the low-k layers further, alterations were made to some of the k-z profiles. In Figure 2.8, two simulations with modified k-z profiles are presented. The first of these k-z profiles is shown in Figure 2.8a, while the numerical simulation using this profile is shown in Figure 2.8b. This k-z profile is based on the $k_{best} - z$ profile from Figure 2.7a. With the original $k_{best} - z$ profile, convection did not occur. In Figure 2.8a, the k_{best} values are used for the coarse and intermediate materials, but the k_{upper} values are used for the fine material. The k-z profile shown in Figure 2.8c (and the resulting temperature distribution shown in Figure 2.8d), are alterations to the k_{upper} profile that was used to produce the k_{upper} results in Figure 2.7a. In the kupper case shown in Figure 2.7a, convection was shown to occur. The altered $k - z$ profile shown in Figure 2.8c has the k_{upper} values used for the coarse and intermediate material, but the k_{lower} values used for the fine material. The results seen in Figure 2.8 show that whether or not convection occurs in the simulations can be controlled by the k values of the fine material. The temperature distribution in Figure 2.8b shows convection occurring in a case where convection did not occur with the original $k_{best} - z$ profile. Similarly, the results from Figure 2.8d show no convection in a profile that originally had convection. These results highlight the impact of low-k layers on the potential for convection in heterogeneous aquifers.

For the purpose of the extraction of heated water for geothermal energy, it is of interest to know whether or not convection occurs, where convection cells are likely to occur, and the temperature of the water in the convective upwellings. Convection can create anomalously high temperatures at shallow depths, which could reduce the cost of geothermal energy and/or expand the range of geothermal applications that may be viable. Table 2.3 shows the maximum temperature and the temperature enhancement (above a conductive heat transfer case) at or above -1000 m depth for each simulation. The depth of -1000 m (below land surface, not model surface which was always at -300 m) was selected somewhat arbitrarily, representing a depth that could be practically drilled without excessive drilling costs. For reference, the temperature expected at -1000 m for a conduction only scenario is 45 °C. The actual depth of the maximum temperature point varies between scenarios. The temperature enhancements range from 0.7 to 23.4 °C, with the amount of enhancement depending largely on convection cell size, which

in turn is a function of aquifer thickness and k. Temperature enhancements at the upper end of this range would make a significant difference to the viability of geothermal energy extraction.

Table 2.3: Maximum temperature and temperature enhancement (relative to a conductive heat transfer case) at depths shallower than z = -1000 m.

Case (as in Figure 2.7)	k interpretation	Maximum T above -1000 m (°C)	Maximum T enhancement above -1000 m (°C)
a	k_{lower}	Not convecting	-
	k_{best}	Not convecting	-
	k_{upper}	54.8	10.2
b	k_{lower}	68.2	23.4
	k_{best}	66.9	22.1
	k_{upper}	58.9	14.1
c	k_{lower}	57.2	12.4
	k_{best}	60.4	15.6
	k_{upper}	58.5	13.7
d	k_{lower}	Not convecting	-
	k_{best}	56.0	11.1
	k_{upper}	51.7	6.8
e	k_{lower}	49.0	4.0
	k_{best}	51.5	6.5
	k_{upper}	45.7	0.7

The simulations presented here do not represent the true 3D structure of the Yarragadee Aquifer or its connectivity to other overlying aquifers in the Perth Basin. These aspects have been investigated by Schilling et al. (2013), who showed that the location of convection cells was influenced by the 3D geometry of the aquifer, and that movement of groundwater through the aquifer (driven by recharge from the overlying aquifers) could cause convection cells to migrate in the direction of through-flow. However, their simulations used homogeneous permeability. This study focused on the impact of heterogeneity on convection, using geologically informed permeability distributions representing locations within the Yarragadee Aquifer. The conclusions of this study would not be changed by the inclusion of realistic aquifer geometry or through-flow.

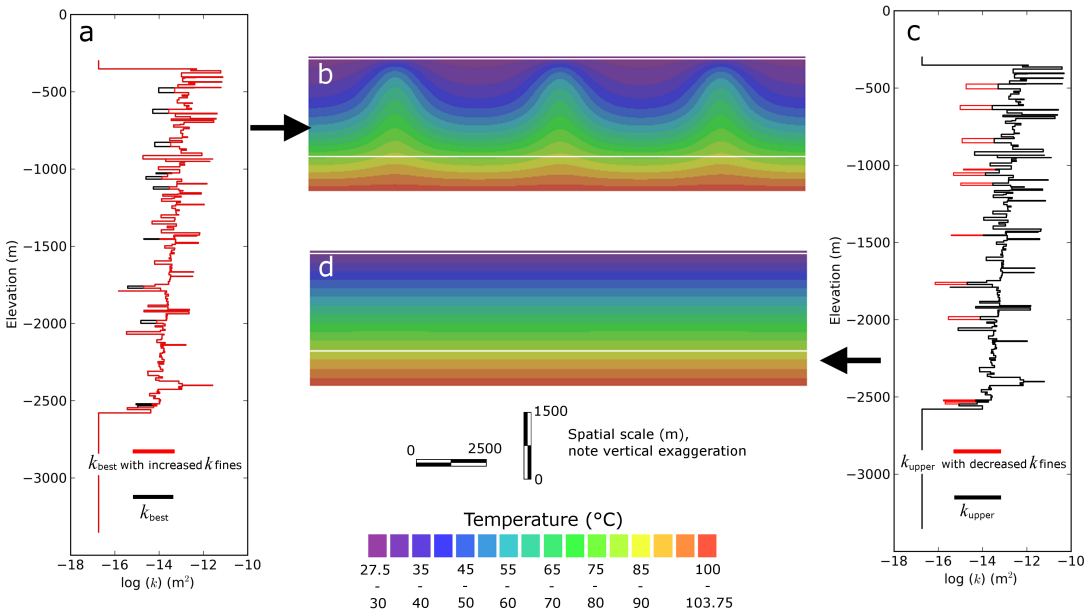

Figure 2.8: Altered k with depth profiles (a and c), and output of FEFLOW simulations using these profiles (b and d). In a, the k_{best} from the case shown in Figure 2.7a is shown in black. The red line is k_{best} for the coarse and intermediate materials, but with k_{upper} for the fine material. The resulting temperature distribution (b) shows convection where it did not occur in the k_{best} scenario in Figure 2.7a. The profile shown in black in c is the k_{upper} as shown in Figure 2.7a. The red line shows k_{upper} for the coarse and intermediate materials (as per scenario shown in Figure 2.7a), but with k_{lower} for the fine material. The temperature distribution plot (d) shows convection does not occur, while convection did occur in the k_{upper} case as shown in Figure 2.7a

2.6 Conclusions

This study incorporated geologically informed permeability profiles from a stratigraphic forward model into an analysis of the influence of aquifer heterogeneity on the likelihood of thermal convection in the Yarragadee Aquifer. Permeabilities and layer thicknesses from the SFM were used to calculate Rayleigh numbers and critical permeabilities, and were used as the basis for 2D hydrothermal simulations. This study shows that free convection is plausible in the Yarragadee, even when representative geologic heterogeneity is incorporated into the analysis. The use of a stratigraphic forward modelling approach provides realistic permeability distributions that are informed by geological understanding and permeability

measurements. The ability to represent heterogeneity in a geologically realistic way is a key benefit of the stratigraphic forward modelling approach over the use of geostatistical methods to represent aquifer heterogeneity.

New evidence for the possibility of thermal free convection in the Yarragadee Aquifer presented in this study includes:

1. Rayleigh number maps, which provide a first-order analysis of where in the Yarragadee Aquifer thermal convection could occur. These maps demonstrate the likelihood of convection on much of the eastern side of the Yarragadee Aquifer in the PMA, where the aquifer is thick and highly permeable. Rayleigh numbers that exceed the critical Rayleigh number occurred in this area for all interpretations of the permeability field (i.e. k_{best}, k_{lower} and k_{upper}). This suggests that, even with a conservative interpretation of permeability (k_{lower}), convection is likely to occur in the Yarragadee Aquifer in some parts of the PMA.

2. Calculations of critical vertical permeabilities, which show that much of the Yarragadee Aquifer is above the critical Rayleigh number. For example, using the k_{best} values, 62.4 % of the Yarragadee Aquifer within the PMA exceeded the critical permeability. The permeability profiles shown in Figure 2.5 include permeabilities up to 3 orders of magnitude above critical permeabilities.

3. 2D hydrothermal simulations, which show convection occurring in geologically informed permeability distributions derived from the SFM. In particular, it should be noted that the occurrence of low-permeability layers ($k < k_{crit}$) within the permeability-depth profile did not prevent thermal convection.

The general agreement between the Rayleigh number analyses and the hydrothermal simulations suggests that the Rayleigh number maps may be a useful tool in determining potential locations for thermal convection, even in heterogeneous systems. The approach used in the calculation of Ra_T/Ra^* and critical permeability values could be applied to any field site where a deep permeability log exists, e.g. a permeability profile derived from a wireline log. The limitation to this approach is that while permeability-depth profiles contain a significant

amount of information about the vertical variation of permeability, they provide no information on horizontal heterogeneity. The SFM approach used in this study provides information about the lateral variability of Ra_T/Ra^*, which in turn provides spatial information about the likelihood of convection.

This study also demonstrated the impact of low permeability layers on the shape of convection cells, and highlighted the difficulties in the representation of heterogeneous permeability distributions in numerical simulations. Future investigations could focus on: 1) Simulating convection in 2D cross-sections of the SFM to investigate the influence of lateral heterogeneity; 2) Expanding the simulations into 3D; and 3) Comparison between the Rayleigh number maps and temperature anomalies measured in the area.

Chapter 3

Heat and solute tracers: How do they compare in heterogeneous aquifers?

Accepted in *Ground Water*. Irvine, D.J., C.T. Simmons, A.D. Werner and T. Graf (in press). Heat and solute tracers: How do they compare in heterogeneous aquifers?. doi: 10.1111/gwat.12146.

3.1 Abstract

A comparison of groundwater velocity in heterogeneous aquifers estimated from hydraulic methods, heat and solute tracers was made using numerical simulations. Aquifer heterogeneity was described by geostatistical properties of the Borden, Cape Cod, North Bay and MADE aquifers. Both heat and solute tracers displayed little systematic under- or over-estimation in velocity relative to a hydraulic control. The worst cases were under-estimates of 6.63% for solute and 2.13% for the heat tracer. Both under- and over-estimation of velocity from the heat tracer relative to the solute tracer occurred. Differences between the estimates from the tracer methods increased as the mean velocity decreased, owing to differences in rates of molecular diffusion and thermal conduction. The variance in estimated velocity using all methods increased as the variance in log-hydraulic conductivity (K) and correlation length scales increased. The variance in velocity for each scenario was remarkably small when compared to $\sigma^2\ln(K)$ for all methods tested. The largest variability identified was for the solute tracer where 95% of velocity estimates ranged by a factor of 19 in simulations where 95% of the K values varied by almost four orders of magnitude. For the same K-fields, this range was a factor of 11 for the heat tracer. The variance in estimated velocity was always lowest when using heat as a tracer. The study results suggest that a solute tracer will provide more understanding about the variance in velocity caused by aquifer heterogeneity and a heat tracer provides a better approximation of the mean velocity.

3.2 Introduction

Groundwater velocity can be estimated using hydraulic methods such as pumping tests (e.g. Theis 1935; Cooper and Jacob 1946, using measured hydraulic conductivity and hydraulic heads), and tracer tests (e.g. Sudicky 1986; LeBlanc et al., 1991; Shook et al. 2001). In relatively simple groundwater systems, estimates of velocity using pumping and tracer tests have been shown to agree (e.g. Pearson and White 1967; Drury et al. 1984). For highly heterogeneous systems, differences in velocity estimates between pumping tests and tracer tests arise due to the sampling of different portions of the aquifer (Larocque et al. 2009). While the performance of solute tracers in providing aquifer parameter, or flow rate estimates for heterogeneous aquifers has been extensively investigated using both field and numerical methods (e.g. Sudicky 1986; LeBlanc et al. 1991; Larocque et al. 2009), investigations into the influence of aquifer heterogeneity on thermal transport and the interpretation of heat as a tracer are less common.

With recent developments in field equipment to measure water temperature, including fibre-optic distributed temperature sensors (e.g. Tyler et al. 2009), it appears that there may be a wide scope of unexplored applications where heat can be used to both understand and constrain groundwater problems. This point is supported by Anderson (2005), who highlights that both temperature data and associated analytical tools are underused in hydrogeology. Water temperature can be measured quickly, easily and cheaply (Birkinshaw and Webb 2010). Measured variations in groundwater temperature can be used to estimate hydraulic and thermal properties of aquifers such as hydraulic conductivity (Bravo et al. 2002) or thermal dispersivity (Vandenbohede et al. 2009). How a heat tracer performs compared to a solute tracer or pumping test to estimate groundwater flow rates has not been comprehensively investigated and demonstrated.

The effect of streambed heterogeneity on the estimation of fluxes between groundwater and streams using heat as a tracer has been investigated by Schornberg et al. (2010), and Ferguson and Bense (2011). Schornberg et al. (2010) used binary hydraulic conductivity (K) fields to generate synthetic temperature data. They found that large differences between K values have a greater influence on estimates of flux than the structure of the K-field. Ferguson and Bense (2011)

performed a similar analysis to Schornberg et al. (2010), however they used stochastic K-fields to represent streambed heterogeneity. Ferguson and Bense (2011) highlighted that conduction of temperature into regions where low flow occurs, can lead to errors in the estimation of fluxes.

Research into the influence of heterogeneity on the transport of heat in groundwater on larger scales have been conducted by Ferguson (2007), Hidalgo et al. (2009), and Chang and Yeh (2012). While these researchers did not explicitly study the interpretation of temperature measurements to determine rates of groundwater flow, they still provide insight into the effect of aquifer heterogeneity on the transport of heat in groundwater. For example, Ferguson (2007) studied the influence of aquifer heterogeneity on the recovery of heat in the process of aquifer thermal energy storage and recovery. He found that even a small degree of aquifer heterogeneity leads to significant variation in temperature distributions in the subsurface. Hidalgo et al. (2009) investigated the influence of aquifer heterogeneity on steady state heat transport with a point source of heat. They found that the lateral spreading of temperature from a point source is proportional to the variance in the $\ln(K)$ field and the mean flow rate. Chang and Yeh (2012) used stochastic analysis of thermal transport to develop a thermal transport equation with effective parameters. They found a linear relationship between the longitudinal and transverse macrodispersivities and variance in $\ln(K)$, suggesting that the dispersive flux of heat (i.e. flow of heat due to temperature gradients) at the field scale increases linearly with heterogeneity in hydraulic conductivity of the medium.

Investigations that have compared thermal and solute tracers to determine aquifer properties, or flow rates are extremely rare. Bons et al. (2013) developed a unified expression for solute and heat dispersion in homogeneous porous media. Using both numerical and laboratory experiments, they showed that thermal transport properties can be determined from solute transport data in homogeneous media. Vandenbohede et al. (2009) assessed the use of heat and solute tracers in two push-pull aquifer tests to determine transport properties of a deep Tertiary aquifer in Belgium. In their study, cooler, fresher water was injected into the aquifer, and changes in temperature and salinity were measured. Fitting values of dispersivity for solute and temperature in their interpretive modelling led to the

conclusion that aquifer heterogeneity has a greater influence on solute transport than thermal transport. This was attributed to the fact that heat is transported through both the pore fluid and the porous medium, and is thereby able to bypass low permeability structures, reducing the control of heterogeneity on heat transport. Rau et al. (2012) performed a systematic comparison of solute and thermal transport under controlled laboratory conditions using sand tank experiments to investigate the magnitudes of solute and thermal dispersivity. They suggested that spatial heterogeneity is a possible explanation for the variance in estimates of velocity using heat as a tracer, although this was not explicitly tested. Constantz et al. (2003) compared the use of diurnal variations in stream and sediment temperature with an applied bromide tracer test in a stream setting. They determined that heat and bromide provide quantitatively similar estimates of hydraulic conductivities and fluxes; however, they highlight that conduction of heat can mask the presence of preferential paths. Heat will move laterally into low K zones more rapidly than a solute, which can mask the presence of the flow path. Whilst a vanishingly small number of papers have simultaneously considered heat and solute tracers to explore groundwater systems (e.g. Constantz et al. 2003; Pavelic et al. 2006; Vandenbohede et al. 2009), they have not done so in a sufficiently generalised way to draw reasonably generalised conclusions about how these tracers compare and contrast when specifically utilised for the objective of groundwater flow rate estimation in heterogeneous aquifers.

In this paper, we perform a systematic and quantitative comparison of the influence of aquifer heterogeneity on groundwater velocity estimated using applied solute and heat tracers on the scale of tens of metres. The utility of heat and solute tracers for the specific objective of groundwater flow rate estimation in heterogeneous aquifers are compared and contrasted within the same quantitative analysis framework. Velocity estimates calculated using hydraulic conductivities from aquifer pumping tests and regional hydraulic gradients are also provided in order to give a hydraulic estimate of velocity for comparison. The investigation is performed using numerical simulations of: 1) flow and transport (solute and thermal) and 2) aquifer pumping tests, for a range of heterogeneous structures and flow velocities (scenarios). The variance in velocity estimates of each scenario and bias in groundwater velocity estimates (relative to a hydraulic control) are used as performance indicators of the tracer and pumping test methods.

3.2.1 Equations of solute and heat transport

Assuming homogeneous and isotropic material properties and uniform flow, the advection-dispersion equation can be written as (e.g. Domenico and Schwartz 1998):

$$D\nabla^2 C - v\nabla C = \frac{dC}{dt} \tag{3.1}$$

Where D is hydrodynamic dispersion (m^2/day), C is solute concentration (kg/m^3), v is pore water velocity (m/day), and t is time (days). The first term on the left-hand side of Equation 3.1 describes the mechanical and molecular spreading of the solute. D can be written as $D = \alpha_{L,T}^{sol} v + D^{sol}$, where $\alpha_{L,T}^{sol}$ is longitudinal or transverse dispersivity (m) and D^{sol} is molecular diffusion (m^2/day). The second term describes the advective transport of the solute by the pore fluid, and the term on the right hand side is the change in concentration with time.

The convection-conduction equation has a similar form to the advection-dispersion equation. Assuming homogeneous and isotropic aquifer properties, and equilibrium between the pore fluid and porous medium temperatures, the convection-conduction equation can be written as (e.g. Domenico and Schwartz 1998):

$$\frac{\kappa_b}{(\rho c)_b} = \nabla^2 T - \frac{\rho_w c_w}{(\rho c)_b}\nabla(Tq) = \frac{dT}{dt} \tag{3.2}$$

Where κ_b is the bulk thermal conductivity (m^2/day), $(\rho c)_b$ is the bulk volumetric heat capacity (J/m^3/C), T is temperature (°C), ρ_w is the density of water (kg/m^3), c_w is the specific heat capacity of water (J/kg/°C) and q is the Darcy velocity (m/day). κ_b is calculated by $\kappa_b = (1-\theta)\kappa_s + \theta\kappa_w$, where subscripts s and w denote solid and water respectively, and θ is porosity (-). $(\rho c)_b$ is calculated as $(\rho c)_b = (1-\theta)\rho_s c_s + \theta\rho_w c_w$. In Equation 3.2, the first term (known as thermal diffusivity) describes the conduction of heat, the second term denotes the transport of heat by flowing groundwater, and the term on the right-hand side is the change in temperature with time. The effect of thermal dispersivity (α^{heat}, m) can be included by adding $\alpha^{heat} q$ to the first term in Equation 3.2. Given that the effect of α^{heat} has been shown to be small relative to α^{sol} (e.g. Vandenbohede et al. 2009; Constantz et al. 2003), and is not required for numerical stability, the effect

of α^{heat} has been omitted from this study. This is further justified on the basis that wide variations in advection due to aquifer heterogeneity is the dominant physical mechanism for large-scale mixing (e.g. Domenico and Schwartz 1998).

While the equations of solute and thermal transport have the same basic form, there are some key differences between them, such as: 1) solutes are transported through the pore spaces only, whereas heat is transported though both the pore spaces and the porous medium, 2) thermal diffusivity is three to four orders of magnitude greater for thermal transport than molecular diffusion (D_{sol}) in solute transport (Anderson 2005).

3.3 Methods

Numerical simulations were performed using HydroGeoSphere (Therrien et al. 2006), which uses the control-volume approach to discretise the equations for groundwater flow and the Galerkin finite element approach for heat and solute transport. Heterogeneous aquifers were generated using the Sequential Gaussian Simulation tool (SGSIM) from the Geostatistical Simulation Library (GSLIB) (Deutsch and Journel 1998).

3.3.1 Conceptual model, boundary conditions and discretisation

Applied heat and solute tracer tests, and aquifer pumping tests were simulated using a numerical model. The model domain was set up to represent a 2D section of heterogeneous porous media (Figure 3.1). For the pumping test simulations, the model domain was a horizontal (xy) plane, as described below. This orientation was also assumed for the transport simulations, however, with the assumptions of constant density, the tracer simulations could also be considered a vertical cross section. The model domain has dimensions of 125 m $\times$ 100 m. A 2D model domain allowed for an extensive number of model simulations compared to a 3D domain because of the reduced computational requirements of 2D modelling. In total, we present results from 724 simulations.

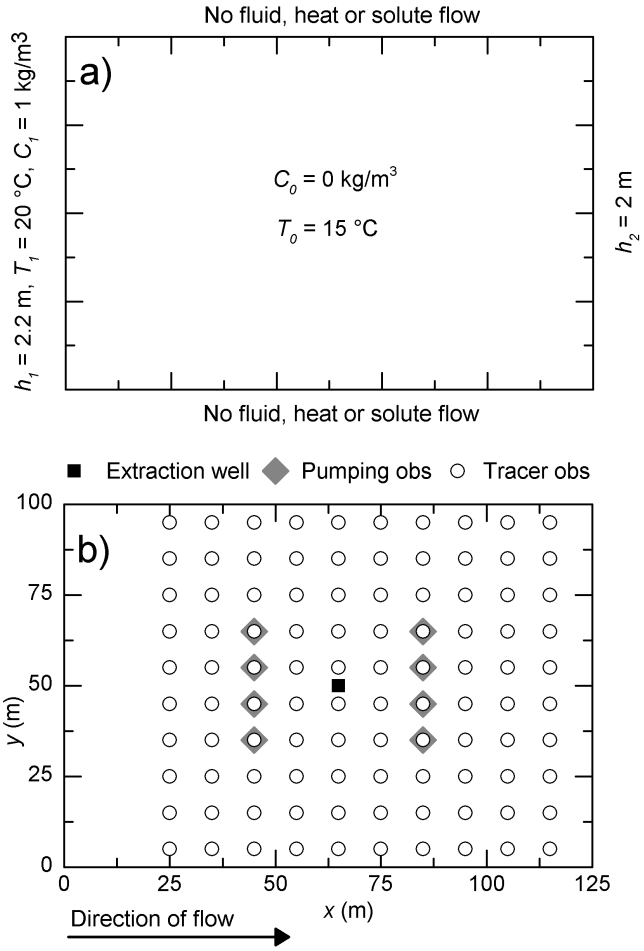

Figure 3.1: (a) Conceptual model with boundary and initial conditions. h_1 and h_2 denote constant head values, C_0 and C_1 are initial and tracer concentrations, and T_0 and T_1 are initial and tracer temperatures, respectively. (b) Model dimensions and locations of observation (obs) wells and extraction well.

The model domain was discretised with a uniform quadrilateral mesh where $\Delta x = \Delta y = 0.25$ m, producing 200,000 elements. For the transport simulations, time steps (Δt) of 0.2 days were used. This spatial and temporal discretisation satisfied the critical values of the thermal and solute grid Peclet ($\leqslant$2) and Courant numbers ($\leqslant$1) to provide numerically stable results (Anderson and Woessner 1992). The solute grid Peclet number was 0.5. Other stability criteria are flow-rate dependent. Using the average flow velocity, the thermal grid Peclet number was 0.35, the solute Courant number was 0.32, and the thermal Courant number was 0.064.

Groundwater flow was controlled by constant head boundaries of $h_1 = 2.2$ m at $x = 0$ m, and $h_2 = 2.0$ m at $x = 125$ m (in later simulations, the hydraulic gradient was altered). All other model boundaries were no-flow boundaries. The tracer source was represented as a constant concentration and constant temperature boundary along the $x = 0$ m boundary for the tracer simulations. The tracer concentration and temperature were 1 kg/m^3 for solute and 20°C for heat, respectively. The initial conditions for transport simulations were an initial solute concentration of 0 kg/m^3 and initial temperature of 15°C. Numerous researchers have investigated the effect of variable density on transport problems in groundwater. For example, Ma and Zheng (2010) for heat transport, and Simmons (2005) for solute transport, show that density effects are not significant for variations in temperature (5°C) and solute concentration (1 kg/m^3) considered in this study, and hence density differences were neglected.

A network of 100 tracer observation wells was distributed throughout the model domain (see Figure 3.1). The locations of the wells were selected to allow for ten estimates of pore water velocity at 10 different distances from the tracer source. No tracer observations were recorded within 25 m of the tracer source to allow the tracers to pass through at least one heterogeneous correlation length prior to any estimate of pore water velocity. Of the 100 tracer observation wells, eight wells were also used to obtain observations of drawdown for aquifer pumping tests (see Figure 3.1). The locations of the observation wells ranged between 20.6 to 25 m from the pumping well, and were not placed near the lateral boundaries to limit the influence of the lateral no-flow boundaries on the pumping test results.

A finer temporal discretisation was required for the aquifer pumping tests relative to the tracer tests. For the pumping test simulations, Δt was set at 0.25 seconds. Further details on the pumping tests are given in the section 'Aquifer pumping test interpretation', below.

3.3.2 Representation of aquifer properties

Hydraulic and thermal parameters were selected to represent a well-sorted, medium-to-coarse sand (Table 3.1).

Table 3.1: Hydraulic and transport parameters

Parameter	Value	Unit
Total porosity (θ)	0.2	-
Hydraulic gradient (I)	0.0008–0.008	-
Geometric mean hydraulic conductivity (K)	50	m/day
Storativity (S)	7.5×10^{-4}	-
Specific heat capacity of solids (c_s)	830	J/kg/°C
Specific heat capacity of water (c_w)	4187	J/kg/°C
Density of solids (ρ_s)	2650	kg/m^3
Density of water (ρ_w)	1000	kg/m^3
Thermal conductivity of solids (κ_s)	2.00	W/m/°C
Thermal conductivity of water (κ_w)	0.57	W/m/°C
Thermal diffusivity (λ)	5.70×10^{-2}	m^2/day
Solute longitudinal dispersivity (α_L^{sol})	0.5	m
Solute transverse dispersivity (α_T^{sol})	0.05	m
Molecular diffusion coefficient (D_{sol})	1.75×10^{-4}	m^2/day
Initial temperature (T_0)	15	°C
Tracer temperature (T_1)	20	°C
Initial concentration (C_0)	0	kg/m^3
Tracer concentration (C_1)	1	kg/m^3

The geostatistical properties of the aquifers were selected to be representative of the heterogeneity of typical field settings e.g. the Borden (Sudicky 1986), Cape Cod (Hess et al. 1992; LeBlanc et al. 1991), MADE (Barlebo et al. 2004; Rehfeldt et al. 1992) and North Bay (Sudicky et al. 2010) sites. In total, 12 combinations of variance (σ^2) in $\ln(K)$ and the correlation length (i.e. the distance over which K values are correlated, τ) were tested. These scenarios are labelled A through to L (see Figure 3.2). In Figure 3.2, τ from field sites (presented in brackets) were adjusted to match the spatial discretisation of the model domain. In all scenarios, τ was isotropic (i.e. $\tau_x = \tau_y$), and all K-fields were stationary. All tracer and aquifer pumping tests were performed using 60 realisations of the $\ln(K)$ field.

The values of $\sigma^2\ln(K)$ cover a range of heterogeneities, from a minor to a high degree of heterogeneity. With the values of $\sigma^2\ln(K)$ considered in this study (0.14, 1.00, 2.00 and 4.50), 95% of$K$ values (i.e. mean $K \pm 2\sigma$) are expected to vary by a factor of 4.5, 55, 286 and 4843 respectively. For example, the 95% range of K in the $\sigma^2\ln(K) = 4.50$ fields spans between three and four orders of

magnitude.

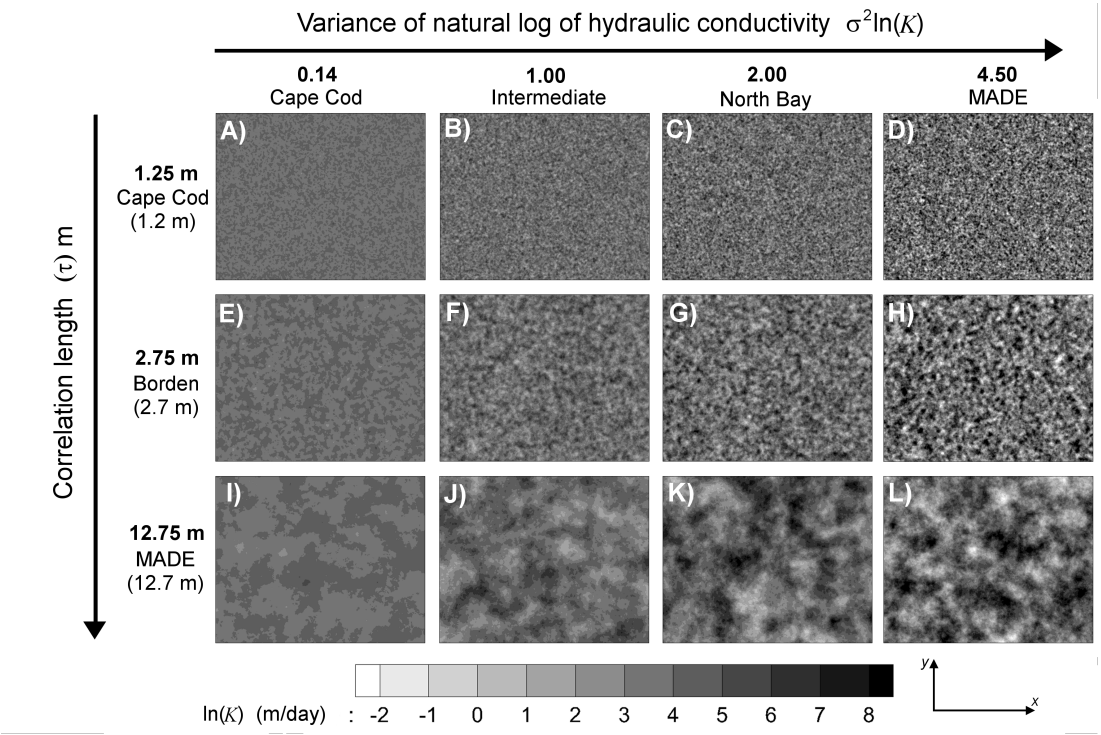

Figure 3.2: Considered geostatistical parameters and scenario names (A–L). The first of 60 realisations of each scenario is shown. All values of $\sigma^2\ln(K)$ and τ are taken from fields sites with the exception of $\sigma^2\ln(K) = 1.00$, which was selected as an intermediate value between the $\sigma^2\ln(K)$ of the Cape Cod and North Bay sites.

3.3.3 Tracer interpretation

For both tracer approaches, 10 estimates of v were obtained for each distance from the tracer source, for each realisation of the K-field. This sampling leads to a sample size of 600 estimates at each distance from the tracer source for each scenario (10 estimates from each realisation, for 60 realisations).

Estimates of v from the solute tracer observations (v_{sol}) were obtained from:

$$v_{sol} = \frac{x}{t_{sol}} \tag{3.3}$$

Where x is the distance from the tracer source/inlet (m), and t_{sol} is the time (days) of breakthrough of the solute at the observation well. For the solute tracer, t_{sol} was taken as the time when the concentration in an observation well reached half of the input concentration (0.5 kg/m^3). The same observation wells were used to measure the time of the breakthrough of temperature (t_{heat}), where v estimated using heat as a tracer (v_{heat}) is determined by:

$$v_{th} = \frac{x}{t_{heat}} \tag{3.4}$$

$$v_{heat} = v_{th} R_{th} \tag{3.5}$$

$$R_{th} = 1 + \frac{(1-\theta)\rho_s c_s}{\theta \rho_w c_w} \tag{3.6}$$

Where v_{th} is the velocity of the thermal front (m/day). The value theat is the time (days) when the temperature in an observation well reached the average of the initial and boundary temperatures. R_{th} (-) is the thermal retardation coefficient as outlined by Palmer et al. (1992). R_{th} reduces v_{th} relative to v because heat is lost to the porous media. In a field setting, the values of the parameters that are used to calculate R_{th} will vary spatially, although they are expected to vary over a smaller range with respect to the range of K (e.g. Waples and Waples 2004; Anderson 2005; Chang and Yeh 2012). As the ranges of thermal parameter values are many orders of magnitude lower than variations in K, variations in θ, ρ_s and c_s have not been included in this analysis. For our parameter values, R_{th} is approximately 3.1.

Initial testing of the tracer approaches in a homogeneous 1D simulation showed that both tracer approaches agreed with calculated velocity using Darcys law, with estimates of v accurate to within 0.5%.

3.3.4 Aquifer pumping test interpretation

The limited spatial extent of the model domain precluded the use of several classical pumping test approaches, such as the Jacob straight-line method (Cooper and Jacob 1946). That is, the lateral no-flow boundary conditions prevented the late-time data plotting on a straight line. For example, for the drawdown data to be linear with respect to $\log(t)$, testing showed that the boundaries at $y = 0$ m

and 100 m would have to be extended by approximately 1000 m to prevent boundary effects. However, it was possible to interpret the early-time drawdown data to determine transmissivity (T, m^2/day) using a derivative drawdown method outlined by Straface (2009). The Straface (2009) method is based on the Theis (1935) solution, and does not require the late-time data to be linear. Here, we briefly outline the derivative drawdown method. For the full derivation of the approach, see Straface (2009).

The drawdown (w) at time (t'), when the derivative $dw/d(ln(t))$ reaches an inflection point, is used to calculate T. The inflection point of $dw/d(ln(t))$ occurs when the value of the second derivative ($d^2w/d(ln(t))^2$) is at a maximum, and when ($d^3w/d(ln(t))^3$) is equal to zero. When the third derivative is equal to zero, the value of t' is known, and with the value of the well function $W(u) = W(1)$, the Theis solution for T reduces to:

$$T = \frac{QW(1)}{4\pi w(t')} \tag{3.7}$$

Where Q is the pumping rate (m^3/day). A graphical example of the Straface (2009) method is shown in Figure 3.3.

For the numerical aquifer pumping tests, a steady Q of 300 m^3/day was used at an extraction well located at $x = 65$ m and $y = 50$ m. A value for v can be calculated from the pumping test using the transmissivity (same as K in a horizontal 2D domain with a unit thickness) obtained from the test, the regional hydraulic gradient (I), and θ (i.e. $v = KI/\theta$). We denote this value v_{pump}. The resulting sample size of pumping test observations was 480 observations per scenario (eight wells and 60 realisations).

Initial testing of the Straface (2009) method in a 2D simulation with homogeneous and isotropic aquifer properties gave estimates of v_{pump} that agreed with calculations using Darcys law, with estimates of v accurate to within approximately 0.1 %.

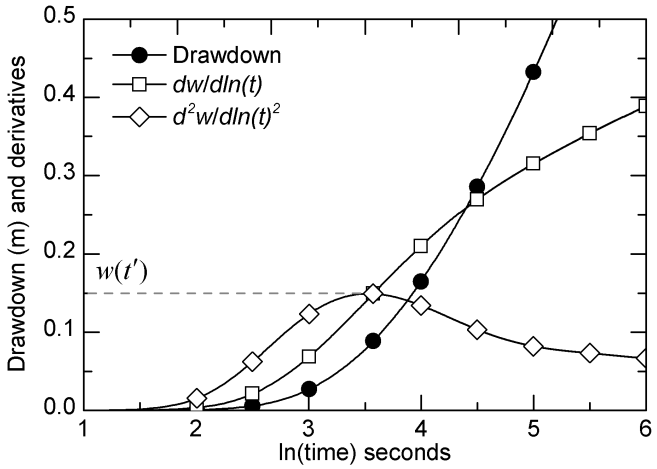

Figure 3.3: Example of aquifer pumping test data using the method outlined by Straface (2009). The value of drawdown at the inflection point of $dw/dln(t)$ (local maximum of $d^2w/dln(t)^2$) is used to calculate transmissivity in Equation 3.7.

3.3.5 Determination of performance indicators

To test the performance of each method to estimate v, we determined 1) the variance in estimates of v (See Variance in velocity estimates, below), and 2) whether any method displays any consistent over- or under-estimation of v (see Mean flow rates and bias, below).

The variance in velocity estimates are presented as $\sigma^2\ln(v)$, because distributions of v ($v_{sol}, v_{heat}, v_{pump}$) are controlled by the K-fields, which also have a natural log distribution. The comparison of $\sigma^2\ln(v)$ and $\sigma^2\ln(K)$ allows for the determination of the relative variability of the K-fields and the values of v estimated from those fields.

To determine whether any of the tracer or pumping test methods introduces any systematic under- or over- estimation (bias), we compared how each velocity estimate compares to a true flow rate for each realisation. A representative value for v was calculated for each realisation from the water balance of a steady-state simulation. The representative v was calculated from the volumetric flux through the model domain at steady state, the cross sectional area of flow (width

of domain multiplied by 1 m) and θ. A determination of bias was obtained by dividing each estimate of v from the tracer and pumping test approaches by the representative flow rate from that realisation. We denote this normalised value as v_{bias}.

3.4 Results and Discussion

3.4.1 Variance in velocity estimates

For the pumping tests, $\sigma^2\ln(v_{pump})$ is expected to reduce as the volume of the aquifer sampled by the test increases (Meier et al. 1998; Larocque et al. 2009). For the heat and solute tracer tests, $\sigma^2\ln(v_{sol})$ is expected to reduce as the number of correlation lengths traversed by the tracer increases (Larocque et al. 2009). The same behaviour is expected for $\sigma^2\ln(v_{heat})$. This point is demonstrated in Figure 3.4, where $\sigma^2\ln(v_{sol})$ (top figure) and $\sigma^2\ln(v_{heat})$ (bottom figure) are plotted against the number of correlation lengths traversed by the tracer (distance of the observation well from the tracer source divided by τ). Results are shown for scenarios where $\tau = 1.25$ m. Figure 3.4 shows that the variance in estimates of velocity are small relative to the variation in the K-field for each distance from the tracer source. For example, the greatest variance in v estimates occurred for the solute test, with a $\sigma^2\ln(v_{sol})$ of 0.052. This is clearly much lower than the $\sigma^2\ln(K)$ of 4.50. Figure 3.4 also demonstrates that for all cases, $\sigma^2\ln(v_{heat})$ is smaller than $\sigma^2\ln(v_{sol})$. For example, for case D, after the tracer passed through 20 correlation lengths (x = 25 m), $\sigma^2\ln(v_{sol})$ was 0.052, while $\sigma^2\ln(v_{heat})$ was 0.018. For case D, 95% of the velocity estimates at $x = 25$ m vary between 0.336–0.537 m/day for solute, and 0.366–0.484 m/day for heat. When the tracers have traversed 92 correlation lengths ($x = 115$ m), $\sigma^2\ln(v_{sol})$ is 0.005 and $\sigma^2\ln(v_{heat})$ is 0.003. 95% of the velocity estimates vary between 0.365–0.484 m/day for solute, and 0.388–0.477 m/day for heat. This demonstrates that $\sigma^2\ln(v)$ increases as $\sigma^2\ln(K)$ increases for both tracers, but that the temperature measurements exhibit less variance. Figure 3.4 demonstrates that the variation in velocity estimates is small relative to the variation in the K-fields, where $\sigma^2\ln(K)$ increases from scenario A through to scenario D.

Figure 3.5 demonstrates how $\sigma^2\ln(v)$ is influenced by both $\sigma^2\ln(K)$ and τ. In

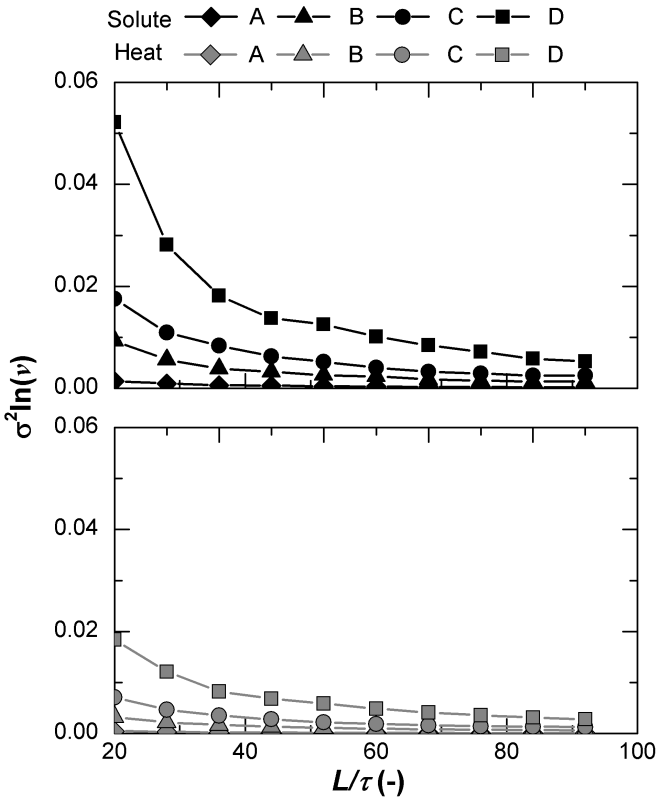

Figure 3.4: $\sigma^2\ln(v_{sol})$ (black markers) and $\sigma^2\ln(v_{heat})$ (grey markers) against the number of correlation lengths covered in the tracer tests for scenarios A-D, where $\tau = 1.25$ m.

Figure 3.5, $\sigma^2\ln(v_{pump})$ for the pumping test wells, and $\sigma^2\ln(v_{sol})$ and $\sigma^2\ln(v_{heat})$ for the wells 55 m from the tracer source are plotted against the $\sigma^2\ln(K)$. The distance of 55 m for the tracer observation wells was selected as it is a mid-range distance, and gave comparable variance in v estimates to the pumping tests. Figure 2.5 demonstrates that $\sigma^2\ln(v)$ from the pumping test and tracer methods are small relative to $\sigma^2\ln(K)$ for all values of τ, with the largest variation occurring in the case of the solute tracer for the highly heterogeneous case L. In this case, the value of $\sigma^2\ln(v_{sol})$ of 0.55 is almost an order of magnitude lower than $\sigma^2\ln(K)$ of 4.50. For case L, 95% of the measurements of vsol ranged between 0.085–1.641 m/day in K-fields where 95% of the K values ranged by a factor of 4843. The largest value of $\sigma^2\ln(v_{pump})$ of 0.38 and the largest value of $\sigma^2\ln(v_{heat})$ of 0.37 also occurred in case L. In case L, 95% of the estimates ranged between 0.08–1.06 m/day and 0.12–1.32 m/day for v_{pump} and v_{heat}, respectively. For case D,

where $\sigma^2\ln(K)$ is identical to case L, but the correlation length is shorter (τ = 1.25 m), 95% of the estimates of v_{pump}, v_{heat} and v_{sol} spanned only 0.317–0.535, 0.366–0.510 and 0.366–0.537 m/day respectively. This shows a clear effect of τ on the variance in v estimates for all methods tested.

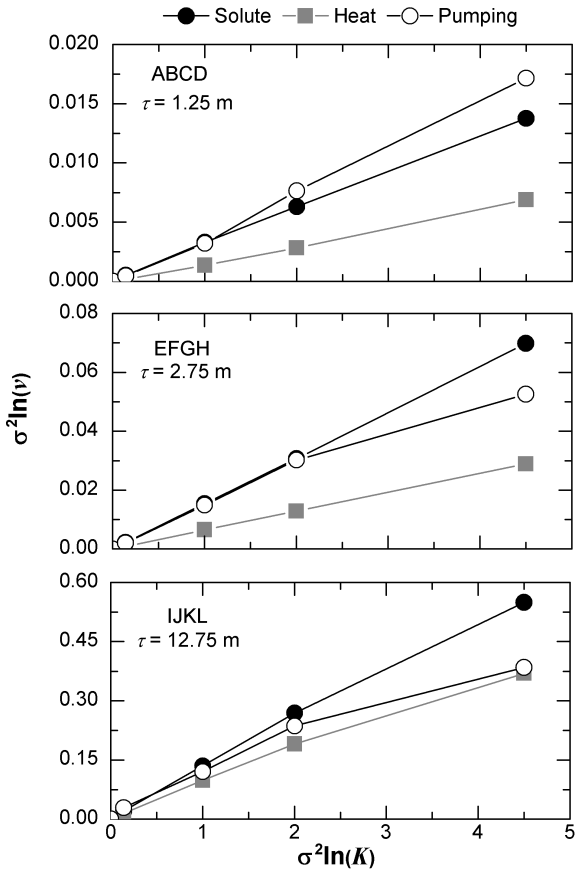

Figure 3.5: $\sigma^2\ln(v)$ against the $\sigma^2\ln(K)$ for 55 m tracer observation wells, and the pumping test observation wells. For details on scenarios A-L, see Figure 3.2. Note that the y-axis scale varies.

The higher $\sigma^2\ln(v_{sol})$ compared to $\sigma^2\ln(v_{heat})$ suggests that the influence of heterogeneity (both τ and $\sigma^2\ln(K)$) on solute tracers is stronger than for heat tracers, as suggested by Vandenbohede et al (2009). The results in Figure 3.5 suggest that if several observation wells are available, a solute tracer test will provide more insight into the heterogeneity of the aquifer because a solute plume is more strongly modified by aquifer heterogeneity. In comparison, a heat tracer will provide an estimate of v that is closer to the average value, as the smoothing of the thermal

front has an averaging effect on the estimated flow velocity.

It should be highlighted that the Straface (2009) method could not be applied to all results. In some simulations from cases H, J, K, and L (where $\sigma^2\ln(K)$ and τ were large), it was clear from interpretations of pumping test data that boundary effects were influencing results at some of the observation wells. For these wells, there was no clear peak in the second derivative of drawdown caused by the cone of depression reaching the no-flow boundaries.

The difference between the aquifer pumping tests and tracer tests depend on the length of the flow path. That is, selecting the observation wells that were a greater distance from the tracer source will result in lower variations in velocity estimates (e.g. see Figure 3.4). The limited extent and boundary conditions of our model domain did not allow for the pumping test observation wells to be placed further from the extraction well (hence sampling a larger proportion of the aquifer).

Figure 3.5 also demonstrates the fact that $\sigma^2\ln(v)$ increases as τ increases. This is an important point given the limited range of τ tested in this study. For example, Larocque et al. (2009) demonstrated that variance in velocity estimates using radioactive tracers and pumping tests increased with τ up to 250 m.

3.4.2 Mean flow rates and bias

The geometric average bias from each method across all 60 realisations of each scenario is shown in Figure 3.6. The data in Figure 3.6 demonstrates how aquifer heterogeneity influences the v_{bias} from the pumping test and tracer methods. A value of v_{bias} greater than one suggests an over-estimation and a value less than one suggests an under-estimation of v, relative to the value determined from the water balance approach.

For cases A and B ($\tau = 1.25$ m), there is little difference in the bias of the tracer and pumping test methods. As $\sigma^2\ln(K)$ increases (cases C and D), the pumping test method under-estimates v which is likely caused by zones of lower K. For cases E, F, G and H ($\tau = 2.75$ m), again, there is little difference between the

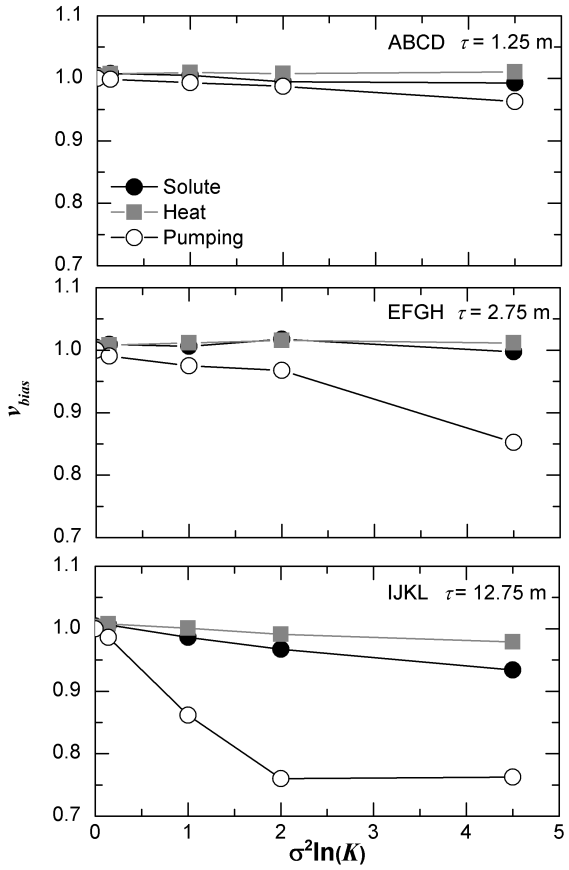

Figure 3.6: Average bias (v_{bias}) against $\sigma^2\ln(K)$. $v_{bias} = v_{sol}$, v_{heat}, or v_{pump} divided by the v determined from the water balance of a steady state model simulation). All plots include the initial homogeneous test case (i.e. $\sigma^2\ln(K) = 0$).

two tracers. For these cases, the pumping tests continue to under-estimate v, with a large change in v_{bias} for the pumping test in case H. The large change in v_{bias} from case G to case H was due to the removal of results that could not be interpreted with the Straface (2009) method. The presence of high K zones resulted in some observation wells being influenced by the boundary conditions. The removal of observations of high transmissivity (and hence high v) explains the apparent underestimation for case H. For the cases I, J, K and L (v_{bias} = 12.75 m), the tracers under-predict v, on average. Even in the most highly heterogeneous scenario (case L), bias was very small for each tracer test method. The largest bias for the solute tracer was an under-estimation of 6.63% (v_{bias} = 0.934) and the largest bias for the heat tracer was a 2.13% underestimation (v_{bias}

= 0.979).

As with case H, the values of vbias from the pumping tests for cases J, K and L under-estimate v due to observations being omitted due to boundary effects. The worst bias from the reliable pumping tests was an under-estimation of 3.25% ($v_{bias} = 0.967$) for case G. For case G, the solute tracer lead to an over-estimation of 1.75% ($v_{bias} = 1.017$) for solute, and an over-estimate of 1.54% ($v_{bias} = 1.015$) for heat.

As $\sigma^2\ln(K)$ increased, all methods tended to under-estimate v. For the tracer tests, this occurs because the presence of lower K zones increases the length of flow paths. This increases the time required for the breakthrough of the tracer, which leads to the estimation of lower flow rates. The under-estimation of v as calculated from derivative drawdown pumping tests has previously been demonstrated by Trinchero et al. (2008). They demonstrate that low K zones delay in the time of t' which in turn leads to the estimation of a lower K than the geometric mean of the K-field.

For the highly heterogeneous cases where $\sigma^2\ln(K) = 4.50$, the estimates of velocity from the solute tracer show a greater under-estimation relative to the heat tracer. Differences in estimates of velocity using heat and solute can be explained by the presence of low$K$ zones. The higher value of thermal diffusivity relative to solute dispersion allows heat to be transported more rapidly through low K zones by conduction, which produces less low velocity estimates (explaining why values of v_{bias} are closer to one, leading to smaller bias in the velocity estimates).

Figure 3.6 does not show a significant bias, on average, for either of the tracer methods. Figure 3.7, below, allows for a direct comparison between estimates of v_{heat} and v_{sol}. Data shown are for the 25 m wells from all realisations from case G. Case G was selected for this analysis because of the mid-range values of $\sigma^2\ln(K)$ and τ. The results in Figure 3.7 show the relationship between estimates of v_{heat} and v_{sol} for three hydraulic gradients. The top row of Figure 3.7 shows results using a low gradient ($I = 0.0008$ m/m), the middle row shows results from the case with the gradient used to produce Figures 3.4, 3.5 and 3.6 ($I = 0.0016$ m/m) and the bottom row shows the results from the case with a high gradient ($I =$

0.008 m/m). Next to each scatterplot are the distributions of solute (left) and heat (right) at the average time of breakthrough of the 10 observation wells that are 25 m from the tracer source. It is important to note that the snapshot of the heat distributions are taken at a time 3.1 times greater than for the solute case (as time lags are proportional to R_{th}). This visual representation demonstrates the influence of the high thermal diffusivity relative to the solute dispersion.

Figure 3.7 clearly shows a systematic difference in the distribution of the two tracers, which influences the prediction of vheat and v_{sol}. In Figure 3.7, the greatest mismatch between the estimates of vsol and vheat is around a factor of 2, which occurs in the case with the lowest background velocity (lowest hydraulic gradient). As with the findings shown in Figures 3.4–3.6, differences on the order of a factor of 2 are small when compared to variations of K, which for case G, 95% of the values of K ranged by a factor of 286 (e.g. between two and three orders of magnitude).

Preferential flow pathways (high K zones) lead to fingering of the tracers. A mismatch in the distribution of the solute and heat fingers will lead to the v_{heat} against v_{sol} data diverging from a 1:1 line. The distribution of fingers for the solute tracer at the time of the average breakthrough at the 25 m wells is essentially identical for all hydraulic gradients tested, however the temperature distribution varies across the three hydraulic gradients tested. For the low hydraulic gradient case (I = 0.0008 m/m), the lateral diffusive heat flux smooths out the thermal front relative to the solute front in the preferential flow pathway. This smoothing of the thermal front explains why heat both under- and over-estimates flow rates comparative to the solute tracer (see top row in Figure 3.7). That is, in the cases where a finger of the solute tracer reaches an observation well (i.e. flow through a preferential flow pathway), the smoothing of the thermal front will increase the time taken for the breakthrough of temperature in the observation well. Under these conditions, the use of heat as a tracer will lead to an estimate of velocity that is slower than the estimate from a solute tracer. When the observation well is located between the solute fingers (in a low K zone), the smoothing of the thermal front will lead to enhanced transport of heat relative to solute, and heat will estimate a greater flow velocity than the solute tracer.

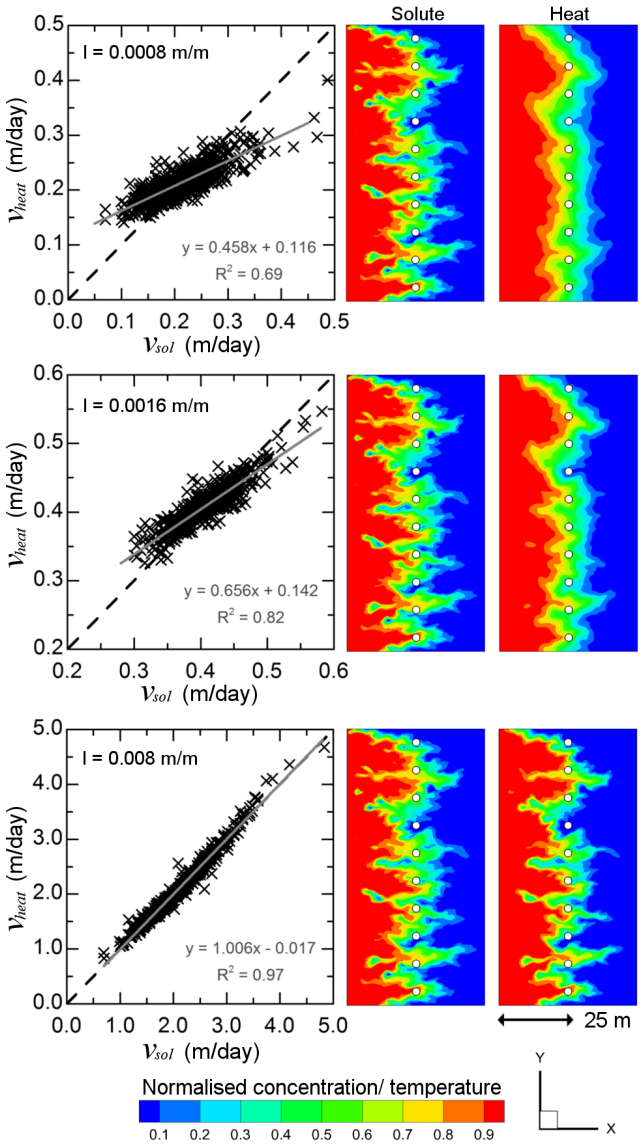

Figure 3.7: Relation between v_{heat} and v_{sol} using the 25 m wells for scenario G ($\sigma^2 ln(K) = 2.00$, $\tau = 2.75$ m, left) for three hydraulic gradients. Dashed black line is the 1:1 line and solid grey line is the linear line of best fit. Note: the axes vary between the scatterplots. The right figures show the distribution of solute and temperature at the average time of the tracer (solute or heat) breakthrough at 25 m from the tracer source from realisation 1. On the tracer distribution plots, white circles denote observation wells.

For higher hydraulic gradients, the influence of the smoothing of the thermal front is reduced, suggesting that there is a Peclet number (ratio of convection

to conduction) control on the distribution of the heat tracer. It appears that the use of heat as an applied tracer is likely to be more suitable in the case of high Peclet numbers (where the influence of convection dominates the influence of conduction). In the case with high gradient ($I = 0.008$ m/m), the distribution of the heat and solute tracers are essentially identical, a point which is shown by the slope in the equation of a line approximately equalling one (Figure 3.7).

Sensitivity analyses (results not shown) demonstrated that both τ and $\sigma^2\ln(K)$ also has an influence on the deviation of the estimates of v_{heat} and v_{sol} from the 1:1 line, however the mean flow rate (as shown in Figure 3.7) has the most pronounced influence. Across all of the scenarios tested, the slope of the line of best fit of v_{heat} against v_{sol} approaches one as either $\sigma^2\ln(K)$ or τ increases. This investigation on the influence of mean flow rate of solute and thermal transport in Figure 3.7 demonstrates that we may not necessarily expect the use of heat and solute tracers to lead to the estimation of the same subsurface hydraulic or transport parameters.

3.5 Summary and conclusions

In this study, we present a systematic comparison of the influence of aquifer heterogeneity on the interpretation of heat and solute tracers to determine groundwater velocity within a unified modelling framework. For a hydraulic comparison, the tracer tests are compared against an aquifer pumping test method. All measurements were presented with no associated error (e.g. measurement error) that would occur with field measurements.

The selection of the most appropriate characterisation/estimation method will be influenced by time and cost constraints, the purpose of the test and sometimes environmental restrictions. The duration of both the solute and heat tracers were influenced by the variance in the $\ln(K)$ field. As $\sigma^2\ln(K)$ increased, typically so did the duration of the test. This was caused by local low-K regions reducing the flow velocity. For the use of heat as a tracer, with $R_{th} \approx 3.1$ as was the case in this study, the duration of heat tracer tests typically was on the order of 3.1 times longer than the solute tracer test.

The analysis of temperature requires the knowledge, or at least an estimate of thermal parameters ($\kappa_s, \theta, \rho_s, \rho_w, c_s, c_w$, see Table 1 for definitions) of which apply to both the medium and the groundwater. While the introduction of these extra parameters does introduce more complexity, thermal parameters vary over a much smaller range than hydraulic parameters such as hydraulic conductivity.

The key findings of this study show that:

1. The variance in flow rates v for each scenario is remarkably small when compared to $\sigma^2\ln(K)$ of that scenario for all methods used. The largest variability identified is for the solute tracer where 95% of the estimates range by a factor of 19 in K-fields where 95% of the values of K range by a factor of 4843 (between three and four orders of magnitude). For the same K-fields, 95% of the velocity estimates using heat as a tracer range by a factor of 11.

2. The values of bias are also small for the tracer and pumping tests. The largest bias that could be determined using the pumping test method is an under-estimation of 3.25% for case G ($\sigma^2 ln(K) = 2.00$, $\tau = 2.75$ m), although the bias is expected to be worse in even more heterogeneous aquifers. The largest bias for the solute tracer is a 6.63% under-estimation, and for heat the largest bias is a 2.13% under-estimation of pore water velocity.

3. The differences that do occur between the two tracers can be explained by the higher value of thermal diffusivity relative to dispersion of solutes. The influence of thermal diffusivity allows heat to be transported through lower K zones by conduction, whereas solutes typically flow around low K zones, or are transported orders of magnitude slower by molecular diffusion. A direct comparison of the tracers shows that the greatest difference in estimates of velocity is around a factor of 2, which is small in comparison to the variation in hydraulic conductivity. This smoothing of the temperature front has an averaging effect on the velocity inferred from temperature data. This may be a key benefit if the objective of a test is to understand average flow behaviour.

4. The non-conservative nature and retardation of heat limit the distance that the use of heat as an applied tracer will be appropriate under a natural gradient. The fact that heat is non-conservative (i.e. heat is lost to the aquifer material) will require the tracer to be applied over a longer duration than a solute tracer. The effect of thermal retardation will extend the duration of the test relative to a solute tracer test.

These results suggest that a solute tracer will typically provide more understanding about the variance in flow rate caused by aquifer heterogeneity and a heat tracer will provide a better approximation of the mean groundwater velocity. Although at extremely low velocities (e.g. 1×10^{-9} m s^{-1}) temperature distributions will become insensitive to advection, and will not provide information on velocity, where a solute tracer may still provide valuable information.

Whereas a solute tracer can be selected that is not present in the groundwater, care must be taken with heat as a tracer. When using heat as a groundwater tracer, it is important to understand the initial temperature distribution of the aquifer prior test conditions. If the test is in the surficial zone (typically the upper 10 m) using heat may be problematic due to seasonal variations in groundwater temperature due to recharge of warmer and cooler waters, changes in temperature due to thermal radiation, or other groundwater- atmosphere interactions.

Future work could be conducted to explore the role that flow dimensionality (e.g., 2D vs. 3D) plays on tracer interpretation, and to examine the effects of more realistic heterogeneity that is constrained using field data. It would be valuable to test these theoretical findings with field data from sites in which hydraulic information as well as heat and solute tracer information are simultaneously available.

Chapter 4

The effect of streambed heterogeneity on groundwater-surface water fluxes inferred from temperature time series

Under review at *Water Resources Research:* Irvine, D.J., R.H. Cranswick, C.T. Simmons, M. Shanafield, L.K. Lautz. The effect of streambed heterogeneity on groundwater-surface water fluxes inferred from temperature time series.

4.1 Abstract

One-dimensional analytical heat transport equations based on temperature time series data have become popular tools to determine the interaction between groundwater and surface water. The influence of non-ideal field conditions on the use of these equations has been assessed for a non-sinusoidal stream temperature signal, uncertainty in thermal parameters, sensor accuracy and for multidimensional flow. Given that streambeds are often highly heterogeneous, the influence of streambed heterogeneity on flow estimates from temperature time series equations requires further investigation. Synthetic streambed temperatures were generated using a two-dimensional numerical model with heterogeneous hydraulic conductivity distributions. Streambed temperatures were used to calculate fluxes between groundwater and surface water for flow fields analogous to losing streams. The influence of streambed structure, degree of heterogeneity, depth of the sensor pair, and location along a flow path were assessed. Errors in calculated fluxes increased with sensor pair depth, the position along a flow path, and with the degree of heterogeneity. These errors were larger for streambeds with a cobble like structure compared with layered streambeds. In heterogeneous streambeds, the use of amplitude ratio method typically produced smaller errors relative to the phase shift method. The simultaneous estimation of strong fluxes using the phase shift method, and an inability to obtain a flux estimate from the amplitude ratio method can suggest the presence of low hydraulic conductivity

zones. When this occurs,flux estimates from the phase shift method should not be used.

4.2 Introduction

Understanding the interaction between groundwater and surface water is important in the management of water resources. Quantifying the rates of stream water loss to groundwater may be important in supporting regionnal stream depletion assessments, and determining safe yields of groundwater extraction from nearby wells. The use of heat as a tracer to determine fluid flux between groundwater and surface water has become a popular technique, with interest demonstrated through recent reviews by Anderson (2005), Constantz (2008), and Rau et al. (2014), and over 100 citations for each of the Stallman (1965), Hatch et al. (2006) and Keery et al. (2007) papers that outline methods to estimate water flow from temperature time series data. Temperature time series based approaches fot the determination of fluxes between streams and groundwater offer many benefits, including the fact that temperature sensors are inexpensive, automated, can be deployed for long periods, highly uncertain properties such as hydraulic conductivity (K) are not required to obtain flux estimates, and automatic techniques to calculate fluxes from temperature time series are freely available (e.g. Swanson and Cardenas (2011); Gordon et al. (2012)).

The use of temperature time series to determine groundwater-surface water interactions was proposed by Suzuki (1960), and later by Stallman (1965). The Stallman equation was adapted by Hatch et al. (2006), and Keery et al. (2007), where the vertical component of Darcy flux can be obtained by iteratively solving equations for the thermal front velocity determined from a pair of temperature time series. More recently, methods have been proposed by McCallum et al. (2012), and Luce et al. (2013) which are also based on the Stallman (1965) equation, but equations are solved directly. These more recent approaches also allow for the calculation of thermal diffusivity, and in the case of Luce et al. (2013), streambed scour. The method to determine streambed scour or deposition has been extended by Tonina et al. (2014). The abovementioned methods are based

on the following assumptions: 1) the water flow is vertical and one-dimensional, 2) the temperature signal at the upper boundary is sinusoidal, 3) there is no thermal gradient with depth in the streambed, 4) there is thermal equilibrium between the pore water and the streambed materials, and 5) the streambed thermal and hydraulic properties are homogeneous. Given that streambeds typically exhibit a large range of K (e.g. Calver 2001) and the use of heat tracing is becoming widespread, an investigation into the influence of heterogeneity on the use of temperature time series methods is required.

The influence of multidimensional flows on errors in fluid flux using the Hatch et al. (2006) equations have been investigated for longitudinal hyporheic flow conditions (Lautz 2010; Roshan et al. 2012; Cuthbert and McKay 2013) and for lateral flow through conditions (Roshan et al. 2012; Cuthbert and McKay 2013). Results from these studies demonstrate that the Hatch et al. (2006) methods perform better for downwelling compared to upwelling flows, and that generally, equations that use the ratio of the amplitudes of the temperature signals are less prone to errors than equations that use phase shift between the time series. Errors in the use of phase shift can be caused by filtering, which can produce spurious phase shifts (Hatch et al. 2006), by low flow rates, or situations where thermal resolution of temperature sensors makes it difficult to determine the exact time of peaks in the temperature signal (Lautz 2010). A non-sinusoidal stream temperature has been shown to produce variable flux estimates when fluxes are constant, but this effect can be reduced by calculating average flux over several days (Lautz 2010). The effect of a thermal gradient has been shown to be negligible for losing conditions (Lautz 2010). The effect of the uncertainty of thermal parameters can be reduced by reducing the spacing of thermal sensors (Shanafield et al. 2011), and the range of fluxes that can be determined for a given combination of thermal parameters and sensor accuracy can also be computed (Soto-Lpez et al. 2011).

Heterogeneity of streambed and aquifer materials can have an influence on the spatial patterns of groundwater-surface water interaction (Kalbus et al. 2009; Irvine et al. 2012). Quantifying exchange between groundwater and surface water can be difficult because streambed materials range from relatively homogeneous to cases where the range of K exceeds six orders of magnitude (Calver et al. 2001). Streambed heterogeneity has been suggested as a potential cause for the

mismatch of flow direction estimated by heat methods and vertical head gradients (Hatch et al. 2010; Rau et al. 2010), although the influence of streambed heterogeneity has not been explicitly tested. The influence of streambed heterogeneity on the estimation of fluxes using point-in-time temperature measurements has been investigated by Schornberg et al. (2010), and Ferguson and Bense (2011). These studies tested analytical solutions that assume steady state temperature boundary conditions (Bredehoeft and Papadopulos, 1965; Turcotte and Schubert, 1982), rather than temperature time series, and only tested these methods for upwelling conditions. There is no systematic study of the influence of streambed heterogeneity on the use of heat as a tracer to determine downwelling, and no studies on the influence of streambed heterogeneity on heat tracing based on diurnal temperature signals.

The objective of this study is to determine the influence of streambed heterogeneity on groundwater-surface water exchange fluxes that are estimated from the Hatch et al. (2006) equations for losing streams. The choice to assess the performance of the Hatch et al. (2006) equations, and not the newer approaches outlined by McCallum et al. (2013) or Luce et al. (2013), was made because the Hatch et al. (2006) equations are widely used, and effects of non-ideal field conditions on the use of the Hatch et al. (2006) equations have been extensively studied, with the exception of streambed heterogeneity. Similar analyses could also be performed on the use of the McCallum et al. (2012) and Luce et al. (2013) equations. The performance of the Hatch et al. (2006) equations are assessed for both deterministically and geostatistically arranged streambed materials, and for a range of sensor pair depths, and positions along a hyporheic flow path. To perform this analysis, synthetic streambed temperature data were generated using a numerical flow and transport model. To isolate the effect of streambed heterogeneity, stream temperatures were restricted to a purely sinusoidal signal. The synthetically generated streambed temperature data were the input into the Hatch et al. (2006) equations, and the output was compared against the 'known' fluxes from the numerical model.

4.3 Methods

4.3.1 Equations of heat transfer

The general 1D form of the conduction-convection equation in homogeneous saturated porous media is defined as (Stallman 1965):

$$\frac{\partial T}{\partial t} = D_{th}\frac{\partial^2 T}{\partial z^2} - q\frac{\rho_w c_w}{(\rho c)_b}\frac{\partial T}{\partial z}, \tag{4.1}$$

where T is temperature (°C), t is time (s), D_{th} is the effective thermal diffusivity (m^2/s), z is distance (m), q is the Darcy flux (m/s), ρ_w is the density of water (kg/m^3), c_w is the specific heat capacity of water (J/kg/°C) and $(\rho c)_b$ is the volumetric heat capacity of the saturated sediments ($J/m^3/°C$). The value of $(\rho c)_b$ is calculated as:

$$(\rho c)_b = \theta\rho_w c_w + (1-\theta)\rho_s c_s, \tag{4.2}$$

where θ is porosity (-), ρ_s is the density of the solids (kg/m^3), and c_s is the specific heat capacity of the solids ($J/m^3/°C$). D_{th} is calculated as:

$$D_{th} = \frac{\kappa_e}{(\rho c)_b} + \beta\frac{\rho_w c_w |q|}{(\rho c)_b}, \tag{4.3}$$

where κ_e is the effective thermal conductivity of the medium (W/m°C), and β is thermal dispersivity (m). Recent work by Rau et al. (2012) demonstrates that the fraction in the second term on the right hand side of Equation 4.3 is squared, although for most fluxes considered in groundwater-surface water interaction, the effect of the inclusion of this square relationship is negligible.

The analytical approach outlined in Hatch et al. (2006) was used to calculate the thermal front velocity (v_{th}, m/s) between two observation points in a numerical model. A value of v_{th} is calculated using either the amplitude ratio ($A_r = A_d/A_s$), where A_d is the amplitude of the deep temperature signal and A_s is the amplitude of the shallow signal (Equation 4.4), or the phase shift ($\Delta\phi = \phi_d - \phi_s$) of the

temperature signals (Equation 4.5):

$$q_{Ar} = \frac{(\rho c)_b}{\rho_w c_w}\left(\frac{2D_{th}}{\Delta z} lnA_r + \sqrt{\frac{\alpha + v_{th}^2}{2}}\right), \tag{4.4}$$

$$|q_\phi| = \frac{(\rho c)_b}{\rho_w c_w}\sqrt{\alpha - 2\left(\frac{4\pi\Delta\phi D_{th}}{P\Delta z}\right)^2}, \tag{4.5}$$

where P is the period of the sine temperature wave (i.e. 86400 s), and α is defined as:

$$\alpha = \sqrt{v_{th}^4 + \left(\frac{8\pi D_{th}}{P}\right)^2}. \tag{4.6}$$

Equations 4.4 and 4.5 must be solved iteratively as v_{th} appears on both sides of each equation (given that $q = v_{th}(\rho c)_b/\rho_w c_w$). All calculations of q from Equations 4.4 and 4.5 were performed using VFLUX (Gordon et al. 2012). A negative flux denotes downwelling, and a positive flux denotes upwelling. Estimated fluxes from the use of $\Delta\phi$ are absolute values, because the value of v_{th} (second term on the right hand side of Equation 4.5) is a square root. Hydraulic heads at observation points were used to determine the sign (and hence the vertical direction of flow) of $q_{\Delta\phi}$.

4.3.2 Numerical modelling

Time series of synthetic streambed temperatures were generated using the numerical simulator HydroGeoSphere (HGS) (Therrien et al. 2006), which uses the control volume approach to discretise equations for flow, and the Galerkin finite element approach for solute and thermal transport. HGS has been used to simulate a range of thermal transport processes (e.g. Graf and Therrien 2009; Brookfield et al. 2009; Irvine et al. in press). All simulations in this study were run assuming steady state flow, but with transient heat transport. Other assumptions include instantaneous change in water temperature and temperature of the medium, and that the influence of variable fluid density can be ignored. Assumptions in the numerical modelling are consistent with previous numeri-

cal modelling experiments (e.g. Lautz 2010; Roshan et al. 2012; Cuthbert and McKay 2013), and the assumption of constant fluid density has been shown to be justified for the temperature range considered in this study (Ma and Zheng 2010).

The model domain (Figure 4.1) is a 2D section, taken along the length of a stream (x direction), with dimensions of 5 m in the x direction, and 3 m in the z direction. Only the losing part of model is simulated, producing the downwelling part of a hyporheic flow cell. The choice to focus on downwelling only was made because temperature both A_r and $\Delta\phi$ methods have been shown to perform well for determining downwelling fluxes, but that A_r methods can be unreliable for determining upwelling fluxes (Roshan et al. 2012). A uniform, quadrilateral mesh was used to discretise the domain, with $\Delta x = 0.02$ m and $\Delta z = 0.01$ m, producing 75 000 elements. Time steps of 60 seconds were used for all simulations. The temporal and spatial discretization produced stable results, satisfying the grid Peclet and Courant numbers for thermal transport. For all simulations, seven days were simulated so that edge effects in filtering the temperature time series was not an issue. For example, Hatch et al. (2006) demonstrated that the filtering of temperature time series can produce lower amplitudes in the first four days. In their example, errors in calculated fluxes during the first four days ranged between 0.1 to 0.6 m/day where the actual flux was 1.0 m m/day.

The hydraulic boundary conditions of the model (Figure 4.1) were no-flow boundaries for the left and bottom boundaries. The top boundary was represented as a constant head boundary, with a hydraulic gradient of 0.1 (-). This gradient produced fluxes which typically ranged between ± 3.0 m/day (although the strongest downwelling flux encountered was -7.9 m/day). The right hand boundary was also represented as a constant head boundary, with the minimum head value from the top boundary applied to the entire boundary. The transport boundaries are Dirichlet boundaries for the top and bottom boundaries. The bottom boundary was represented with a constant temperature of 22 °C. The top boundary was represented as a sinusoidal temperature signal with temperature varying between 22 and 29 °C according to Equation 4.7.

$$T_{(t)} = T_0 + \Delta T sin\left(\frac{2\pi(t - [P/4])}{P}\right) \tag{4.7}$$

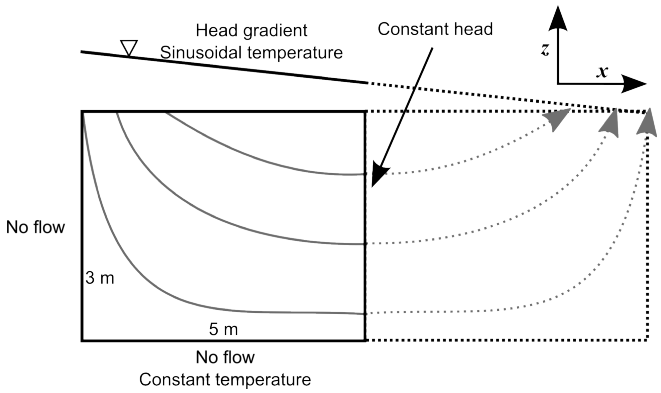

Figure 4.1: HydroGeoSphere model domain. Only the losing part of the model domain (solid lines) was simulated. No flow boundaries were applied at the left and bottom boundary. Constant head boundaries were used for the top and right boundaries. Thermal boundary conditions were a sinusoidal top boundary condition, and a constant temperature bottom boundary.

where T_0 is the average temperature (25.5 °C), ΔT is the amplitude of the temperature signal in the stream (3.5 °C). The term $P/4$ (i.e. 86400 s / 4) was included so that the starting temperature of the temperature signal was at its minimum value. For this study, typical temperature ranges from data from Cranswick et al. (under review) were used.

Streambed temperatures (with diurnal signals) are typically measured to depths of 1.0 m (e.g. Fanelli and Lautz 2008; Rau et al. 2010; Gordon et al. 2012). However, in highly permeable (e.g. sandy) streambeds, temperature signals can propagate further into the streambed, making estimates of q at greater depths possible. For example, Cranswick et al. (under review) estimated q at depths of up to 1.2 m below the streambed surface.

To capture a range of flow behaviour (including fluxes at depths which exceed 1.0 m), observation points were positioned at locations along the length of the model (x = 0.5, 1.0 and 2.5 m), and at a range of depths (z = 0.0 to 1.5 m in 0.1 m increments). All calculations of q using either A_r or $\Delta\phi$ where performed using Δz = 0.1 m, resulting in up to 45 estimates of and $q_{\Delta\phi}$ from each simulation. It was not possible to calculate a value of q for every sensor pair, as Equations 4.4 and 4.5 cannot be iteratively solved where $A_r > 1$, or $\Delta\phi < 0$.

As 1D tracer methods assume vertical flow, but flow paths in natural streambeds are inherently 2D or 3D, it is assumed that 1D methods estimate the vertical component of flux (q_z), which is representative of the midpoint between the two sensors (e.g. Figure 4.2b). This is in comparison to Figure 4.2a, where the estimate of q will be representative of any point between the temperature sensor pair.

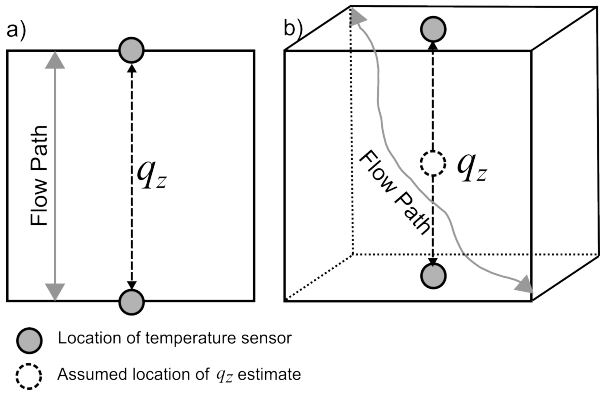

Figure 4.2: The grey lines denote a flow path, and dashed black lines denote the vertical component of flux. Solid grey circles denote temperature observation points, and dashed white circle denotes the hypothetical location where the flux estimate applies when 3D flow occurs. a) Shows the assumptions of the Stallman (1965) and resulting Hatch et al. (2006) models, with vertical 1D flow. The flux at any point between the observation points will be identical. b) Shows a more realistic case with a flow path that is 3D. It is assumed that flux estimates are representative of the vertical component of flux (q_z), which is applied at the mid-point between two sensors.

To compare the q estimated from the A_r or $\Delta\phi$ against a 'known' flux from the model (which we denote q_{HGS}), the arithmetic mean q_z between a pair of observation points was calculated, an approach also used by Roshan et al. (2012). The use of an arithmetic mean was chosen over harmonic or geometric means, as both positive and negative fluxes were present.

4.3.3 Representation of streambed properties

The values of streambed properties are shown in Table 4.1. All streambed properties in the model were spatially uniform, with the exception of hydraulic con-

ductivity.

Table 4.1: Thermal and hydraulic parameters

Parameter	Unit	Symbol	Value
Thermal conductivity of solids	W/m/°C	κ_s	2.00
Thermal conductivity of water	W/m/°C	κ_w	0.6
Specific heat capacity of solids	J/kg/°C	c_s	830
Specific heat capacity of water	J/kg/°C	c_w	4187
Density of solids	kg/m^3	ρ_s	2650
Density of water	kg/m^3	ρ_w	999.7
Total porosity	-	θ	0.3
Hydraulic conductivity	m/s	K	Varies

The three arrangements of K considered in the study are shown in Figure 4.3. For the first set of investigations (Figure 4.3a), the streambed was represented as a high K material ($K = 1 \times 10^{-4} m/s$) with a 0.2 × 0.2 m zone of low K ($K = 1 \times 10^{-5} m/s$). The low K material was moved to a range of locations in the model domain to investigate the influence of heterogeneity in a manner that could be easily controlled. Later, the streambed was represented using multi-Gaussian geostatistics. For all geostatistically arranged streambeds, the geometric mean K was approximately 1 × 10^{-4} m/s. Figure 4.3b shows a typical ln(K) field from a case which is to represent cobble structured streambed materials. In these simulations the correlation lengths (τ, m) in the horizontal (τ_x) and vertical (τ_z) direction were both set at 0.2 m. Figure 4.3c shows a layered streambed setting, where τ_x = 2.0 m, and τ_z = 0.2 m. For each of the two streambed structures, three degrees of heterogeneity were considered, with variance (σ^2) of ln(K) values of 0.1, 0.74 and 2.5. This range of σ^2ln(K) spans the range from a low to a relatively high degree of heterogeneity, with an intermediate value that was taken from Cardenas and Zlotnik (2003). All ln(K) fields were generated using the Sequential Gaussian Simulation (SGSIM) tool from the Geostatistical Simulation Library (GSLIB) (Deutsch and Journel 1998). For each of the six scenarios (combination of correlation structure and σ^2ln(K)), 50 realisations were simulated, which provided a sufficiently large number of q estimates to calculate average errors in Section 3.3. For example, the minimum number of q_{Ar} estimates used to calculate average errors was 86 (average of 124 values), and minimum

number of estimates of $q_{\Delta\phi}$ was 61 (average 132 values).

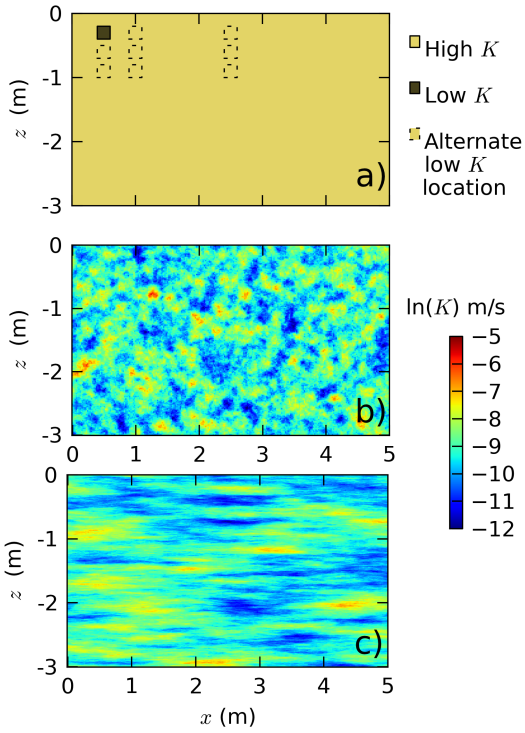

Figure 4.3: Heterogeneous structures. a) Showing deterministic arrangements of high K (sand colour), and low K (brown colour). Dashed lines denote alternative locations of low K zone (i.e. only a single low K zone is present in each simulation), b) geostatistical distributions of ln(K) with cobble like structure, and c) geostatistical distributions of ln(K) with layered structure.

4.4 Results and Discussion

4.4.1 Simulations with a single low K zone

The resulting streambed temperature signals from a homogeneous (dotted lines) and heterogeneous simulation with a single low K zone (solid lines) are shown in Figure 4.4. Figure 4.4 shows that heterogeneities in the streambed can cause $A_r > 1$ (i.e. the amplitude of the signal at z = -0.5 m is greater than the amplitude at z = -0.3 m). It should be mentioned that instances where $A_r > 1$ could be resolved by increasing the sensor spacing and that filtering of temperature time

series can also cause $A_r > 1$ (Gordon et al. 2012). When $A_r > 1$, flux estimates cannot be produced, as the A_r equation cannot be iteratively solved. In the simulation presented in Figure 4.4, observation points are located so that they pass through the low K zone, with observation points located above, within and below the low K zone. In the simulation with a homogeneous streambed (dotted lines), the signal amplitude decreases with depth, and phase shifts increase with depth, between all sensor pairs.

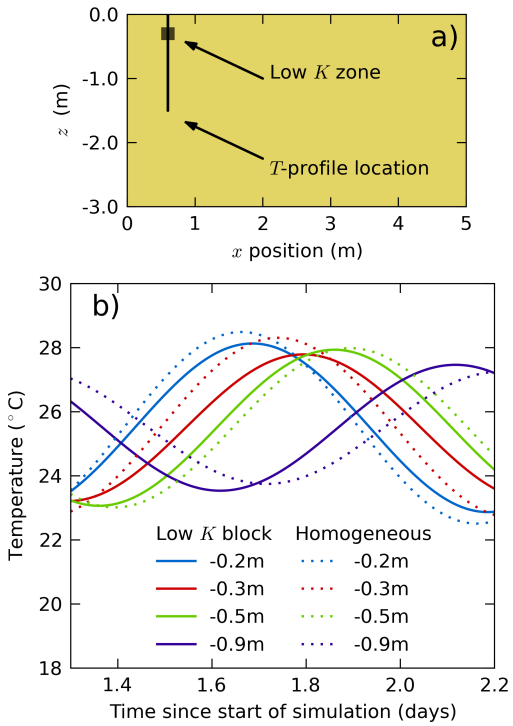

Figure 4.4: Representation of the K distribution and location of temperature sensors of a HGS model. For the sand coloured material, $K = 1 \times 10^{-4}$ m/s, and for the brown coloured material $K = 1 \times 10^{-5}$ m/s. b) Synthetic temperatures from two HGS simulations. Solid lines are from the K distribution in a), and dotted lines are from a homogeneous model where $K = 1 \times 10^{-4}$ m/s. The temperature time series with the low K block resemble the data shown in Figure 4.5.

The results from the simulation with the low K zone (solid lines, Figure 4.4b) show that the temperature signal from within the low K zone (z = -0.3m, shown in red) has a decreased amplitude and increased phase relative to the homogeneous

simulation. The reduction in amplitude occurs in such a way that no calculation of is possible using the z = -0.3 and -0.5 m sensor pair. While the phase of the temperature signal at z = -0.3 m is also influenced by the low K zone, the timing of the temperature peaks increases with depth between all sensors pairs, making estimates of $q_{\Delta\phi}$ possible between all sensor pairs. The presence of the low K zone influences the amplitude and phase of all temperature data shown in Figure 4.4b.

Figure 4.5 shows unfiltered temperature data from a vertical profile taken from the Haughton River in northern Queensland, Australia (see Cranswick et al. (under review) for details). The temperature signals in Figure 4.5 follow the general pattern as shown in Figure 4.4, suggesting that heterogeneities in the streambed could be a possible explanation for these temperature signals. Interestingly, the data presented in Figure 4.5 could be used to obtain an estimate of $q_{\Delta\phi}$, as $\Delta\phi$ increases with depth between all sensor pairs.

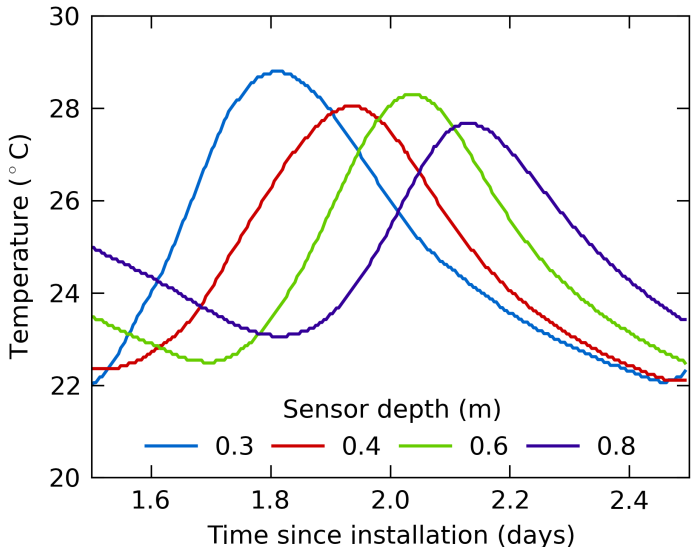

Figure 4.5: Temperature data at four depths from the Haughton River, Queensland, Australia. Between the -0.4 m, and -0.6 m sensors $A_r > 1$, and a value of q_{Ar} cannot be calculated.

In order to determine the influence of streambed heterogeneities on the estimation of q using either A_r or $\Delta\phi$, the location (in x and z) of the low K zone

was varied, and fluxes were calculated from the resulting temperature data. The centre point of the low K zone was positioned at x = 0.5, 1.0 and 2.5 m, and at z = -0.3, -0.7 and -1.1 m, producing nine combinations of x and z. The results in Figure 4.6 show the influence of the position of a single low K zone on the estimates of q_{Ar} and $q_{\Delta\phi}$ relative to q_{HGS} (where the element by element q_{HGS} is shown).

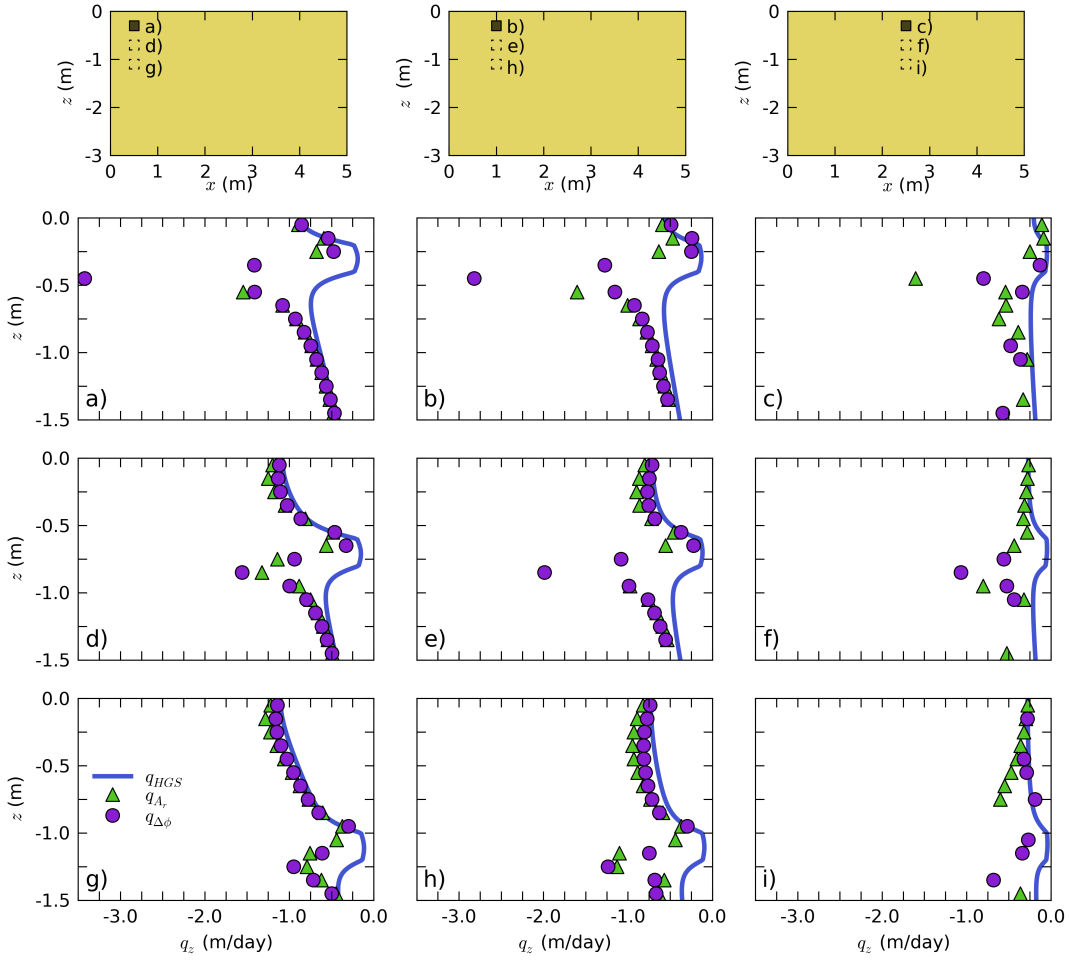

Figure 4.6: Top row shows the location of the low K zones tested. For the sand coloured material, $K = 1 \times 10^{-4}$ m/s, and for the brown coloured material $K = 1 \times 10^{-5}$ m/s. The dashed lines represent alternative locations of the low K zone. From left to right, the centroid of the low K zone (in x) is 0.5 m (left), 1.0 m (centre) and 2.5 m (right). From top to bottom the centroid of the low K zone (in z) is -0.3 m (top), -0.7 m (middle) and -1.1 m (bottom). In Figures 4.6a-i, blue line denotes q_{HGS}, circle marker denotes q_{Ar}, and triangle marker is $q_{\Delta\phi}$.

In all cases shown in Figure 4.6, the observation points are positioned so that the points pass through the low K zone. For simulations with the sensors located at x = 0.5 and 1.0 m, the sudden increase in q_{HGS} (i.e. q approaches zero, see blue line where z $\approx$ -0.25 m in Figure 4.6a) caused by the low K zone leads to a sudden decrease (i.e. q is more strongly negative) in the estimate of both q_{Ar} and $q_{\Delta\phi}$. This effect is more pronounced in cases where the low K zone is closer to the surface (as shown in Figures 4.6a and 4.6b), compared to cases where the low K zone is located deeper in the profile (as shown in Figures 4.6g and 4.6h). Estimates of q_{Ar} and $q_{\Delta\phi}$ at locations above the low K block are typically close to q_{HGS} or estimate stronger downwelling fluxes. For example, at z = -0.35 m in Figure 4.6d, the error (calculated as calculated as q_{HGS} - q_{Ar} or $q_{HGS} - q_{\Delta\phi}$) in q_{Ar} is 0.13 m/day, and the error in $q_{\Delta\phi}$ is 0.10 m/day where q_{HGS} = -0.78 m/day. Presented as percentages, these errors are 14.33 and 11.29 % respectively. Figure 4.6 suggests that the simultaneous estimate of strong downwelling from the use of $\Delta\phi$ and an inability to obtain an estimate of q_{Ar} suggests that streambed heterogeneity is influencing $q_{\Delta\phi}$, and that the estimate is not reliable (e.g. Figures 4.6a, 4.6b). Figure 4.6 also shows that generally, errors are smaller for $q_{\Delta\phi}$ compared to q_{Ar} except where the low Kzone strongly influences flux estimates.

Figure 4.7 is an alternative method of presenting the results from Figure 4.6. In Figure 4.7, errors in q_{Ar} or $q_{\Delta\phi}$ are presented as a function of the vertical distance of the flux estimate from the low K zone (either the upper or lower edge). The extent of the low K zone is shown by the grey bar. Given that the majority of q values are negative (i.e. downwelling), a positive error denotes a more strongly downwelling flux estimate.

Errors in Figure 4.7 for both q_{Ar} and $q_{\Delta\phi}$ are generally comparable, except when one of the observation points used in a flux estimate was in the low K zone. Errors in flux estimates where one or more observation points were in a low K zone are generally larger for $\Delta\phi$ relative to A_r. The strong downwelling estimates of $q_{\Delta\phi}$ shown in Figures 4.6a and 4.6b correspond to the large errors in the top right figure in Figure 4.7. These large errors (2.95 m/day where q_{HGS} was -0.48 m/day for the x = 0.5 m, and 2.47 m/day where q_{HGS} was -0.35 m/day for the x = 1.0 m case) occur where no estimate of q_{Ar} is possible.

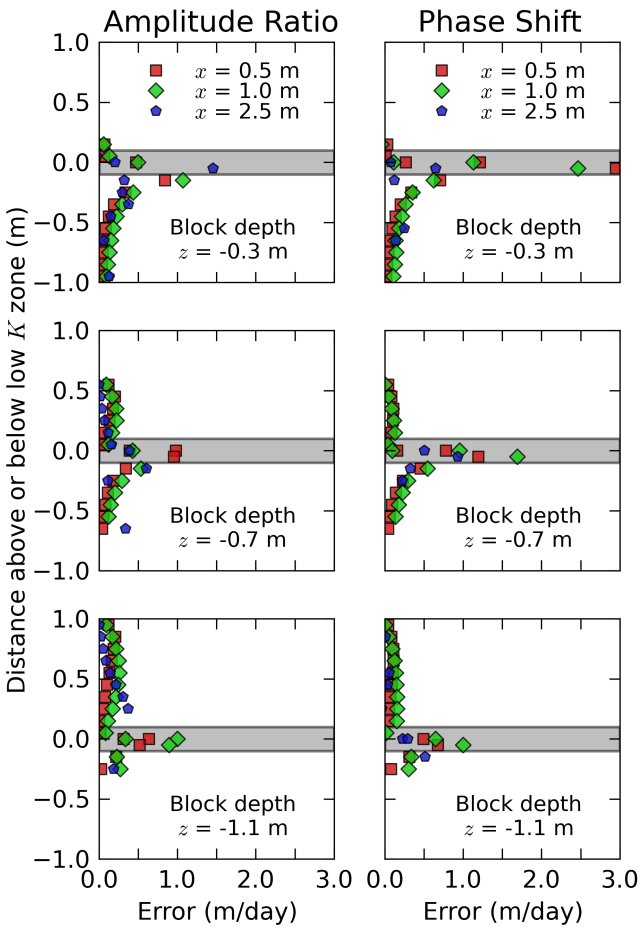

Figure 4.7: Errors in estimated fluxes from A_r (left) and $\Delta\phi$ (right) from the HGS simulations considered in Figure 4.6. Results are presented for the depth of the low K zone at z = -0.3 m (top), z = -0.7 m (middle), and z = -1.1 m (bottom). Errors are presented for the distance of the q estimate (from either the top or the bottom) of the low K zone. The grey bar denotes the vertical extent of the low K zone.

The non-linear flow patterns that occur above the low K zone in the upper 1.0 m of the profile (e.g. Figures 4.6d, 4.6e, 4.6g and 4.6h), were generally reproduced, and estimates of q_{Ar} and $q_{\Delta\phi}$ approached q_{HGS} below the low K zone. There were cases where the $\Delta\phi$ method also failed to produce a flux estimate. For the deterministic scenarios, the failure of the $\Delta\phi$ approach was limited to the simulations where the temperature observations were taken at x = 2.5 m. It appears that errors are caused by filtering of weak temperature signals at depth.

In general, the performance of q_{Ar} and $q_{\Delta\phi}$ is poor as the horizontal component of q increases relative to q_z (e.g. Figures 4.6c, 4.6f, 4.6i), a finding consistent with Lautz (2010), Roshan et al. (2012), and Cuthbert and McKay (2013).

The difference in K of an order of magnitude represents a relatively mild degree of heterogeneity. For example, in detailed investigations of streambed hydraulic conductivity, Cardenas and Zlotnik (2003) and Ryan and Boufadel (2007) recorded K distributions which spanned approximately 3 orders of magnitude. The influence of streambed heterogeneity for K-fields that include and exceed these ranges are assessed in section 4.4.2.

4.4.2 Log-normally distributed K values

The results presented in Figure 4.8 are for streambeds structures that are intended to represent cobbled streambeds. In Figure 4.8, the degree of heterogeneity increases from left (σ^2 ln(K) = 0.1) to right (σ^2 ln(K) = 2.5), and the x position of the temperature sensors increases from top (x = 0.5 m) to bottom (x = 2.5 m). In each case, a flow field from HGS is presented. In Figures 4.8 and 4.9, estimates of q_{Ar} and $q_{\Delta\phi}$ are presented for the first realization of each heterogeneous scenario.

For the $\sigma^2 ln(K) = 0.1$ case (Figure 4.8, left column), estimates of both and $q_{\Delta\phi}$ are generally in agreement with q_{HGS} for the majority of the vertical profile, with the exception of the range of z = -0.15 to z = -0.35 m (top row), and estimates below z = -0.35 m (bottom row). Errors in estimated fluxes for the σ^2ln(K) = 0.1 typically ranged between -0.30 and 0.33 m/day (on the order of ±35 %). As with the case shown in Figure 4.6, estimates of stronger downwelling flows are estimated where rapid changes in flow velocity and direction occur (e.g. z = -0.15 to -0.35m, for x = 0.5m, σ^2ln(K) = 0.1) . This effect is shown more clearly for example the σ^2ln(K) = 2.5, x = 2.5 m case (Figure 4.8, right column, bottom row), where an error of $q_{\Delta\phi}$ = -3.34 m/day occurs where q_{HGS} = 0.33 m/day at z = -0.55 m (i.e. an error of 1008 %). As with the results shown in Figure 4.6, errors in estimates of q_{Ar} and $q_{\Delta\phi}$ become greater as the horizontal component of flux increases relative to the vertical component. For the higher 2ln(K) cases (Figure 4.8 centre and right column) both q_{Ar} and $q_{\Delta\phi}$ follow the general trends in flow, even for the highly variable fluxes shown.

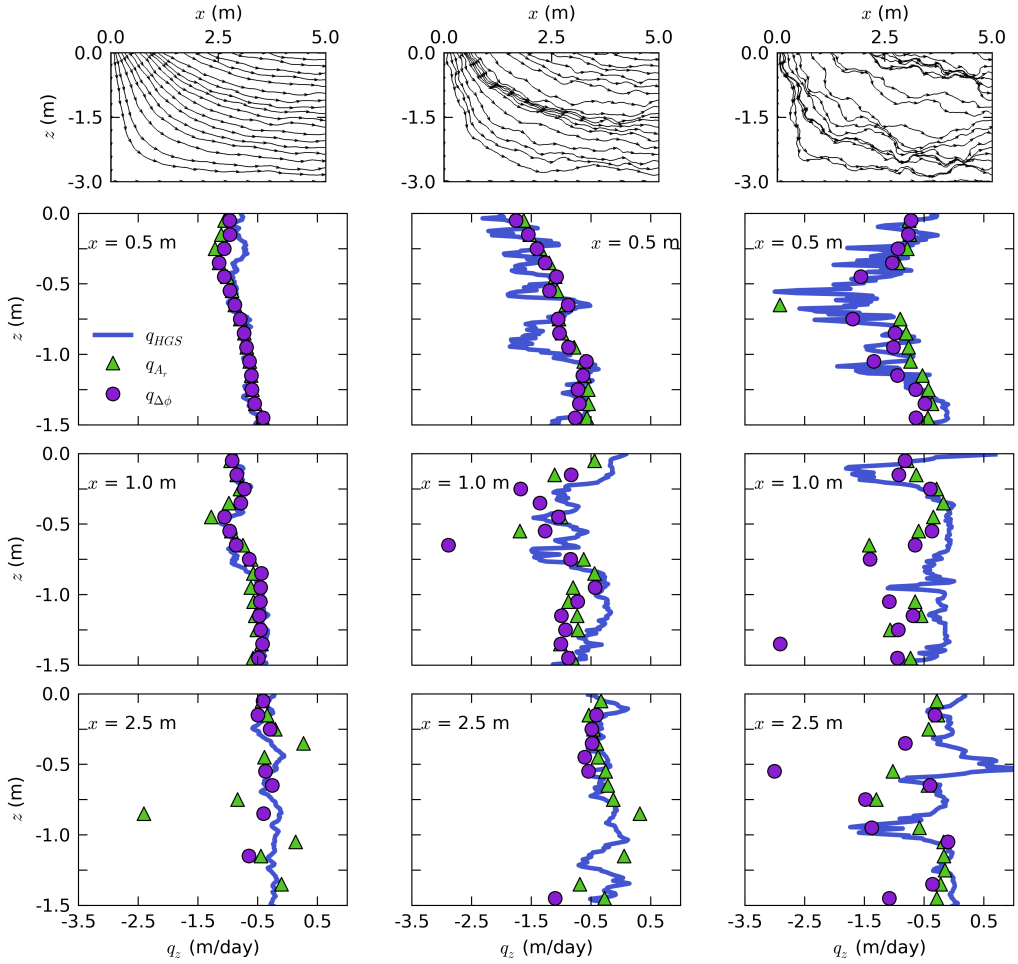

Figure 4.8: Flow fields and plots of q_{HGS}, q_{Ar}, and $q_{\Delta\phi}$ for cobble structured streambeds. Top row shows flow the HGS flow field, with σ^2 ln(K) increasing from left to right column. In scatterplots, blue line denotes q_{HGS}, circle marker denotes q_{Ar}, and triangle marker denotes $q_{\Delta\phi}$.

The investigation into the effect of streambed heterogeneity with more continuous, layered structures is presented in Figure 4.8. The layout of Figure 4.9 mimics that of Figure 4.8.

The case where $\sigma^2 \ln(K) = 0.1$ (Figure 9, left column) shows that both the A_r and $\Delta\phi$ equations perform well for all depths and positions along the flow path. For the $\sigma^2 \ln(K) = 0.1$ and $x = 0.5$ m case, the greatest errors for both q_{Ar} and $q_{\Delta\phi}$ occurred at z = -0.15 m were errors of 0.26 m/day (-22.9 %) and 0.10 m/day

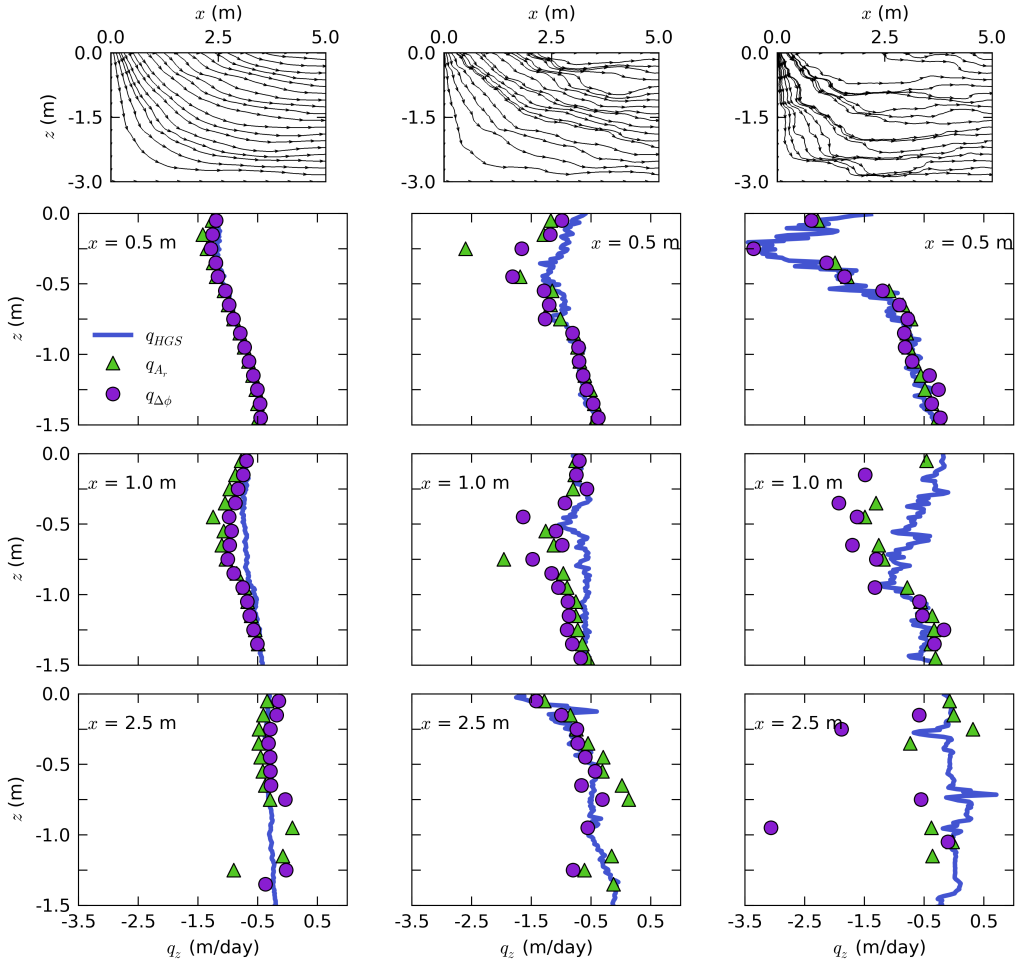

Figure 4.9: Flow fields and plots of q_{HGS}, q_{Ar}, and $q_{\Delta\phi}$ for layered structured streambeds. Top row shows flow field from HGS simulation, with $\sigma^2\ln(K)$ increasing from left to right column. In scatterplots, blue line denotes q_{HGS}, circle marker denotes q_{Ar}, and triangle marker denotes $q_{\Delta\phi}$.

(-9.0 %) for q_{Ar} and $q_{\Delta\phi}$ respectively, where q_{HGS} was -1.15 m/day. Errors were larger for the $\sigma^2\ln(K) = 0.1$ and $x = 1.0$ m case, with errors up to 0.50 m/day (67.9 %) for q_{Ar} , 0.23 m/day (31.6 %) for $q_{\Delta\phi}$ where q_{HGS} was -0.74 m/day. Within the upper 0.7 m for the $x = 2.5$ m, $\sigma^2\ln(K) = 2.5$ case, errors were within 0.15 m/day for both q_{Ar} and $q_{\Delta\phi}$. In the $\sigma^2\ln(K) = 2.5$ simulation (right column), both the A_r and $\Delta\phi$ approaches are able to reproduce the flow behaviour extremely well for the $x = 0.5$ m time series, producing estimates of q with errors on the order of $\pm$ 0.2 m/day. As with the high $\sigma^2\ln(K)$ case presented in Figure 4.8, the estimates of both q_{Ar} and $q_{\Delta\phi}$ are erratic for the case where $x =$

2.5 m, producing errors in excess of 1.0 m/day (in excess of 500 %). Generally, the A_r and $\Delta\phi$ approaches produce more strongly negative estimates of q (i.e. downwelling), however Figures 4.8 and 4.9 also show cases where more positive fluxes are predicted, as well as the fact that generally both estimates of both q_{Ar} and $q_{\Delta\phi}$ have the correct sign. Estimates of q with the incorrect sign occurred for cases where q_{HGS} was close to zero. Estimates of $q_{\Delta\phi}$ and q_{Ar} for both cobble structured (Figure 4.8) and layer structured (Figure 4.9) streambeds typically reproduced q_{HGS} in the upper 0.3 m. The largest errors typically occurred for cases where the vertical component of flux was small.

In order to generalise the findings from Figures 4.8 and 4.9, average errors across the 50 realisations are calculated for each geostatistical scenario. Average errors are calculated for x = 0.5, 1.0 and 2.5 m in 0.3 m depth increments (i.e. fluxes estimated using Δz= 0.1 m, in the depth range from z = 0.0 to z = -0.3 m, ..., z = -1.2 to z = -1.5 m). This sampling produced up to 3 estimates of q_{Ar} or $q\Delta\phi$ in each $x - z$ range considered, from each realisation. Owing to the difficulties in calculating average values when both positive and negative values are present, average errors are presented using two calculation methods. The results shown in Figure 4.10a are the arithmetic mean errors, presented in m/day. The benefit of an arithmetic mean is that the sign of the error is maintained; however, the overall average will be dominated by large (positive or negative) errors. An alternative to the arithmetic mean (or similar approaches such as Root Mean Square Error) is to calculate a geometric mean error. A drawback of the use of a geometric mean is that negative values cannot be used, so the units of the results presented in Figure 4.10b are |%|. Errors presented as a percentage are more easily generalizable, and with the presentation of the geometric mean, the overall value is not dominated by large errors. However, errors expressed as a percentage exaggerate errors as fluxes approach zero (i.e. as x or z increases). By definition, for q_{HGS} = 0, any error presented as a percentage would equal infinity. For results presented in both Figures 4.10a, and 4.10b, cases where no solution was possible from q_{Ar} or $q_{\Delta\phi}$, or where estimates are clearly erroneous (errors of $\pm$ 10.0 m/day) were omitted from calculations. These large errors only occurred for the use of $\Delta\phi$ where no estimate from A_r was possible, and were more prevalent for the cobbled structured scenarios compared to the layered scenarios, for higher $\sigma^2\ln(K)$, and as the x location of the sensors increased.

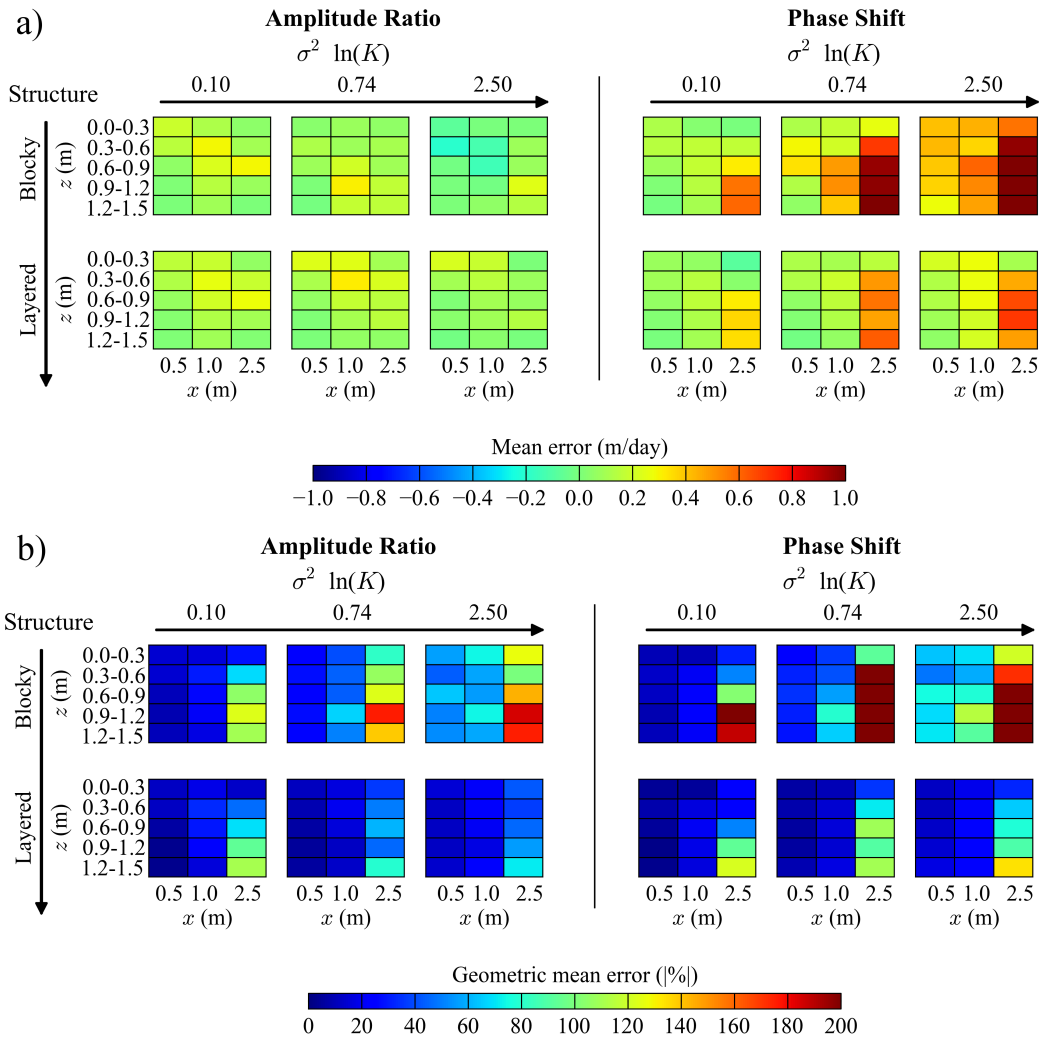

Figure 4.10: Showing a) arithmetic error (in m/day), and b) geometric mean error in (|%|). For both figures, results from the use of A_r are shown on the right, and results from the use of $\Delta\phi$ are shown on the left. The top row of panels is for a cobble structure, and the bottom row of panels is for a layered structure. Columns of panels are for the range of $\sigma^2\ln(K)$. In each panel, averaged results for three x positions, and five depths (in 0.3 m increments) are presented.

The results shown in Figure 4.10a show that flux estimates from both A_r and $\Delta\phi$ typically produce q estimates that are greater (stronger downwelling) for all parameters in our analysis (location of sensor pair, structure of streambed, degree of heterogeneity and use of A_r or $\Delta\phi$). It is clear that the use of A_r produces

smaller errors relative to the use of $\Delta\phi$. The trend in the $q_{\Delta\phi}$ estimates shows that greater errors occur as x and z increase. It is also clear in the $\Delta\phi$ data in Figure 4.10a that errors are larger for cobble structured streambeds compared to the layered structure. For example, for the $\sigma^2\ln(K) = 2.5$ case, with a cobble structure for $x = 1.0$ and $z = 0.0$ to -0.3 m, the average error from the use of $\Delta\phi$ is 0.44 m/day, and for the layered streambed is 0.18 m/day. The maximum error presented in Figure 4.10b (which occurred for the z interval of -1.2 to -1.5 m, $x =$ 2.5 m and using $\Delta\phi$) was 507 %, although as previously stated, the presentation of errors as a percentage is problematic as q approaches zero, and that errors increased with depth and x location of the sensor pair. Figure 4.10b shows that on average, estimates of q_{Ar} were accurate within 49.6 % in the upper 0.6 m of the streambed for the layered materials (and accurate within 14.9 % at $x = 0.5$ m), and 127.1 % for the cobble materials (56.5 % at $x = 0.5$ m). On average, estimates of $q_{\Delta\phi}$ in the upper 0.6 m were accurate within 71.2 % for the layered materials (12.3 % at $x = 0.5$ m), and 202.7 % for cobble structure streambeds (63.3 % at $x = 0.5$ m). While these errors may seem large, it is important to consider alternative approaches. For example, fluxes calculated using measurements of K and hydraulic gradients are expected to be highly uncertain, given the potential range in streambed K values. The findings shown in Figure 4.10 suggest that the use of heat as a tracer in cobble structured streams should be used with caution, where rapid changes (spatially) in flow direction can influence how temperature is distributed in the streambed. Also, in and around large cobbles, temperature changes within a cobble will be slower than surrounding regions where thermal transport will be dominated by convection rather than conduction.

4.5 Summary and Conclusions

This study is the first quantitative and systematic analysis of the influence of streambed heterogeneity on the interpretation of temperature time series data to estimate the exchange between groundwater and surface water. In both deterministically and geostatistically arranged streambed materials, our investigation assessed the influence of 1) streambed structure, 2) the degree of streambed heterogeneity, 3) the vertical and horizontal position of sensors along a flow path, and 4), the performance of the use of amplitude ratios or phase shifts to calculate

fluxes.

Results show that fluxes typically have the correct sign (direction), but fluxes are typically over-estimated (more strongly downwelling). Results from Figure 6 show that estimates of strong downwelling from phase shifts are unreliable if no estimate of flux is possible from the amplitude ratio method for the same sensor pair. The influence of the key parameters assessed in this study on the estimation of fluxes are as follows:

1. Flux estimates from the Hatch et al. [2006] equations are more reliable for layered streambeds compared to cobble structured streambeds. The cobble structured streambeds have complex flow paths that change direction rapidly over short spatial scales, and small regions where conduction dominates convection, leading to these regions changing temperature more slowly than surrounding material. This effect decreases the amplitude, and increases the time of the peak of the temperature signal. In the combination of parameters tested here, this effect led to the over-estimation of downwelling from the use of phase shifts, and caused the amplitude ratio equation to fail.

2. Errors in flux estimates increase with the degree of heterogeneity (i.e. $\sigma^2 \ln(K)$) of the streambed material. The effect of the degree of streambed heterogeneity was greater on flux estimates using phase shifts compared to amplitude ratios.

3. Errors in flux estimates increased with depth of the sensor pair, and with position along the flow path. Estimates of fluxes in the upper 0.3 m were generally the most reliable, with the greatest errors for the amplitude ratio of 127 % for the cobble streambeds, and 42 % for the layered structure, and greatest errors for the phase shift of 120 % for cobble streambeds and 32 % for layered structure. It should be highlighted that all of these errors occurred in the most heterogeneous streambeds (i.e. $\sigma^2 \ln(K) = 2.5$), and where the horizontal component of flux was large relative to the vertical component (i.e. where $x = 2.5$ m). In cases where temperature measurements are in locations with stronger downwelling, the use of amplitude ratio to calculate flux produces smaller errors than those obtained from the use

of phase shifts.

4. Errors were typically comparable from the use of phase shift or amplitude ratios. However, the use of the phase shift equation resulted in much larger errors for the case where vertical velocity was nearly zero ($x = 2.5$ m), and as depth increased.

The findings of this study have been obtained through the use of synthetic 2D modeling. More complex flow paths are expected in 3D simulations. Directions for further work could include an investigation into the performance of temperature time series in 3D fields, the upscaling of point estimates of flux, or an investigation into the benefits and drawbacks of more recent solutions presented by McCallum et al. (2012) and Luce et al. (2013). An investigation of the influence of heterogeneity on the fluxes estimated from the McCallum et al. (2012) and Luce et al. (2013) equations would be of particular interest, given that they use both phase shift and amplitude ratio in the estimation of flux, and streambed heterogeneity appears to influence the phase shift and amplitude ratios differently.

Chapter 5

Conclusions

5.1 Summary of findings

The three studies contained in this thesis investigated the influence of heterogeneity in porous media on flow dynamics, and the estimation of flow rates using heat as a groundwater tracer. Processes that were investigated ranged from thermal free convection (a process that occurs on the kilometer scale), the interpretation of applied solute and temperature tracers (on the scale of tens of metres) and the interpretation of applied and natural temperature signals in streambeds to determine flow rates (centimetre scale).

The key findings from each of the three specific studies are as follows:

i. The use of a stratigraphic forward model of an aquifer in the study of the potential for thermal free convection allows for the use of plausible permeability distributions that are based of field measurements. This is a significant advancement to previous approaches that are based on geostatistics (with measured or assumed mean and variance of log-K), or homogeneous permeability fields. In our study, Rayleigh number maps and numerical hydrothermal simulations both suggest that thermal convection is a plausible process in the Yarragadee Aquifer. These findings could be used as a basis for regions to explore for geothermal energy extraction in the Perth metropolitan area in Western Australia, and the approach used in our study could be applied in other site investigations.

ii. The variance in estimates of groundwater velocity are shown to be remarkably small in comparison to the variance in $\ln(K)$. On average, estimates of groundwater velocity from the use of heat as an applied tracer were closer to the known mean velocity and displayed less variance in comparison to the use of applied solute tracers. This suggests that estimates of velocity from the use of applied heat tracers produce estimates that are closer to the mean velocity,

owing to the diffusive nature of thermal transport. The higher variance of velocity estimates from the interpretation of applied solute tracers suggests that the use of a solute tracer will produce a better understanding of aquifer heterogeneity.

iii. Estimates of flux, in a groundwater–surface water interaction context, using one-dimensional heat transport equations based on temperature time series data are shown to produce reliable estimates of exchange fluid fluxes, even in highly heterogeneous streambeds. Errors in flux estimates are shown to increase with variance in $\ln(K)$, for cobble structured streambeds compared to layered structures, and were larger using equations based on phase shift compared to amplitude ratios. Errors for layered streambeds using the amplitude ratio were generally less than 40 %, errors which are small in comparison to methods which require measurements of K and head gradients.

5.2 Future work

All simulations contained in this thesis were restricted to two dimensions (either x-z as with Chapters 2 and 4, or x-y in the case of Chapter 3). In all cases, the reasoning behind the use of 2D simulations rather than 3D was to make it possible to investigate behaviour across a number of realisations or scenarios. Thus, all of the situations considered in this thesis could also be considered in 3D. Further work could also include:

i. The extension of the geothermal modelling presented in Chapter 2 into 3D would be of interest, as any simulation convecting in 2D would also convect in 3D, but the opposite is not also true. For example, discontinuities in low permeability layers may allow for thermal convection to occur. The influence of non-continuous layers was not considered in the study. 3D sections from the stratigraphic forward model of the Yarragadee Aquifer could be simulated, which would be useful. A logical next step in the study of the potential for thermal convection both in the Yarragadee Aquifer, but also other sites, is to move towards the use of 3D and realistic aquifer structures. Other directions for future work would be for an investigation into the correlation between elevated bottom hole temperatures presented in Sheldon et al. (2012) with

Rayleigh number maps to determine whether elevated temperatures occur in these regions.

ii. A field investigation into the differences in flow rates estimated from applied solute and temperature tracers in an field setting would be of interest. Our study suggests that we should not necessarily expect the same estimates of groundwater velocities from solutes and heat tracers. It would be of interest to determine whether these findings are reproduced in the field. In addition, the use of heat as a tracer could be more extensively tested in cases of aquifer storage and recovery, where typically there are many observation wells, and high hydraulic gradients exist.

iii. The use of heat as a tracer to determine the exchange fluxes between surface water and groundwater is a current research area of much interest, and there is much work that can be done in this area. As with previous chapters, an extension of heterogeneous simulations from 2D to 3D could be considered. There are also several key areas in the use of heat as a tracer in stream settings that require further attention. A compassion between the widely used Hatch et al. (2006) method and newer methods that simultaneously use amplitude ratio and phase shifts, such as those by McCallum et al. (2012), and Luce et al. (2013) will be able to demonstrate the benefits that these methods may offer. It may also be of interest for a clear comparison of the temperature time series methods (e.g. Hatch et al. 2006) and point in time methods (e.g. Bredehoeft and Papadopulos 1965) methods. A key limitation of the use of heat as a tracer in streams is that estimates are limited to point measurements. Methods that could upscale point measurements to providing more spatially distributed estimates of flux would be a key step forward in the use of heat as a tracer in a stream setting. For example, Lautz and Ribaudo (2012) provide methods to produce maps of flux from point measurements.

iv. Other exciting possibilities for the use of heat in constraining groundwater problems are surely to arise from the use of Distributed Temperature Sensors. The ability to capture both fine spatial and temporal resolution data sets has already been used in a groundwater–surface water context, and it is likely that this will continue. The use of Distributed Temperature Sensors to obtain near continuous estimates of flux with depth (i.e. Briggs et al.

2012) in streambeds, or the ability to obtain spatially (horizontal) distributed streambed or wetland temperatures will likely provide detailed understanding of groundwater–surface water interactions. Distributed Temperature Sensors may also become more widely used in the identification of fractures (e.g. Leaf et al. 2012; Banks et al; 2014).

v. Other equipment capable of recording temperature measurements are beginning to show promise, particularly in the field of surface water-groundwater interactions. For example Angermann et al. (2012) provide guidance on the use of 'heat pulse sensors' which use a heat pulse, and a 3D network of temperature sensors to determine 3D flows on the centimetre scale in the hyporheic zone. This heat pulse technique is capable of determining horizontal flow components, a capability that is not possible with many of the 1D analytical techniques. Also thermal imaging cameras show promise for identification of processes such as submarine groundwater discharge (Duarte et al. 2006) or to locate areas of upwelling in streambeds (Chen et al. 2008).

Tools are available to record temperature measurements from the point scale to continuous measurements of 10s to 100s of metres, and the ability to capture from point in time to years. With the increased availablity of these tools to record temperature measurements, coupled with the improved ability to interpret temperature data, it is likely that there is a bright future for the use of temperature tracing in hydrogeology.

Appendix A

Conversion from permeability to hydraulic conductivity

Much of the discussion in Chapter 2 is focused on permeability (k; m^2), which is related to hydraulic conductivity (K, m/s) by the expression $K = k\rho g/\mu$, where ρ and μ are fluid density and viscosity. For hydrothermal simulations which include variable density and viscosity, the numerical simulator FEFLOW requires K to be entered at a reference temperature. The Beta-Gamma plugin (Magri 2009) allows the thermal expansion term to vary with temperature, and requires that the reference temperature be set to 0 °C. At 0 °C and 1 bar, the reference density ρ_0 is 999.84 kg/m^3 and reference viscosity μ_0 is 0.001792 Pa s (Wagner et al. 2000). Thus the multiplying factor from k to K is $\rho_0 g/\mu_0 = 5474907$ $m^{-1}s^{-1}$.

Appendix B

Quantitative evaluation and comparison of heat and solute tracers in heterogeneous aquifers

National Groundwater Association Confecence, 2012

Dylan J. Irvine[1], Craig T. Simmons[1], Adrian D. Werner[1] and Thomas Graf[2]

[1]School of the Environment, Flinders University, NCGRT, Adelaide, Australia,

[2]Institute of Fluid Mechanics in Civil Engineering, Leibniz Universität, Hannover, Germany

Tracer tests are a powerful tool for quantifying transport and hydraulic subsurface parameters. Anderson (2005) suggests that hydrogeologists should capitalize on recent improvements in temperature sensors, and that heat data should be collected and interpreted more widely. Heat data are increasingly used in groundwater-surface water interaction studies, and have proven useful in calibrating numerical models. It would appear that there is an opportunity for more widespread use of heat as a tracer in hydrogeology, but the use of heat is currently inhibited by a lack of quantitative guidance and intuition on situations where heat is an appropriate tracer. Furthermore, it is not immediately obvious what advantages heat tracers offer over solute tracers. These two tracer types have not been systematically evaluated within the same framework to allow for a rigorous quantitative comparison. The most fundamental differences between solute and heat tracers are that thermal diffusivity is 3-4 orders of magnitude greater than molecular diffusion, and heat can be transported through both the connected pore spaces and the porous medium. How this affects flow rate determination using the tracers in both homogeneous and heterogeneous geologic settings requires exploration. In this study, we use a numerical model to compare and contrast solute and heat tracers in order to develop quantitative guidance for the applicability of these tracers in natural hydrogeologic settings. A numerical model is an efficient tool to perform this analysis because the problem can be well constrained, and flow velocities are known. Results suggest that the uncertainties and bias which arise from using tracers are greater compared to hydraulic methods. Uncertainties and bias are lower for heat tracers compared to solute tracers; however heat tracer tests require a longer duration due to thermal retardation, which under some circumstances may be a significant drawback.

Appendix C

Simulating thermal free convection in complex layered media using FEFLOW

FEFLOW Down Under, 2013

Dylan J. Irvine[1,2], Heather A. Sheldon[2], Craig T. Simmons[1] and Adrian D. Werner[1]

[1]School of the Environment, Flinders University, National Centre for Groundwater Research Training, Adelaide, Australia,

[2]CSIRO Earth Science and Resource Engineering, Perth, Western Australia, Australia

Investigations into thermal free convection that attempt to incorporate field observations of material properties are rare owing to the difficulty in obtaining sufficient data to represent aquifer heterogeneity. Because of this difficulty, aquifer properties such as permeability are typically represented as simple stratigraphic layers or modelled as stochastic distributions. An alternative approach is to utilise sparse field observations of permeability-porosity profiles to condition stratigraphic forward models, where physical deposition and erosion processes are numerically simulated. In this investigation, a stratigraphic forward model of the Yarragadee aquifer in the Perth Basin is used to investigate the influence of complex layering of aquifer materials on the potential for thermal free convection. Classical Rayleigh number analyses were performed (assuming equivalent homogeneous and anisotropic media) and these were used to identify critical permeabilities, where thermal convection can occur if this permeability value is exceeded. Findings from the Rayleigh number analysis were compared against two-dimensional flow and transport simulations performed with FEFLOW to compare outcomes of analyses where heterogeneity is included (numerical simulations) and neglected (Rayleigh number analysis). It was previously believed that aquifer heterogeneity would inhibit convection in the Perth Basin. Numerical modelling suggests that large-scale thermal free convection can occur in areas where the classical Rayleigh number suggests that convection is unlikely. This occurs because while the average permeability is sub-critical, layers in the aquifer have permeabilities that promote convection. Our findings provide additional lines of evidence for the possibility of thermal free convection in the Perth Basin, which has implications for geothermal energy.

Appendix D

Did heterogeneity kill convection? Building the case for thermal convection in the Yarragadee aquifer, Perth, Western Australia

IAH Conference 2013, (abstract accepted, but withdrawn due to absence)

Dylan J. Irvine[1,2], Heather A. Sheldon[2], Craig T. Simmons[1] and Adrian D. Werner[1]

[1]School of the Environment, Flinders University, National Centre for Groundwater Research Training, Adelaide, Australia,

[2]CSIRO Earth Science and Resource Engineering, Perth, Western Australia, Australia

Thermal convection of groundwater can lead to anomalously high temperatures occurring at relatively shallow depths. These elevated groundwater temperatures could be exploited for geothermal energy. It is therefore useful to know if and where thermal convection might occur and how strong it is. The likelihood of thermal convection is controlled by a number of key factors, including aquifer thickness, geothermal gradient and permeability. Given that permeability can span several orders of magnitude within an aquifer, and varies spatially on length scales ranging from centimetres to hundreds of metres, it is perhaps the most important parameter in determining whether convection is possible. While studies into the influence of heterogeneity on convection processes have been performed using simple layered systems or multi-Gaussian permeability fields, studies which investigate the impact of realistic aquifer permeability distributions on convection are extremely rare. In this study, a stratigraphic forward model of the Yarragadee aquifer in the Perth Basin (Western Australia) is used to provide a realistic permeability distribution for the aquifer. Theoretical and numerical analyses of this permeability distribution are performed to determine whether thermal convection could potentially occur. These analyses include comparisons of permeability-depth profiles against estimates of the critical permeability for convection in an equivalent homogeneous anisotropic medium, and two-dimensional hydrothermal simulations with permeability-depth distributions taken from the stratigraphic forward model. Findings from the theoretical analyses indicate that convection may occur on the eastern side of the aquifer where it is thick (>2500 m in places) and has high average permeability. Convection is not expected to occur on much

of the western side of the aquifer, where low permeability marine sediments are present. Results from numerical modelling support the findings of the theoretical analyses, demonstrating the occurrence of large-scale thermal convection in simulations that use the stratigraphic forward model to represent aquifer properties.

References

Anderson, M.P., and W.W. Woessner. 1992. Applied groundwater modeling. Simulation of flow and advective transport. Sydney: Academic Press Inc.

Anderson, M.P. 2005. Heat as a ground water tracer. Ground Water 43 no. 6: 951-968.

Angermann, L., J. Lewandowski, J.H. Fleckenstein, and G. Nützmann. 2012. A 3D analysis algorithm to improve interpretation of heat pulse sensor results for the determination of small-scale flow directions and velocities in the hyporheic zone. Journal of Hydrology, 475, 1-11.

Bair, E.S. and M. A. Metheny. 2002. Remediation of the Wells G & H superfund site, Woburn Massachusetts. Groundwater 40 no. 6: 657-668.

Banks, E.W., M.A. Shanafield, and P.G. Cook. 2014. Induced temperature gradients to examine groundwater flowpaths in open boreholes. Groundwater doi: 10.1111/gwat.12157.

Barlebo, H.C., M.C. Hill, and D. Rosbjerg. 2004. Investigating the Macrodispersion Experiment (MADE) site in Columbus, Mississippi, using a three-dimensional inverse flow and transport model. Water Resources Research 40 no. 4.

Birkinshaw, S.J., and B. Webb. 2010. Flow pathways in the Slapton Wood catchment using temperature as a tracer. Journal of Hydrology 383 no. 3-4: 269-279.

Bons, P.D., B.P. van Milligen, and P. Blumm. 2013. A general unified expression for solute and heat dispersion in homogeneous porous media. Water Resources Research 49, doi:10.1002/wrcr.20488.

Bravo, H.R., F. Jiang, and R.J. Hunt. 2002. Using groundwater temperature data to constrain parameter estimation in a groundwater flow model of a wetland system. Water Resources Research 38, no. 8.

Bredehoeft, J.D., I.S. Papadopulos. 1965. Using groundwater temperature data to constrain parameter estimation in a groundwater flow model of a wetland system. Water Resources Research 1 no. 2.

Briggs, M.A., L.K. Lautz, J.M. McKenzie, R.P. Gordon, and D.K. Hare. 2012. Using high-resolution distributed temperature sensing to quantify spatial and temporal variability in hyporheic flux. Water Resources Research 48, doi: doi:10.1029/2011WR011227.

Burnett, R.D., and E.O. Frind. 1987. Simulation of contaminant transport in three dimensions

2. Dimensionality Effects. Water Resources Research 23 no. 4: 695-705.

Calver, A. 2001. Riverbed permeabilities: Information from pooled data, Ground Water, 39(4), 546-553.

Cardenas, M. B., and V. A. Zlotnik. 2003. Three-dimensional model of modern channel bend deposits, Water Resources. Research 39(6).

Carslaw, H.S. and J.C. Jaeger. 1959. Conduction of heat in solids. Oxford: Clarendon Press.

Chang, C.M., and H.D. Yeh. 2012. Stochastic analysis of field-scale heat advection in heterogeneous aquifers. Hydrology and Earth System Sciences 16 no. 3: 641-648.

Chen, X., J. Song, C. Cheng, D. Wang, and S.O. Lacket. 2008. A new method for mapping variability in vertical seepage flux in streambeds. Hydrogeology Journal, 17, 519-525.

Constantz, J., M.H. Cox, and G.W. Su. 2003. Comparison of heat and bromide as ground water tracers near streams. Ground Water 41 no. 5: 647-656.

Constantz, J. 2008. Heat as a tracer to determine streambed water exchanges, Water Resources Research 44.

Cooper, H.H.J., and C.E. Jacob. 1946. A generalized graphical method for evaluating formation constants and summarizing well-field history. Transactions, American Geophysical Union 27: 526-34.

Corbel, S., O. Schilling, F.G. Horowitz, L.B. Reid, H.A. Sheldon, N.E. Timms, P. Wilkes 2012a Identification and geothermal influence of faults in the Perth metropolitan area. Thirty-Seventh Workshop on Geothermal Reservoir Engineering, Stanford, California

Corbel, S., C. Griffiths, abd C. Dyt. 2012b. Hot sedimentary aquifer characterization using forward modelling, Perth Basin, Australia. Thirty-Seventh Workshop on Geothermal Reservoir Engineering, Stanford, California

Cranswick, R.H., P.G. Cook, M.A. Shanafield, and S. Lamontagne. In press. The vertical variability of hyporheic fluxes inferred from riverbed temperature data. Water Resources Research, doi: doi:10.1002/2013WR014410.

CSIRO. 2007. PressurePlot. CSIRO, Perth, Australia. www.pressureplot.com

Cuthbert, M. O., and R. Mackay. 2013. Impacts of nonuniform flow on estimates of vertical streambed flux, Water Resources Research 49 no. 1, 19-28.

Darcy, H. 1856. Les Fontaines Publiques de la Ville de Dijon, Dalmont, Paris.

Deutsch, C.V., and A.G. Journel. 1998. GSLIB Geostatistical Software Library and User's Guide. 2nd ed. ed. New York: Oxford University Press.

Domenico, P.A., and F.W. Schwartz. 1998. Physical and chemical hydrogeology, 2nd ed. New York: Wiley.

Drury, L.W., G.E. Calf, and D. J.K. 1984. Radiocarbon dating of groundwater in tertiary sediments of the Eastern Murray Basin. Australian Journal of Soil Research 22 no. 4: 379-387.

Epherre, J.S. 1975. Creterion for the appearance of natural convection in an anisotropic porous layer. International Journal of Chemical Engineering 17 615-616.

Fanelli, R.M., and L.K. Lautz 2008. Patterns of water, heat and solute flux through streambeds around small dams. Ground Water, 46 no. 5: 671-687.

Ferguson, G. 2007. Heterogeneity and thermal modeling of ground water. Ground Water 45 no. 4: 485-490.

Ferguson, G., and V. Bense. 2011. Uncertainty in 1D Heat-Flow Analysis to Estimate Groundwater Discharge to a Stream. Ground Water 49 no. 3: 336-347.

Fick, A. 1855. Über Diffusion (About Diffusion) Annalen der Physik und Chemie (Annals of Physcis and Chemistry) 94 59-86.

Fourier, J.P.J. 1822. Théorie analytique de la chaleur (The Analytic Theory of Heat). Paris.

Frei, S., J. H. Fleckenstein, S. J. Kollet, and R. M. Maxwell. 2009. Patterns and dynamics of river-aquifer exchange with variably-saturated flow using a fully-coupled model. Journal of Hydrology, 375(3-4), 383-393.

Frind, E.O. 1982. Simulation of long term density-dependent transport in groundwater. Advances in Water Resources 5 7397.

Gordon, R. P., L. K. Lautz, M. A. Briggs, and J. M. McKenzie. 2012. Automated calculation of vertical pore-water flux from field temperature time series using the VFLUX method and computer program. Journal of Hydrology, 420, 142-158.

Griffiths, C., C. Dyt, E. Paraschivoiu, and K. Liu. 2001. Sedsim in hydrocarbon exploration. In: Merriam, D. and J. Davis (eds), Geologic modelling and simulation. Kluwer Academic,

New York.

Hall, F.R. and A.F. Moench. 1972. Application of the convolution equation to stream-aquifer relationships. Water Resources Research 8 no. 2: 487-493.

Hatch, C. E., A. T. Fisher, J. S. Revenaugh, J. Constantz, and C. Ruehl. 2006. Quantifying surface water-groundwater interactions using time series analysis of streambed thermal records: Method development, Water Resources Research, 42(10).

Hatch, C. E., A. T. Fisher, C. R. Ruehl, and G. Stemler. 2010. Spatial and temporal variations in streambed hydraulic conductivity quantified with time-series thermal methods, Journal of Hydrology, 389(3-4), 276-288.

Hess, K.M., S.H. Wolf, and M.A. Celia. 1992. Large-scale natural gradient tracer test in sand and gravel, Cape-Cod, Massachusetts.3. Hydraulic conductivity variability and calculated macrodispersivities. Water Resources Research 28 no. 8: 2011-2027.

Hidalgo, J.J., J. Carrera, and M. Dentz. 2009. Steady state heat transport in 3D heterogeneous porous media. Advances in Water Resources 32 no. 8: 1206-1212.

Hot Dry Rocks Pty Ltd. 2008. Geothermal energy potential in selected areas of Western Australia (Perth Basin). Hot Dry Rocks Pty Ltd, Melbourne.

Irvine, D.J., P. Brunner, H.-J. Hendricks-Franssen, and C.T. Simmons. 2012. Heterogeneous or homogeneous? Implications of simplifying heterogeneous streambeds in models of losing streams. Journal of Hydrology.

Irvine, D.J., C.T. Simmons, A.D. Werner, and T. Graf (in press) Heat and solute tracers: How do they compare in heterogeneous aquifers?, Ground Water, doi: 10.1111/gwat.12146.

Kae'eo Duarte, T., H.F. Hemond, D. Frankel, and S. Frankel. 2006. Assessment of submarine groundwater discharge by handheld aerial infrared imagery: case study of Kaloko fishpond and bay, Hawai'i. Limnology and Oceanography: Methods, 4, 227-326.

Kalbus, E., C. Schmidt, J. W. Molson, F. Reinstorf, and M. Schirmer. 2009. Influence of aquifer and streambed heterogeneity on the distribution of groundwater discharge, Hydrology and Earth System Sciences. 13(1), 69-77.

Keery, J., A. Binley, N. Crook, and J. W. N. Smith. 2007. Temporal and spatial variability of groundwater-surface water fluxes: Development and application of an analytical method using temperature time series, Journal of Hydrology. 336(1-2), 1-16.

Kühn, M., F. Dobert, and K. Gessner. 2006. Numerical investigation of the effect of heterogeneous permeability distributions on free convection in the hydrothermal system at Mount Isa, Australia. Earth and Planetary Science Letters 244: 655-671.

Lapham, W.W. 1989. Use of temperature profiles beneathr streams to determine rates of vertical ground-water flow and vertical hydraulic conductivity. USGS water-supply paper 2337.

Larocque, M., P.G. Cook, K. Haaken, and C.T. Simmons. 2009. Estimating Flow Using Tracers and Hydraulics in Synthetic Heterogeneous Aquifers. Ground Water 47 no. 6: 786-796.

Lautz, L. K. 2010. Impacts of nonideal field conditions on vertical water velocity estimates from streambed temperature time series, Water Resources Reseach 46.

Lautz, L.K., and R.E. Ribaudo. 2012. Scaling up point-in-space heat tracing of seepage flux using bed temperatures as a quantitative proxy, Hydrogeology Journal, 20: 1223–1238.

Leaf, A.T., D.J. Hart, and J.M. Bahr. 2012. Active thermal tracer tests for improved hydrostratigraphic characterization. Ground Water.

LeBlanc, D.R., S.P. Garabedian, K.M. Hess, L.W. Gelhar, R.D. Quadri, K.G. Stollenwerk, and W.W. Wood. 1991. Large-scale natural gradient tracer test in sand and gravel, Cape-Cod, Massachusetts .1. Experimental-design and observed tracer movement. Water Resources Research 27 no. 5: 895-910.

Luce, C.H., D. Tonina, F. Gariglio, and R. Applebee. 2013. Solutions for the diurnally forced advection-diffusion equation to estimate bulk fluid velocity and diffusivity in streambeds from temperature time series, Water Resources Research, 49. 488-506, doi: 10.1029/2012WR012380.

Ma, R., and C.M. Zheng. 2010. Effects of Density and Viscosity in Modeling Heat as a Groundwater Tracer. Ground Water 48 no. 3: 380-389.Meier, P.M., J. Carrera, and X. Sanchz-Villa. 1998. An evaluation of Jacobs method for the interpretation of pumpingtests in heterogeneous formations. Water Resources Research 34, no. 5: 10111025.

Macfarlane, P.A., A. Forster, D.F. Merriam, J. Schrotter, and J.M. Healey. 2002. Monitoring artificially stimulated fluid movement in the Cretaceous Dakota aquifer, western Kansas. Hydrogeology journal. 10 no 6: 662-673.

Magri, F. 2009. Derivation of the coefficients of thermal expansion and compressibility for the use in FEFLOW finite element subsurface flow and transport simulation system. White Papers volume III, WASY, Berlin 13-14.

Magri, F., T. Akar, U. Germici, and A. Pekdeger. 2010. Deep geothermal groundwater flow in

the Seferihisar-Balçova area, Turkey: Results from transient numerical simulations of coupled fluid flow and heat transport processes. Geofluids 10: 388-405.

McCallum, A.M., M.S. Andersen, G.C. Rau, and R.I. Acworth (2012) A 1-D analytical method for estimating surface watergroundwater interactions and effective thermal diffusivity using temperature time series. Water Resources Research 48.

McKibbin, R., and M.J. O'Sullivan. 1980. Onset of convection in a layered porous-medium heater from below. Journal of Fluid Mechanics 96: 375-393.

McKibbin, R., and P.A. Tyvand. 1983. Thermal-convection in a porous-medium composed of alternating thick and thin layers. International Journal of Heat and Mass Transfer 26: 761-780.

Nield, D.A., and C.T. Simmons. 2007. A discussion on the effect of heterogeneity on the onset of convection in a porous medium. Transport in Porous Media 68: 413-421.

Nield. D.A., A.V. Kuznetsov, and C.T. Simmons. 2009. The effect of strong heterogeneity on the onset of convection in a porous medium. Non-periodic global variation. Transport in Porous Media 77: 169-186.

Ohm, G.S. 1827. Die galvanische kette: mathematisch (The Galvanic Circuit Investigated Mathematically) Berlin.

Palmer, C.D., D.W. Blowes, E.O. Frind, and J.W. Molson. 1992. Thermal-energy storage in an unconfined aquifer .1. Field injection experiment. Water Resources Research 28 no. 10: 2845-2856.

Pavelic, P., P.J. Dillon, and C.T. Simmons. 2006. Multiscale characterization of a heterogeneous aquifer using an ASR operation. Ground Water 44 no. 2: 155-164.

Pearson, F.J.J., and D.E. White. 1967. Carbon 14 ages and flow rates of water in Carrizo Sand, Atascosa County, Texas. Water Resources Research 3 no. 1: 251-261.

Philips, O.M. 1991. Flow and reactions in permeable rocks. Cambridge University Press, Cambridge.

Pinder, G.F. and H.H. Cooper. 1970. A numerical technique for calculating the transient position of the saltwater front. Water Resources Research 6 no. 3 875882.

Prassad, A. and C.T. Simmons. 2003. Unstable density-driven flow in heterogeneous porous media: A stochastic study of the Elder 1976b "short heater" problem. Water Resources Research 39 no 1.

Rau, G. C., M. S. Andersen, A. M. McCallum, and R. I. Acworth. 2010. Analytical methods that use natural heat as a tracer to quantify surface water-groundwater exchange, evaluated using field temperature records, Hydrogeology Journal 18(5), 1093-1110.

Rau, G.C., M.S. Andersen, and R.I. Acworth. 2012. Experimental investigation of the thermal dispersivity term and its significance in the heat transport equation for flow in sediments. Water Resources Research 48: 3511-3511.

Rau, G.C., M.S. Andersen, A.M. McCallum, H.Roshan and R.I. Acworth. 2014. Heat as a tracer to quatify flow in near-stream sediments. Earth-Science Reviews 1 29: 40-58.

Rehfeldt, K.R., J.M. Boggs, and L.W. Gelhar. 1992. Field-study of dispersion in a heterogeneous aquifer .3. Geostatistical analysis of hydraulic conductivity. Water Resources Research 28 no. 12: 3309-3324.

Reid, L.B., G. Bloomfield, C. Botman, L.P. Ricard, and P. Wilkes. 2011. Temperature regime in the Perth metropolitan area: Results of temperature and gamma logging and analysis, June/July 2010. CSIRO EP111422, CSIRO, Perth, Australia.

Renard, P. 2005. The future of hydraulic tests. Hydrogeology Journal 13: 259-262.

Roshan, H., G. C. Rau, M. S. Andersen, and I. R. Acworth. 2012. Use of heat as tracer to quantify vertical streambed flow in a two-dimensional flow field. Water Resources Research 48.

Ryan, R.J., and M.C. Boufadel. 2007. Evaluation of streambed hydraulic conductivity heterogeneity in an urban watershed, Stochastic Environmental Research and Risk Assessment 21, 309-316, doi: 10.1007/s00477-006-0066-1.

Schilling, O., H.A. Sheldon, L.B. Reid, and S. Corbel. 2013. Hydrothermal models of the Perth Metropolitan Area, Western Australia: Implications for geothermal energy, Hydrogeology Journal.

Schornberg, C., C. Schmidt, E. Kalbus, and J.H. Fleckenstein. 2010. Simulating the effects of geologic heterogeneity and transient boundary conditions on streambed temperatures - Implications for temperature-based water flux calculations. Advances in Water Resources 33 no. 11: 1309-1319.

Sharp, J.M., and M. Shi. 2009. Heterogeneity effects on possible salinity-driven free convection in low-permeability strata. Geofluids 9: 263-274.

Shanafield, M., C. Hatch, and G. Pohll. 2011. Uncertainty in thermal time series analysis

estimates of streambed water flux. Water Resources Research, 47.

Sheldon, H.A., B. Florio, M.G. Trefry, L.B. Reid, L.P. Ricard, K.A.R. Ghori. 2012.The potential for convection and implications for geothermal energy in the Perth Basin, Western Australia. Hydrogeology Journal 20: 1251-1268.

Shook, G.M. 2001. Predicting thermal breakthrough in heterogeneous media from tracer tests. Geothermics 30, 573-589.

Simmons, C.T., T.R. Fenstemaker, and J.M. Sharp. 2001. Variable-density groundwater flow and solute transport in heteroegneous porous media: approaches, resolutions and future challenges. Journal of Contaminant Hydrology 52: 245-275.

Simmons, C.T. 2005. Variable density groundwater flow: From current challenges to future possibilities. Hydrogeology Journal 13 no. 1: 116-119.

Simmons, C.T., A.V. kuznetsov, and D.A. Nield. 2010. Effect of strong heterogeneity on the onset of convection in a porous medium: Imporance of spatial dimensionality and geologic controls. Water Resources Research 46.

Soto-López, C.D., T. Meixner, and T.P.A. Frerré. 2011. Effects of measurement resolution on the analysis of temperature time series for stream-aquifer flux estimation, Water Resources Research 47. doi:10.1029/2011WR010834.

Straface, S. 2009. Estimation of transmissivity and storage coefficient by means of a derivative method using the early-time drawdown. Hydrogeology Journal 17 no. 7: 1679-1686.

Sudicky, E.A. 1986. A natural gradient experiment on solute transport in a sand aquifer - spatial variability of hydraulic conductivity and its role in the dispersion process. Water Resources Research 22 no. 13: 2069-2082.

Sudicky, E.A., W.A. Illman, I.K. Goltz, J.J. Adams, and R.G. McLaren. 2010. Heterogeneity in hydraulic conductivity and its role on the macroscale transport of a solute plume: From measurements to a practical application of stochastic flow and transport theory. Water Resources Research 46.

Suzuki, S. 1960. Percolation measurements based on heat flow through soil with special reference to paddy fields. Journal of Geophysical Research 65, no. 9: 28832885.

Stallman, R.W. 1965. Steady one-dimensional fluid flow in a semi-infinite porous medium with sinusoidal surface temperature, Journal of Geophysical Research. 70, 2821-2827.

Swanson, T.E., and M.B. Cardenas. 2011. Ex-Stream: A MATLAB program for calculating fluid flux through sediment- water interfaces based on steady and transient temperature profiles, Computers and Geosciences, 37, 1664-1669.

Taniguchi, M. 1993. Evaluation of vertical groundwater fluxes and thermal properties of aquifers based on transient temperature-depth profiles. Water Resources Research 29 No 7: 2021-2026.

Taniguchi, M., J. Shimada, T. Tanaka, I. Kayane, Y. Sakura, Y.Shimano, S. Dapaah-Siakwan, and S. Kawashima. 1999.Disturbances of temperature-depth profiles due to surface climate change and subsurface water flow: 1. An effect of linear increase in surface temperature causedby global warming and urbanization in the Tokyo metropolitanarea, Japan. Water Resources Research 35 (5) 15071517.

Tezlaff, D.M., and J.W. Harbaugh. 1989. Simulating clastic sedimentation; computer methods in the geosciences, Van Nostrand Reinhold, New York.

Theis, C.V. 1935. The relation between the lowering of the piezometric surface and the rate and duration of discharge of a well using groundwater storage. Transactions, American Geophysical Union 2: 519-524.

Therrien, R., R.G. McLaren, E.A. Sudicky, and S.M. Panday. 2006. HydroGeoSphere. Waterloo, Canada: Groundwater Simulations Group, University of Waterloo.

Timms, N.E., S. Corbel, H. Olierook, P.G. Wilkes, C. Delle Piane, H.A. Sheldon, R. Alix, F.G. Horowitz, M.E.J. Wilson, K.A. Evans, C. Griffiths, L. Stütenbecker, S. Israni, P.J. Hamilton, L. Esteban, P. Cope, C. Evans, L. Pimienta, C. Dyt, X. Huang, J. Hopkins, and D. Champion. 2012. Perth Basin assessment program project 2: Geomodel. Western Australian Geothermal Centre of Excellence, Perth, Australia.

Tonina, D., C.H. Luce, and F. Gariglio. 2014. Quantifying streambed deposition and scour from stream and hyporheic water temperature time series, Water Resources Research. 50 287-292, doi: 10.1002/2013WR14567.

Townley, L.R. and M.G. Trefry. 2000. Surface water– groundwater interaction near shallow circular lakes: Flow geometry in three dimensions. Water Resources Research. 36 no. 4: 935-949.

Trinchero, P., X. Sanchez-Vila, N. Copty, and A. Findikakis. 2008. Ground Water 46 no 1: 133-143.

Turcotte, D. and G. Schubert. 1982. Geodynamics: Application of continuum physics to geological problems. New York: Wiley.

Tyler, S.W., J.S. Selker, M.B. Hausner, C.E. Hatch, T. Torgersen, C.E. Thodal, and S.G. Schladow. 2009. Environmental temperature sensing using Raman spectra DTS fiber-optic methods. Water Resources Research 45.

Vandenbohede, A., A. Louwyck, and L. Lebbe. 2009. Conservative Solute Versus Heat Transport in Porous Media During Push-pull Tests. Transport in Porous Media 76 no. 2: 265-287.

Wagner, W., J.R. Cooper, A. Dittmann, K. Kijima, H.J. Kretzschmar, A. Kruse, R. Mares, K. Oguchi, H. Sato, I. Stocker, O. Sifner, Y. Takaishi, I. Tanishita, J. Trubenbach, and T. Willkommen. 2000. The IAPWS industrial formulation 1997 for the thermodynamic properties of water and steam. Journal of Engineering for Gas Turbines and Power: ASME 122: 150-182.

Waples, D.W., and J.S. Waples. 2004. A Review and Evaluation of Specific Heat Capacities of Rocks, Minerals, and Subsurface Fluids. Part 1: Minerals and Nonporous Rocks. Natural Resources Research 13 no. 2: 97-122.

Weatherill, D., C.T. Simmons, C.I. Voss, and N.I. Robinson. 2004. Testing density-dependent groundwater models: Two-dimensional steadt state unstable convection in infinite and finite inclined poous layers. Advancse in Water Resources 27.